Treatment of a PHC Source Zone using Land Application of Sulfate

by

Yunxiao Wei

A thesis
presented to the University of Waterloo
in fulfillment of the
thesis requirement for the degree of
Master of Science
in
Earth Sciences

Waterloo, Ontario, Canada 2015
© Yunxiao Wei 2015

Author’s Declaration

I hereby declare that I am the sole author of this thesis. This is a true copy of this thesis, including any required final revisions, as accepted by the examination committee.

I understand that this thesis may be made electronically available to the public.

Yunxiao Wei

Abstract

This pilot-scale experiment was performed in the sand pit area at the University of Waterloo Groundwater Research Facility at CFB Borden located near Alliston, ON. A multicomponent PHC source zone (3 m x 3 m) was emplaced in 2012 between 1 and 3 m below ground surface inside a sheet pile walled experimental gate.

Simulation tools were used to design an optimal sulfate dosage system that would satisfy the reagent delivery and remediation requirements. Three episodes of sulfate release (5 m^3 of 5-20 g/L Na_2SO_4, and 0.3 g/L $(NH_4)_2SO_4$) at the ground surface were conducted over an 8-month period. A host of multilevel monitoring wells in conjunction with a real-time resistivity data collection system was employed to continuously track sulfate patterns and migration.

Treatment performance was evaluated based on changes in sulfate concentration in the plume and PHC mass discharge across a downgradient monitoring fence line. Results from compound specific isotope analysis (CSIA) and biomarker tools were combined with the conventional monitoring data to assess enhanced sulfate reduction of the PHCs.

General sulfate migration pathway was captured during EC monitoring. These results demonstrated 5 g/L Na_2SO_4 did not provide sufficient infiltration, while 15-20 g/L Na_2SO_4 created strong density-dependent flow. EC results of sulfate monitoring showed the real-time resistivity system allowed the collection of high resolution data. PHC mass discharge results showed significant attenuation of benzene, toluene and xylene after the sulfate application. CSIA data showed the occurrence of PHCs biodegradation associated with sulfate reduction. The sulfate isotope data support the occurrence of sulfate reduction. The concentration and isotope patterns observed for DIC are also linked to PHCs biodegradation. The microbiological data showed the occurrence of biodegradation under both aerobic and anaerobic conditions in the PHC plume.

Acknowledgement

I would like to thank my main supervisor, Dr. Jim Barker, for his continuous support and guidance during my whole Master study, not only the guidance in academic and research, but also in my career path and well being. He is a role model in my life. The same thank goes to Dr. Ramon Aravena. Without his support I could not have the opportunity to involve in such a great and challenging project, nor could I finish my degree. I would also like to thank Dr. Neil Thomson, for his appreciation and recognition to my efforts. His encouragement intensives me to strive for excellence. Thank Dr. Jon Jones for reviewing my thesis and for being a committee member of my defense.

Special thank goes to Dr. Massimo Marchesi, who is my field teacher. His patience and generous help ensured the completion of many tough field works. Dr. John Molson provided kind help and prompt feedback in modeling works. I am also grateful for his support.

Technical staffs at Waterloo made huge contributions in this project. Thank Bob Ingleton and Paul Johnson for their quality field support; thank Shirley Chatten, Wayne Nobel for their timely lab results; thank Terry Ridgeway, Cailey McCutcheon and David Stevenson for their help in developing the data logger; also than Richard Elgood for his help in sample coordination and lab method tutorial.

Thank you to Felipe Solano, Summer Jin, Kyle Jong, Christopher Bartlett, Christian Larsen and Mahsa Shayan, for their personal help in fieldworks.

This research was funded by Chevron Energy Technology Company and API. Their funding ensures the project to be carried out.

Finally, I would like to thank Xiang Ding and my parents Hong Wei, and Shaofen Zhou. Their countless support throughout my graduate study let me successfully complete my Master’s degree.

Table of Contents

Author's Declaration ii
Abstract iii
Acknowledgement iv
Table of Contents v
List of Figures vii
1. Introduction 1
1.1 General Introduction 1
1.2 Geochemical Considerations 2
1.3 Sulfate Delivery 3
1.4 Previous Studies and Background 4
1.5 Objectives 5
1.6 Thesis Overview 5
2. Experimental Design and Methods 7
2.1 Site Description 7
2.2 Numerical Modeling 8
2.2.1 Introduction of SALTFLOW 8
2.2.2 Model Domain 9
2.2.3 Modeling Processes 10
2.3 Monitoring Wells 11
2.4 Resistivity Data Logger System 12
2.4.1 Background 12
2.4.2 Resistivity Probes 13
2.4.3 Data logger 13
3. Methods 23
3.1 Monitoring Well Installations 23
3.2 Resistivity Data Logger Installation and Operation 23
3.3 Sampling 24
3.3.1 Sampling Overview 24
3.3.2 Field Sampling Methods 24
3.3.3 Sample Preparation 25
3.3.4 Lab Measurements 26
3.4 Land Application 28
4. Result and Discussion 39
4.1 Sulfate Application and Migration 40
4.1.1 EC Manual Measurement 40
4.1.1.1 Application I 40
4.1.1.2 Application II 41
4.1.1.3 Application III 43
4.1.2 Resistivity Data Logger System Measurement 43
4.1.3 Comparison between SALTFLOW and Actual Sulfate Migration 45

4.1.4 Water Table Fluctuation during Sulfate Application 45
4. 2 Mass Discharge Monitoring 46
4.2.1 Sulfate 47
4.2.2 Hydrocarbons 48
4.2.2.1 Residual NAPL and Initial Mass Discharge 48
4.2.2.2 PHC Mass Discharge Monitoring Results, Sulfate Application Phase 49
4.2.2.3 Source Depletion and Natural Attenuation 51
4.2.2.4 Sulfate Consumption 54
4.2.3 Sulfide 54
4. 3 Progress Monitoring 55
4.3.1 Source Area (S5-D3) 56
4.3.2 Row 3 (R3-M4-D1) 58
4.3.3 Biomarkers 59
5. Summary and Conclusion 108
Reference 110
Appendix A 114
Appendix B 116
Appendix C 118
Appendix D 131
Appendix E 132
Appendix F 137
Appendix G 140

List of Figures

Figure 2.1: Plan-view layout of pre-existing monitoring wells, residual source, and hydrocarbon plume (Kovacik, 2013) in the API gate. 15
Figure 2.2: Cross-section of sampling point layout at Row 3 or Row 4 multilevel monitoring transects..... 15
Figure 2.3: 3D grid model for API gate (Unit m). Each surface or boundary is described by a label and by a number. 16
Figure 2.4: Modeling result simulates sulfate applied on surface above source zone and passively infiltrated by precipitation. Sulfate concentration = 35 g/L, time of continuous application = 100 days. The red rectangular represents the residual source zone. C is the relative concentration compared to the initial value ($c = C/C_0$)..... 16
Figure 2.5: Two-step modeling result simulates sulfate water ponded above source zone at height of 0.6 m for 12 hours (Left) and its migration in the subsurface for 60 days. Initial sulfate concentration = 35 g/L. Red rectangular represents the residual hydrocarbon source zone and the yellow dashed lines show the approximately depth of monitoring wells at Row 3 and Row 4. 17
Figure 2.6: Two-step modeling result simulates sulfate ponded above source zone at height of 0.1 m. Sulfate concentration = 5 g/L, migration time = 45 days. Red rectangular represents the residual source zone. 17
Figure 2.7: Different types of new monitoring wells for Borden sulfate land application. 18
Figure 2.8: The plan-view layout of monitoring wells. Red black-dotted circles are EC multilevels, stars are multilevel suction lysimeters, green circles are Waterloo multilevel monitors and blue points are pre-existing multilevel wells. 18
Figure 2.9: The resistivity probe used in the lab test, modified based on the design in Stevenson (2013) 19
Figure 2.10: Field resistivity probes attached on the EC multilevel. Resistivity probe leads extend to the ground and connect to the data logger. 19
Figure 2.11: The interior of the data logger. The bundles of wires are input port for the multiplexer that connected to resistivity probe leads. 20
Figure 2.12: Data logger field data viewing. Field laptop and data logger connected by USB/RS 232 cable. 20
Figure 3.1: Geoprobe® 7720DT at Borden field. Another casing would be added to the top of the previous one as the pushing proceeded. 29
Figure 3.2: The field-view for installed wells. 29
Figure 3.3: Connection between data logger and probe lead extensions at field. 30
Figure 3.4: Manifold sampler. 30
Figure 3.5: Cole-Parmer 7553-70 pump and controller. 31
Figure 3.6: Sampling containers. 31
Figure 3.7: Field instruments for parameter measurement 32
Figure 3.8: Conceptual design for the sulfate application. 32
Figure 3.9: Groundwater wells and the pump. 33

Figure 4.1: The pond created by planks and bermed sand. Prepared sulfate water stored in the tank to the right of the pond area. 61
Figure 4.2: Bermed pond at constant water level during the first application. 61
Figure 4.3: Background EC contours on Day -9. Top diagram, EC distribution at Row 3; bottom, EC distribution at Row 4. Red dots represent sampling points reported. Red dots represent points where EC was measured. 62
Figure 4.4: EC contour at Row 3 on Day 23. Red dots represent EC measurement points..... 63
Figure 4.5: EC contour at Row 3 on Day 37. Red dots represent EC measurement points..... 64
Figure 4.6: EC contour at Row 3 on Day 58. Red dots represent EC measurement points..... 65
Figure 4.7: EC contour at Row 3 on Day 86. Red dots represent EC measurement points. No data available at R3-M1 and R3-M6 due to winter conditions. 66
Figure 4.8: EC contour at Row 3 on Day 103. Red dots represent EC measurement points. No data available at R3-M1 and R3-M6 due to winter condition. 67
Figure 4.9: Relationship between EC and datalogger reading for field test. 67
Figure 4.10: Resistivity data logger readings (X) at A) EC1, B) EC2, C) EC5 for a period of 78 days after the third application. The red arrow indicates the estimated arrival of sodium sulfate. 68
Figure 4.11: The layout of water table monitoring wells. 73
Figure 4.12: Sulfate concentration at Row 3 and Row 4 on Day -9. Red dots are EC data points. 74
Figure 4.13: Relationship between EC and sulfate on Day 58. 75
Figure 4.14: Sulfate concentration at Row 3 on Day 86. Red dots are sampled points. 75
Figure 4.15: Sulfate concentrations at Row 3 and Row 4 on Day 277. Red dots are sampled points 76
Figure 4.16: UVOST survey boreholes 1-13. 77
Figure 4.17: NAPL distribution. A) top, plan-view; B) bottom, cross-section view relative to Row 3. 78
Figure 4.18: Representative area blocks and sampling points (red dots) from Kovacik, 2013. Contour is the NAPL cross-section projected onto Row 3. 79
Figure 4.19: Distribution of BTXN on Day -9 at Row 3 and Row 4. Red dots are sampled points. 80
Figure 4.20: Distribution of BTXN on Day 86 at Row 3. 81
Figure 4.21: Distribution of BTXN on Day 277 at Row 3 and Row 4. 82
Figure 4.22: Distribution of BTXN on Day 394 at Row 3 and Row 4. 83
Figure 4.23: Raoult's Law model of mass discharge ratio for BTXN 84
Figure 4.24: Raoult's Law model of mass discharge compared with field mass discharge results. A) benzene, B) toluene, C) xylene and D) naphthalene. 86
Figure 4.25: Progress results for S5-D3. 88
Figure 4.26: Progress results for R3-M4-D1. 90
Figure 4.27: Dual isotope for A) benzene, B) toluene and C) o-xylene at S5. The red arrow is the anticipated evolution of compounds undergoing aerobic biodegradation, while the green arrow is the evolution anticipated under anaerobic conditions. The Day of the sampling is also indicated beside each point. 92

Figure 4.28: Dual isotope for A) benzene, B) toluene and C) o-xylene at R3-M4. The red arrow is the anticipated evolution of compounds undergoing aerobic biodegradation, while the green arrow is the evolution anticipated under anaerobic conditions. The Day of the sampling is also indicated beside each point. 94

List of Tables

Table 2.1: Constituents of injected PHC NAPL 15
Table 2.2: Boundary conditions 21
Table 2.3: Borden hydrogeological parameters used in SALTFLOW 22
Table 3.1: List of connected EC probes. 34
Table 3.2: Flux sampling events schedule. 35
Table 3.3: Schedule for progress sampling events. 36
Table 3.4: Sampling points selected for flux monitoring. 37
Table 3.5: Sampling points selected for progress monitoring. 38
Table 4.1: Schedule of field events. 95
Table 4.2: Summary of applications 96
Table 4.3: EC in source area on Day 10 97
Table 4.4: EC in source area on Day 23 98
Table 4.5: EC in source area on Day 37 99
Table 4.6: EC in source area on Day 68 100
Table 4.7: EC at source area on Day 86 101
Table 4.8: EC at well EC2 on Day 103 101
Table 4.9: EC at S5, Row 3 and Row 4 on Day 197 102
Table 4.10: Water table fluctuation at MW4 during the first sulfate application. 103
Table 4.11: Water table fluctuations during the second sulfate application. 103
Table 4.12: Water table fluctuations during the third sulfate application. 103
Table 4.13: Baseline sulfide concentration on Day -9. 104
Table 4.14: Sulfide concentration on Day 197. 105
Table 4.15: Summary of BTXN mass discharge for PHC flux sampling (g/day). 106
Table 4.16: Summary of emplaced NAPL properties and theoretical SO_4^{2-} consumption per unit PHC degradation (mol SO_4^{2-}/ mol PHC). 107

1. Introduction

1.1 General Introduction

For the remediation of petroleum hydrocarbon (PHC) contaminated groundwater, the majority of traditional technologies have concentrated on passive natural attenuation by microorganisms (i.e. monitored natural attenuation, MNA). Other more active technologies involve removing mass from the source zone (i.e. dig and dump), volatilizing the non-aqueous liquid phase into the gas phase (air sparging and soil vapor extraction), and pumping the water-soluble fraction from the plume (Suthersan et al., 2011). Each of these technologies has advantages for a specific contaminated site, and it is acknowledged that no single technology can be treated as all-purpose (Khan et al., 2004). The attractiveness of these traditional technologies is usually degraded by the high cost and long time frame, so there is an interest for economic and efficient alternative techniques (Suthersan et al., 2011).

For PHC contaminated sites, one of the most important attenuation mechanisms is biodegradation that contributes to the decline in contaminant concentration in both source and plumes (Wiedemeier et al., 1999). PHC attenuation by anaerobic bio-oxidation (ABOx) is spontaneous and universal (Atlas, 1981; Leahy and Colwell, 1990; Chapelle, 1999; Suthersan et al., 2011). It has been demonstrated that the utilization the ABOx is cost-effective; however, the lack of electron acceptors (EA) occurs in most cases so that engineered application of ABOx has become more attraction (Lunardini and Dickey, 2003, Suthersan et al., 2011). In these systems, selected soluble non-oxygen EAs (e.g. sulfate, ferric salt and nitrate) are applied to anaerobic environments to stimulate biodegradation (Suthersan et al., 2011).

Among the ABOx, sulfate has been estimated to account for about 70% of the overall natural biodegradation capacity (Wiedemerier et al., 1999). From an engineered perspective, the characteristics of sulfate such as high solubility, widespread naturally occurring sulfate consuming microorganisms, low cost, and high persistence in the subsurface, are advantages (Suthersan et al., 2011). The use of sulfate can not only reduce the remedial time frame when compared to natural attenuation, but it also can reduce the cost when compared to traditional active remediation technologies (Suthersan et al., 2011). Therefore, sulfate land application in

becoming a popular technology for PHC remediation.

1.2 Geochemical Considerations

Dissolved oxygen is consumed rapidly in PHC contaminated groundwater and the rate of oxygen recharge is not able to meet the aerobic biodegradation demand so that anaerobic conditions usually develop (Suthersan et al., 2011). The dosing of sulfate in such environments supplies an EA for the PHC degradation via sulfate reduction (Suthersan et al., 2011). When sulfate is reduced in an anaerobic environment with benzene as the electron donor, as a representative organic compound at fuel spill sites, it can be described by (Suthersan et al., 2011, Anderson and Lovley, 2000):

$$C_6H_6 + 3.75\ SO_4^{2-} + 3\ H_2O \rightarrow 1.875\ H_2S + 1.875\ HS^- + 6\ HCO_3^- + 0.375\ H^+ \quad (1.1)$$

This sulfate reduction produces sulfide and bicarbonate which undergo further reactions. Although the byproduct is bicarbonate, the actual byproduct from PHC oxidation is carbon dioxide, which is dissolved in the groundwaer and transformed into bicarbonate as controlled by:

$$CO_2 + H_2O \rightarrow H_2CO_3 \quad (1.2)$$

$$H_2CO_3 \rightarrow HCO_3^- + H^+ \quad (1.3)$$

The formation of alkalinity contributes to the decrease of pH over time, and if not controlled, the decreasing pH will suppress the sulfate reduction rate (Suthersan et al., 2011). However, acidity will usually be buffered at most sites (Suthersan et al., 2011).

Under methanogenesis condition, CO_2 will also react with H_2 and form methane (Appelo and Postma, 2005):

$$CO_2 + 4\ H_2 \rightarrow CH_4 + H_2O \quad (1.4)$$

Excessive sulfide accumulation will inhibit PHC biodegradation under sulfate-reducing conditions (Suthersan et al., 2011). Previous research has reported that sulfide concentrations between 8.5 and 320 milligrams per liter (mg/L) reduce the rate of sulfate reduction by one-third (Roychoudhury and McCormick, 2006). However, in the anaerobic biodegradation zone, natural occurring iron oxide can reduced the excess sulfide by the precipitation of FeS (Appelo and Postma, 2005) as given by:

$$2\ FeOOH + 3\ HS^- \rightarrow 2\ FeS + S^0\ (s) + H_2O + 3\ OH^- \qquad (1.5)$$

The capacity for sulfide-precipitation depends on the natural abundance of ferric iron and the rate of sulfide formation (Suthersan et al., 2011). Moreover, at the fringe of the anaerobic zone, the presence of oxygen will consume sulfide so rapidly that sulfide accumulation will be limited at most of sites (Deutch, 1997; Suthersan et al., 2011).

1.3 Sulfate Delivery

In a sulfate land application, the sulfate must be delivered to the target region to produce the optimal geochemical environment for effective biodegradation. It has been reported that the threshold sulfate concentration to sustain biodegradation is approximately 100 mg/L (Habicht et al., 2005), and the maximum rate for microbial-mediated reactions is reached when sulfate is 2000 mg/L. At intermediate concentrations, sulfate is not a rate-limiting factor (Roychoudhury and McCormick, 2006), but nutrients (N, P, etc.) are usually not sufficient to support a very high sulfate-reducing rate. Therefore, the strategy to deliver sulfate that can achieve the treatment goals is the most important issue in the design. The selection of a specific strategy depends on the remediation objective, the characteristics of the reagents, the hydrogeological setting, aquifer nutrient levels, and water chemistry (e.g. the presence of iron; pH). Either solid sulfate or sulfate in solution can be applied. Solid sulfate land application is a cheaper and easier approach, while dissolved sulfate can provide better sulfate distribution and infiltration.

Since the migration of the sulfate and, in some cases, contaminants are the concern in the remediation process, monitoring their migration and distribution is critical to an efficient and effective remedial system (Stevenson, 2013).

1.4 Previous Studies and Background

Several studies related to sulfate reduction and hydrocarbon biodegradation had been conducted in the lab and at University of Waterloo's Research Aquifer Facility at Canadian Forces Base (CFB) Borden, Ontario, Canada. (Acton and Barker, 1992; Chen et al., 2007, 2008).

In situ column experiments were conducted by Acton and Barker (1992) to evaluate the potential to enhance in situ biodegradation of various aromatic hydrocarbons under anaerobic conditions at Borden through application of nitrate and sulfate. Under sulfate reducing conditions, rapid toluene attenuation, but no benzene biodegradation, was observed (Acton and Barker, 1992). Other PHCs including m-xylene, ethylbenzene, 1,2,4-TMB, o-xylene, and chlorobenzene were also recalcitrant to biodegradation under sulfate reduction (Acton and Barker, 1992). Although the direct addition of EAs did not enhance aromatic hydrocarbon biodegradation, significant sulfate-reducing activity was noted when lactate and yeast extract was added, suggesting nutrients may be one of the limiting factors for sulfate-reducing anaerobic biodegration at Borden (Acton and Barker, 1992).

In laboratory experiments, Chen et al. (2007; 2008) confirmed the potential for anaerobic monoaromatic PHC biodegradation under nitrate- and iron-combined conditions in the Borden aquifer (Chen et al. 2007). Chen et al. observed benzene biodegradation under iron-reducing conditions, after denitification removed hydrocarbons that may have suppressed benzene utilization (Chen et al. 2007). The addition of sulfate was unsuccessful in promoting monoaromatic PHC (including toluene) biodegradation in the Borden aquifer material. Chen et al. also found that BTEX biodegradation was significantly inhibited by the presence of ethanol, probably due to the preferential consumption of ethanol and its intermediate product acetate by the anaerobic EAs (Corseuil et al., 1998; Chen et al. 2007)

These studies demonstrated the potential for PHC biodegradation under nitrate- and iron-reducing conditions, while the feasibility of sulfate-reducing biodegradation remained controversial. Although nitrate and ferric iron were also shown to be more effective than sulfate by Cunningham et al. (2001), these are less desirable EAs as the regulatory maximum concentration for nitrate in groundwater is only 10 mg/L, and ferric iron is not practical to inject due to its low solubility at neutral aquifer pH (Cunningham et al. 2001). Therefore, the usability of sulfate land application at Borden was pursued.

1.5 Objectives

The remediation objective of this project is to treat both hydrocarbon residual source and the plume by a practical sulfate land application. The present sulfate land application study will comprehensively characterize sulfate plumes using diagnostic tools and so assess enhancement of biodegradation of specific PHC compounds generated by the sulfate application. Approaches to address the experimental objectives include:

(1) Utilize a numerical modeling tool to design a sulfate land application technique that ensures the sulfate plume flows through both contaminated source and plume;

(2) Design a practical sulfate dosage method to meet the reagent delivery and remediation requirements for this field site;

(3) Develop a real-time resistivity monitoring system that continuously tracks the migration of sulfate in the subsurface;

(4) Estimate the remediation effects using field and analytical data (VOC, DIC, sulfide and methane concentration etc.), and evaluate the enhancement of biodegradation by isotope analysis of sulfate and DIC, compound specific isotope analysis (CSIA) and biomarkers.

1.6 Thesis Overview

This thesis consists of four chapters plus references and appendices. The first chapter provides an introduction to the background of sulfate reduction and engineered sulfate

application.

Chapter 2 describes the experimental design.

Chapter 3 explains details of experimental methods.

Chapter 4 shows results and interpretations of the monitoring and analyses.

Chapter 5 summarizes the conclusions, lessons learned and achievements in this research.

2. Experimental Design and Methods

2.1 Site Description

The CFB Borden field site is located about 80 km north-west of Toronto. It has been used as a hydrogeology research facility by the University of Waterloo since the 1970s (Sudicky and Illman, 2011). Field hydrogeological parameters are summarized by King and Barker (1999). The field site is underlain by an unconfined aquifer that consist of median to fine grained sand, with dispersed silt, silty-clay, and coarse sand layers (King and Barker, 1999; Sudicky and Illman, 2011). The glaciolacustrine aquifer grades into glacial till (mainly silt and clay) at about 9 meters below ground surface (mbgs) forming an aquitard (King and Barker, 1999). The average hydraulic conductivity for the aquifer is approximately 8×10^{-5} m/s and the horizontal groundwater flow velocity is about 9 cm/day (Fraser, 2007).

The research for this thesis was conducted in the middle of three API gates at the Borden research site. Several groundwater studies had been done at the API gates (some references would be useful; doesn't need to be complete). Sheet piling on the east and west sides constrain the groundwater and contaminant flow in channels or gates and some sampling wells remained from previous research (Freitas, J.G., M.T. Mocanu, J.L.G. Zoby, J.W. Molson and J.F. Barker, 2011. Migration and fate of ethanol-enhanced gasoline in groundwater: A modeling analysis of a field experiment. J. Contam. Hydrol., 119, 25-43) that were re-used in the current sulfate land application project. Three groundwater monitoring transects or fences: Row 2, Row 3 and Row 4 were used as sampling wells (Figure 2.1). Each of these fences consist of six monitoring wells, designated as Multilevel 1 to 6 (M1-M6). Figure 2.2 shows the cross-section of a monitoring fence. Each well has 14 sampling points. Depth 1 to 13 (D1-D13) are evenly distributed from 1.5 mbgs to 3.84 mbgs at 0.19 m intervals, while D14, the deepest, is screened between 4.8 and 5.3 mbgs.

Prior to the current project about 110 liters of well-characterized PHCs (Table 2.1) were injected to approximate 2 meters below ground surface (mbgs) in August, 2012 in the gate. PHC distribution was characterized by a UVOST tool, which is described in Section 4.2.2.1 (Kovacik, 2013). The location of the residual source is also indicated in both Figure 2.1 and

2.2. The source is about 3 m long, 3 m wide and 2 m deep. For the map view, the source is situated about 1.5 m downgradient of Row 2, between the monitoring well R2-M3 and R2-M4 (Figure 2.1). In the cross-section view, it is located between 0.75 mbgs to 3 mbgs (Figure 2.2).

2.2 Numerical Modeling

2.2.1 Introduction of SALTFLOW

In order to evenly distribute and mix the applied sulfate water in both PHC source and plume for sufficient time (>40 days), the sulfate delivery must ensure the sulfate water penetrates through the total depth of the source and then flow laterally along with the plume.

In order to achieve the dosage objective, a numerical modeling tool was used to simulate the migration behavior of the applied sulfate water. Given the high sulfate concentration of applied water to be employed, density-dependent flow was considered. The model used in the experimental design was SALTFLOW developed by Molson and Frind (2013). This model is coded for modeling complex density-dependent flow and mass transport cases in one, two or three dimensions, based on equations for 3D saturated density-dependent groundwater flow and 3D advection-dispersion (Molson and Frind, 2013).

The density-dependent flux is derived from the Darcy equation for density-dependent flow (Molson and Frind, 2013; Bear, 1972) as given by:

$$q_i = -\frac{k_{ij}}{\mu}\left(\frac{\partial p}{\partial x_j} + \rho g \frac{\partial z}{\partial x_j}\right) \tag{2.1}$$

where q_i is the Darcy flux, k_{ij} is the permeability, μ is the dynamic viscosity, and ρ is the fluid density.

As pointed out by Frind (1982), the use of concentration in the Darcy equation gives more precise simulation than density. The main density-dependent flow constant γ considered in

SALTFLOW depends on the concentration of the target plume, which is expressed as (Molson and Frind, 2013):

$$\gamma = \frac{\rho_f + \alpha(C - C_f)}{1000} - 1 \qquad (2.2)$$

where ρ_f is the density of background groundwater (assumed 1000g/L), α is a dimensionless constant used to relate fluid density to salt concentration that equals to 0.7246 (Mohsen and Singh, 1990), C is the total dissolved solids (salts) (TDS) concentration, and C_f is the TDS in the background groundwater (assumed 500 mg/L).

The density constant γ related to density is given by:

$$\rho = \rho_0(1 + \gamma c) \qquad (2.3)$$

where ρ_0 is the reference fresh water density, γ is a constant defined in equation 2.3, and c is the relative concentration. Further details of SALTFLOW are provided by Molson and Frind (2013).

2.2.2 Model Domain

In the model, a 3D numerical grid was created to define the source and plume area in the API gate (Figure 2.3). The scale of the modeled aquifer is 25 m×12 m×3.65 m, and the number of nodes set in the model calculation is 100, 15 and 20 for the x-, y-, and z-axis, respectively, which provides 30,000 hexahedral brick elements. The x-axis is the direction of groundwater flow, the y-axis is horizontally perpendicular to x-axis, and the z-axis is the vertical direction.

Boundary conditions used for the model are listed in Table 2.2. Each boundary is labelled in Figure 2.3. Hydrogeological variables cited from previous studies (Mackay et al., 1986;

Sudicky et al., 1983, 1986; Linderfelt, 1994) are summarized in Table 2.3.

For the other design considerations, the model domain assumes a homogeneous aquifer, a constant water table at 0.5 mbgs, and evenly infiltrated sulfate water.

2.2.3 Modeling Processes

The process of modeling is inseparably interconnected to the experimental design, especially the consideration of sulfate flow. The goal for the design is to achieve at least 10% of initial sulfate concentration residing in the source zone after 40 days of the sulfate application. This minimizes the number of applications required.

Initially, solid-phase sulfate directly applied on the ground and dissolved passively by precipitation was considered as the dosage strategy. A model was constructed to simulate the migration of a high concentrated (35 g sulfate/L) sulfate plume created by this continuous infiltration (Figure 2.4). The result shows that although the concentration of sulfate in the source zone is still satisfactory after 100 days, only half of the source zone was covered by the sulfate plume. This did not fulfill the delivery requirements. Moreover, a pronounced sinking downgradient of the source caused by density-dependent flow can be observed. This would take the applied water and dissolved hydrocarbons below the existing monitoring network. Therefore, an application of water with dissolved sodium sulfate with a lower concentration was considered in the subsequent design.

To intensify the initial infiltration of sulfate water in the source zone, the application was then modified in two steps. The first step was to simulate flow with the constant water level mounding during the application. A new variable, the height of mounding water above the initial water table, was thereupon considered in the new simulations. The second step simulates the migration of sulfate in the subsurface after the infiltration has finished and the mound has collapsed.

The modeling results for a 35 g/L sulfate solution that maintained a pond level 0.6 m above the initial water table is given in Figure 2.5. This result indicates a better initial infiltration than solid-sulfate applied on the ground. However, the shape of the sulfate plume at Day 45 also suggests a very strong sinking due to density-dependent flow. The sinking

effect has the potential to bring the hydrocarbon plume into poorly monitored depths.

As a result of a series of modeling trials with different parameters, a 5 g/L sodium sulfate solution and an artificial pond with a constant level of 0.1 m above the ground (0.6 m above the initial water table) was selected for the first sulfate application (Figure 2.6). A total of 5 m^3 sulfate solution (25 kg of sodium sulfate) would be applied, as 5 cubic meters of 5 g/L sodium sulfate water.

2.3 Monitoring Wells

As described in Section 2.1, monitoring well fences Row 3 and Row 4 existed at the field site prior to the present experiment. They were used in PHC concentration and mass discharge sampling. To monitor the migration of PHC and sulfate at other than Row 3 and Row 4, three types of new monitoring wells were designed and installed, including 4-point multilevel suction lysimeters, 8-point Waterloo source multilevel monitors (Cherry and Johnson, 1982; Eniarson, 2006), and EC multilevels (Figure 2.7). All of these wells are of 24 mm diameter, 3 mm thick PVC pipes, with Teflon tubing attached and extending to the desired sampling depth.

Suction lysimeters were designed following Freitas and Barker (2008) to monitor shallow areas above and below the water table (varies from 0.4 to 0.9 mbgs) at Row 3 and Row 4, because the shallowest sampling point on the old monitoring wells is 1.5 mbgs. The 4 suction lysimeters are screened at 0.5, 0.75, 1 and 1.25 mbgs (L-D1 to L-D4, respectively), and the length of the lysimeter is about 1.5 m.

Source multilevel monitors were installed in the residual source zone to monitor the distribution and impact of applied sulfate water in that area. There are eight sampling points consisting of Teflon tubing with screens ranged from 0.5 to 4 mbgs with a 0.5 m interval (S-D1 to S-D8).

A total of 11 resistivity multilevels (labeled as EC- wells) were installed in the source, and at Row 3 and Row 4 (Figure 2.8). Two functions are assigned to resistivity multilevels: groundwater sampling and resistivity probe measurements. Six sampling points were created

with Teflon tubing terminating at depths that ranged from 0.5 to 5.5 mbgs with a 1 m interval. Electrical conductivity would be measured in water samples collected from these points, aiming to compare EC values with those detected by EC probes at the same depth. There are 11 EC probes attached on the EC multilevels, ranged from 0.5 to 5.5 mbgs with 0.5 m interval (EC-D1 to EC-D6). A brief description of the resistivity data-logger system and resistivity probe is in Section 2.4. Further details are given by Stevenson (2013).

The plan-view layout of all wells at the study site is shown in Figure 2.9. Multilevel suction lysimeters, source multilevel monitors and EC multilevels are prefixed R3-L- or R4-L, S-, and EC-, respectively.

2.4 Resistivity Data Logger System

2.4.1 Background

The monitoring of an applied reagent is a challenge due to the complexity of the subsurface, especially at highly heterogeneous sites. Although manually sampling from multi-level depths is an obvious strategy (Suthersan et al., 2011), it has shortcomings: labor intensity, cost, maintaining the quality of the sample during shipping, and technical difficulties in obtaining a representative sample. Therefore, taking advantage of in-situ monitoring of the applied sodium sulfate in real-time with low expense was essential for monitoring the progress and distribution of the sulfate plume in this study.

High concentrations of inorganic salts used in enhanced bioremediation (Na_2SO_4, in this case) and in situ chemical oxidation technologies means that electrical conductivity (EC) can be used as the signature of salt arrival and distribution (Stevenson, 2013). Although several commercial probes are able to monitor real-time EC in groundwater, their high cost and vulnerability to strong oxidants reduce their benefits in real-time monitoring (Stevenson, 2013).

In order to build a cost-effective and robust EC system for reagent flow and distribution monitoring, Stevenson elaborated the design and manufacture of self-made resistivity probes in his MASc. thesis (Stevenson, 2013). The resistivity probe measures relative resistivity that

can be related to the change of EC. After extensive lab tests and two field trials, his work demonstrated the practicability of the probe system (Stevenson, 2013). The present sulfate land application project represents the first application of this system in an actual field remedial demonstration. For this project, the resistivity probes and the data-logger system were modified, calibrated, and provided an excellent evaluation of the migration of the applied sulfate solution.

2.4.2 Resistivity Probes

Resistivity probes used in this project were slightly modified based on the design given by Stevenson (2013), in order to fit the needs of the current study, but their function and operation were not changed. The probe shown in Figure 2.9 is for the lab tests; the figure provides the appearance upon original manufacture. For the field model, 2/3 of the PVC pipe on the lab-probe was cut longitudinally and the remained measuring side (the side with metal wire) was attached to the EC well at designed depths (Figure 2.10). The lead extension of each probe was also fixed along the well by electrical tape and extended to the ground surface to be connected to the data logger system (Figure 2.10).

2.4.3 Data logger

The data logger consisted of three parts: battery, multiplexer and data logger (Figure 2.11).

The 12 V battery provides power for the data logger and multiplexer for 3-4 months.

The multiplexer is the part that receives the signal from multiple probes (32 in our case) and forwards them to the data logger. It is the intermediate device joining the resistivity probes and the data logger (Figure 2.11).

The data logger (Campbell Sci. CR 1000) takes the signal from the probes, usually via the multiplexer (Figure 2.11). CRBasic program code was sent to the data logger from a PC, which instructs the data logger to transfer and organize the signal from probes for

subsequently interpretation. The laptop and the CR 1000 data logger are connected by USB/RS 232 cable (Figure 2.12).

The desired data logger reading X can be described by formula 2.4.

$$X(-) = \frac{R_f}{R_f + R_s} \tag{2.4}$$

where R_f is a constant resistance in the data logger circuit and R_s is a variable resistance in the measured solutions. Therefore, X is a dimensionless value that reflects the relative magnitude of water resistance. X is read from the PC and, since R_f is a known value, the resistance in the solution can be calculated. By repeating the measurement for solutions of known EC, the groundwater EC relative to a standard is estimated.

EC is proportional to the distance between electrode plates (d), and inversely proportional to the resistivity (R) and the cross-sectional area of the plates (Stevenson, 2013), which is described as follows:

$$EC = \frac{1}{R}\left(\frac{d}{A}\right) \tag{2.5}$$

Based on equation 2.3 and 2.4, under the same circuitry, the higher the EC, indicated by lower R_s, the higher the data logger reading "X". The d and A terms in equation 2.5 indicate that the length of the lead connected to the data logger is also a variable affecting the X reading, while the cross-sectional area can be treated as a constant.

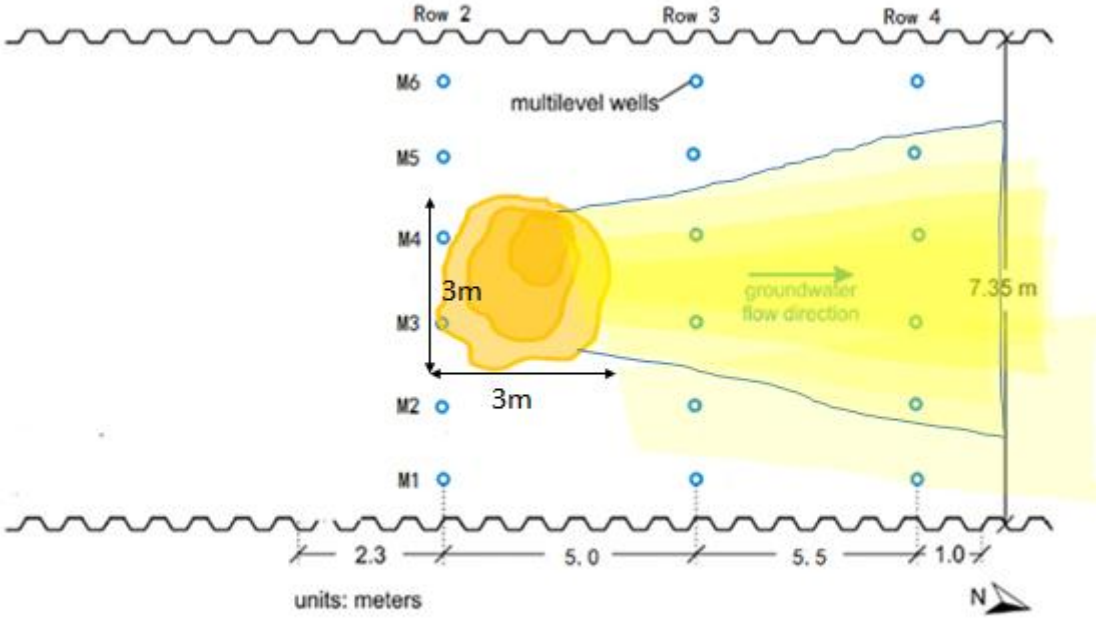

Figure 2.1: Plan-view layout of pre-existing monitoring wells, residual source, and hydrocarbon plume (Kovacik, 2013) in the API gate.

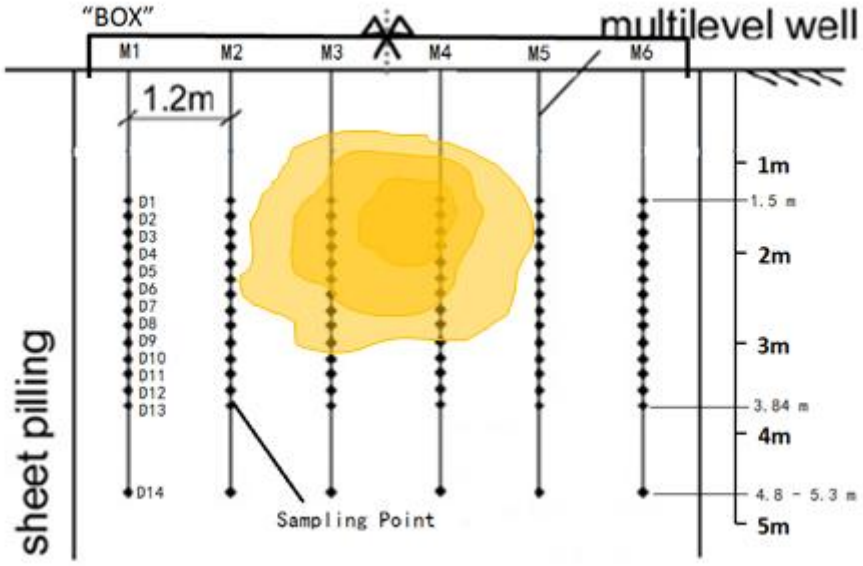

Figure 2.2: Cross-section of sampling point layout at Row 3 or Row 4 multilevel monitoring transects.

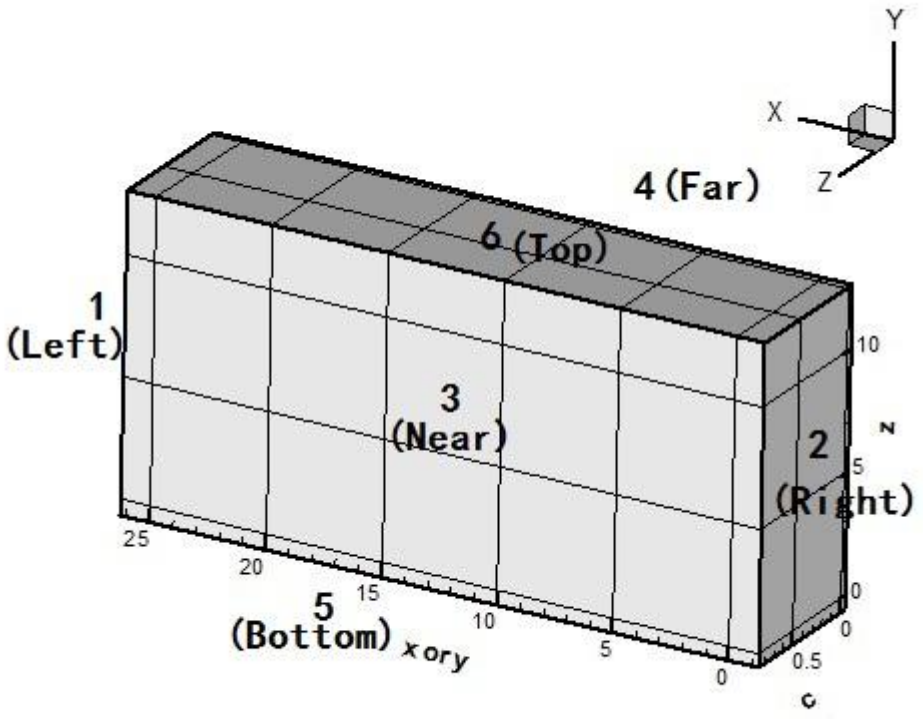

Figure 2.3: 3D grid model for API gate (Unit m). Each surface or boundary is described by a label and by a number.

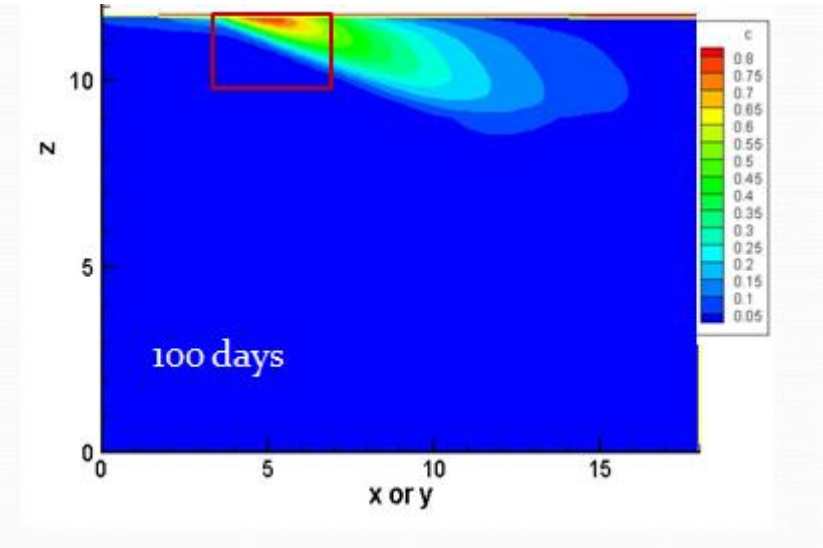

Figure 2.4: Modeling result simulates sulfate applied on surface above source zone and passively infiltrated by precipitation. Sulfate concentration = 35 g/L, time of continuous application = 100 days. The red rectangular represents the residual source zone. C is the relative concentration compared to the initial value ($c = C/C_0$).

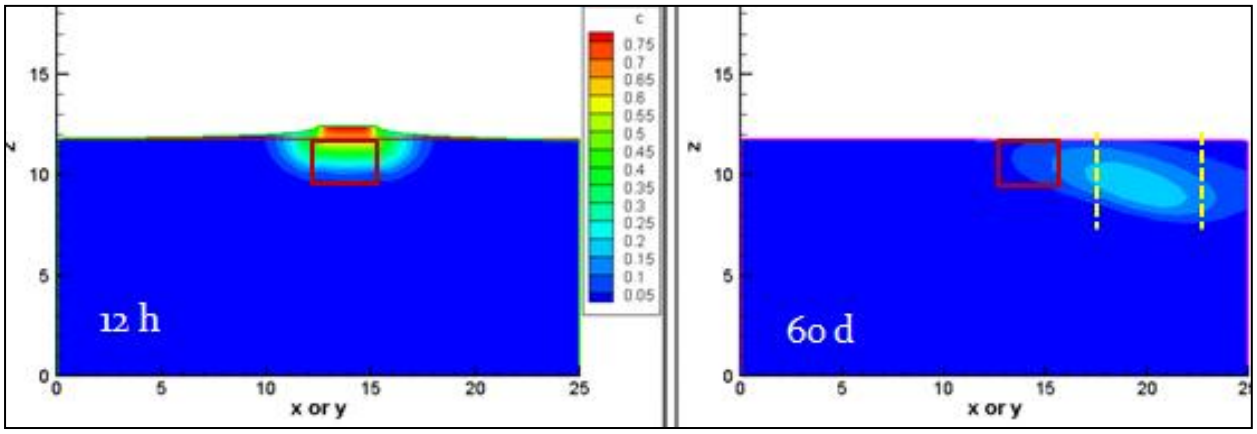

Figure 2.5: Two-step modeling result simulates sulfate water ponded above source zone at height of 0.6 m for 12 hours (Left) and its migration in the subsurface for 60 days. Initial sulfate concentration = 35 g/L. Red rectangular represents the residual hydrocarbon source zone and the yellow dashed lines show the approximately depth of monitoring wells at Row 3 and Row 4.

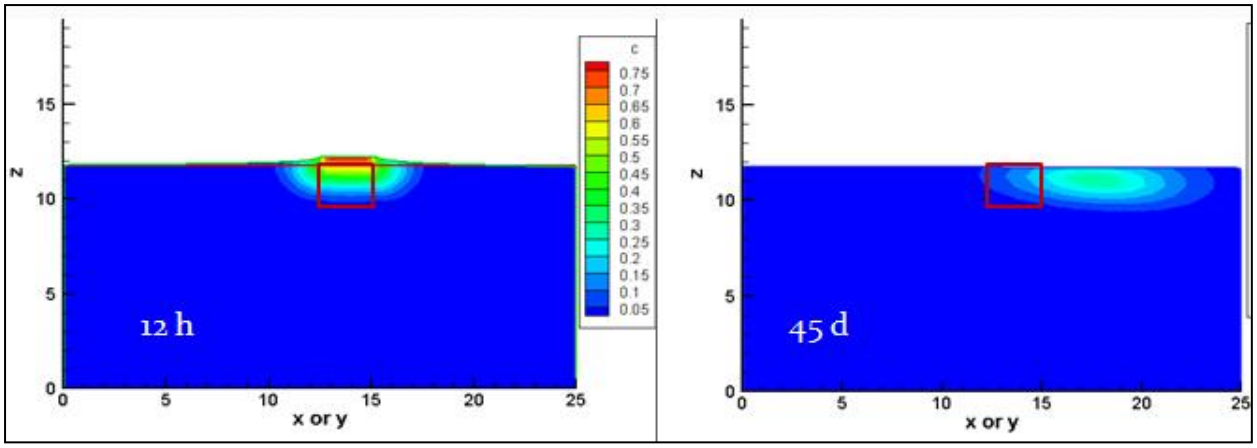

Figure 2.6: Two-step modeling result simulates sulfate ponded above source zone at height of 0.1 m. Sulfate concentration = 5 g/L, migration time = 45 days. Red rectangular represents the residual source zone.

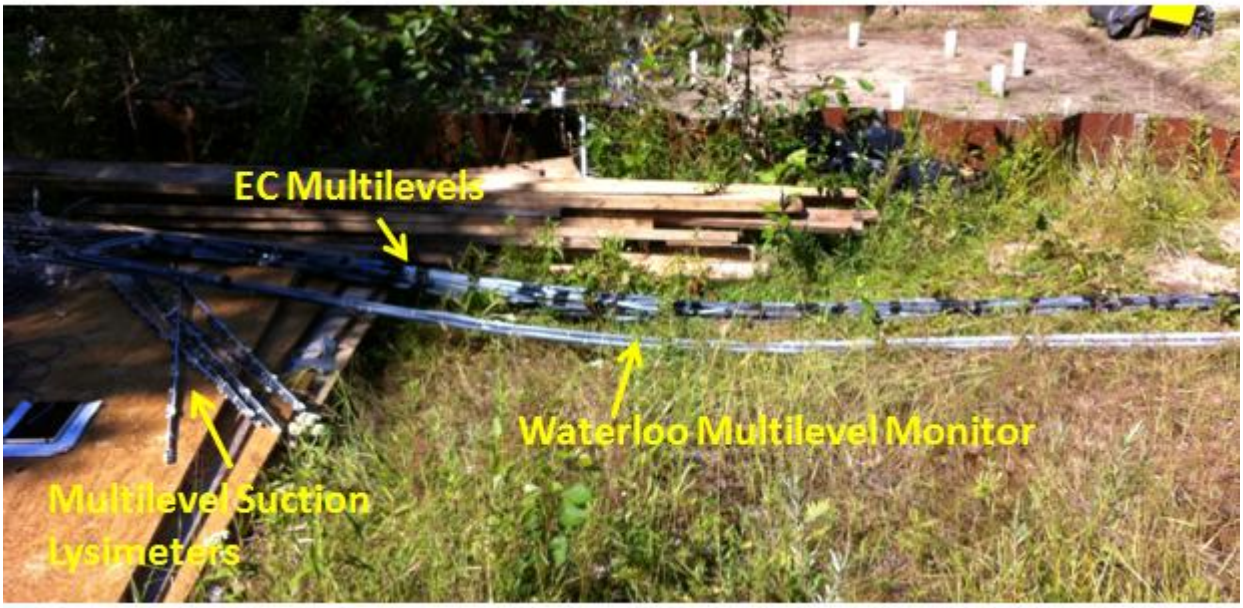

Figure 2.7: Different types of new monitoring wells for Borden sulfate land application.

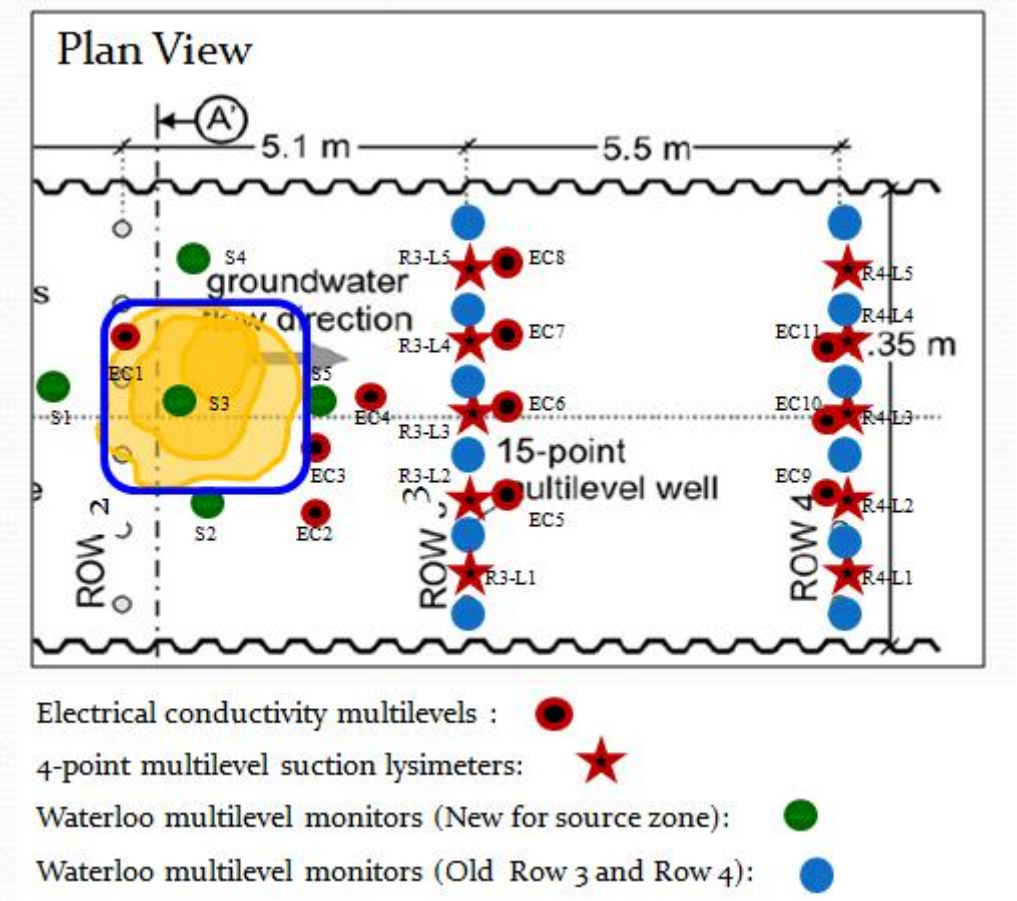

Figure 2.8: The plan-view layout of monitoring wells. Red black-dotted circles are EC multilevels, stars are multilevel suction lysimeters, green circles are Waterloo multilevel monitors and blue points are pre-existing multilevel wells.

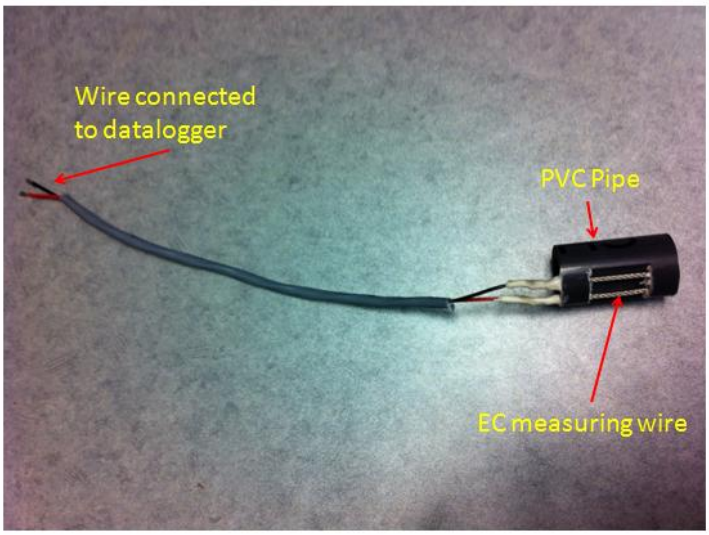

Figure 2.9: The resistivity probe used in the lab test, modified based on the design in Stevenson (2013)

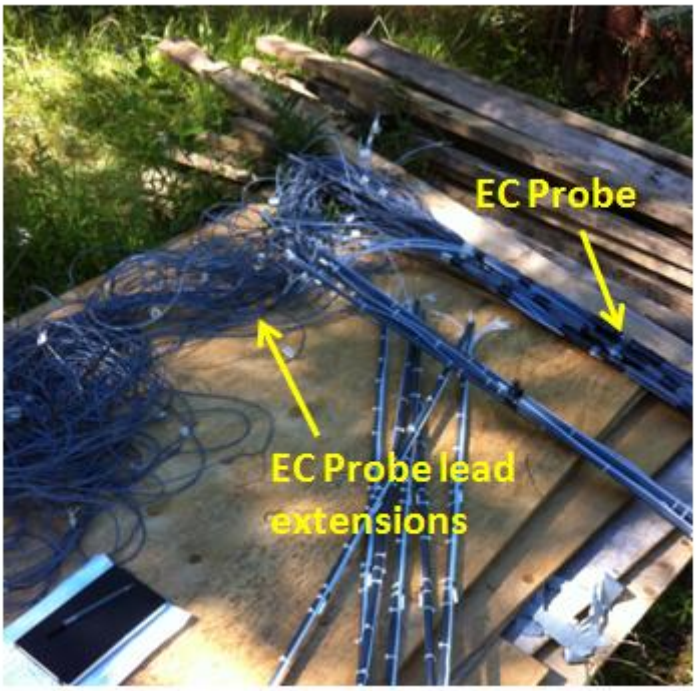

Figure 2.10: Field resistivity probes attached on the EC multilevel. Resistivity probe leads extend to the ground and connect to the data logger.

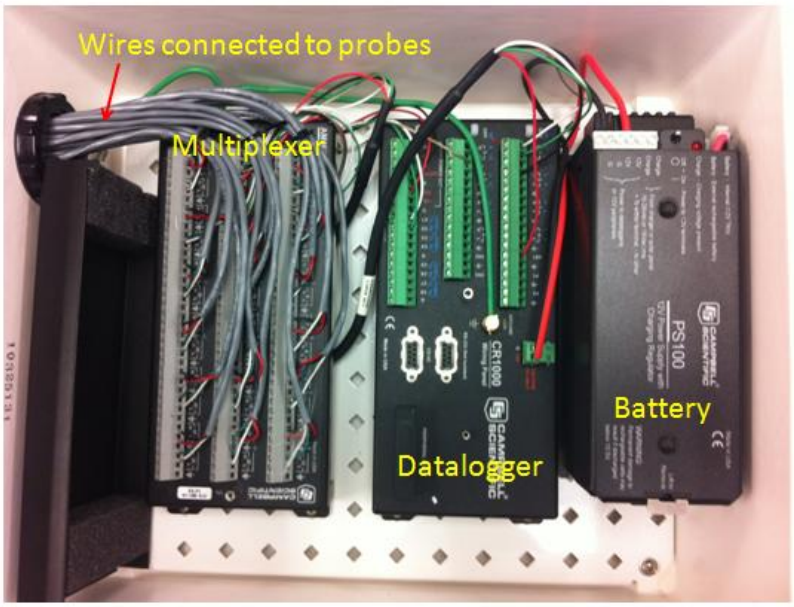

Figure 2.11: The interior of the data logger. The bundles of wires are input port for the multiplexer that connected to resistivity probe leads.

Figure 2.12: Data logger field data viewing. Field laptop and data logger connected by USB/RS 232 cable.

Table 2.1: Constituents of injected PHC NAPL

Compound	Volume (L)	Mass (kg)
2,2,4 Trimethanepentane	25	17.3
Isopentane	25	15.4
Cyclopentane	10	7.51
Octane	10	7.03
Benzene	2.5	2.19
Toluene	1.25	1.09
Naphthalene	1	1.14
o-Xylene	0.5	0.44
1-2-4 Trimethylbenzene	0.5	0.44
Methyl-tert-butyl-ether	0.25	0.19
Pentane	16	10.0
Hexane	20	13.1
TOTAL	**112**	**75.83**

Table 2.2: Boundary conditions

Face	Flow Condition	Mass Transport Condition
1	Fixed head	Zero concentration gradient
2	Fixed head	Zero concentration gradient
3	No-flow	Zero concentration gradient
4	No-flow	Zero concentration gradient
5	No-flow	Zero concentration gradient
6	Flux boundary	Cauchy mass flux

Table 2.3: Borden hydrogeological parameters used in SALTFLOW

Parameter	Value		Source
Porosity	0.33		Mackay et al., 1986
Hydraulic Conductivity	Horizontal	9.75×10^{-5} m/s	Sudicky, 1986
	Vertical	4.88×10^{-5} m/s	
Depth to Water Table	0.75 m		Measured in field, varied in season
Hydraulic Gradient	0.004		Linderfelt, 1994
Groundwater Velocity	0.09 m/day		Fraser, 2007
Dispersivity	Longitudinal horizontal 0.08		Sudicky et al., 1983
	Longitudinal vertical 0.01		
	Transversal horizontal 0.03		
Diffusion Coefficient	10^{-10} m^2/s		Sudicky et al., 1983

3. Methods

3.1 Monitoring Well Installations

All of wells were installed using a direct-push method, Geoprobe® model 7720DT (Figure 3.1). When the machine was in position, a 1.52 m (5 feet) long × 0.05 m OD Geoprobe casing was attached to the percussion drilling hammer, and the casing was directly pushed down into the sediment (Figure 3.1). After reaching the target depth, the well was inserted into the Geoprobe casing until it reached the bottom. Finally, the Geoprobe pulled the casing up as the sand collapsed around the well.

Drilling depth for suction lysimeters was 1.5 m (5 feet), for source multilevel monitor 4 m (13 feet), and for EC multilevels 5.5 m (18 feet). The field view of installed wells in the source area and Row 3 is shown in Figure 3.2.

3.2 Resistivity Data Logger Installation and Operation

The Data logger was set up at the field site prior to the first sulfate application, in order to test its feasibility (Figure 3.3). Quick connectors were used to connect leads between EC probes and the multiplexer in the data logger.

As simulated by SALTFOW, the designed sulfate water concentration for the first application of 5 g Na_2SO_4/L was expected to infiltrate to about 2 mbgs in the source zone and then flow laterally at about the same level (Figure 2.6). Therefore, the data logger was placed between the source area and Row 3 to collect data from probes placed from 0.5 mbgs to 3 mbgs (Figure 3.2). EC multilevels that were monitored include EC1 to EC7. The detailed list of connected EC probe is shown in Table 3.1.

“X” readings from each probe that connected to the data logger could either be viewed on the field laptop in real-time, or could be downloaded as a spreadsheet for further reference. The delay between each data logging was 100 milliseconds and the frequency of

measurement was every 2 minutes.

Field results recorded from the data logger and the process of data logger development will be discussed in chapter 4.

3.3 Sampling

3.3.1 Sampling Overview

Sampling basically can be classified into two categories: flux sampling and progress sampling. The purpose of flux sampling is to monitor the changes in mass discharge or mass flux of compounds and evaluate the attenuation of volatile organic compounds (VOCs), while the purpose of progress sampling is to monitor the migration of the applied sulfate and the potential biodegradation of hydrocarbons, especially by sulfate reduction. Flux sampling includes VOCs, sulfate, sulfide, and electrical conductivity; progress sampling includes VOCs, sulfate, sulfide, EC, pH, dissolved oxygen (DO), oxidation reduction potential (ORP, or Eh), ^{34}S-sulfate, ^{13}C-dissolved inorganic carbon (DIC), compound specific isotope analysis (CSIA) on BTEX, and biomarkers including genes encoding select reactions and metabolites characteristic of select reactions. The schedule for sampling events designed at the beginning of the project is given in table 3.2 and 3.3.

Sampling points for flux monitoring were selected to cover the areas at Row 3 and Row 4 where the bulk of the mass discharge was expected, based on previous sampling of the hydrocarbon plumes. Progress sampling points were selected depending on where the sulfate water was anticipated to flow through the source, Row 3 and Row 4. These points are mostly between 0.5 mbgs and 3 mbgs. All sampling points picked for flux and progress sampling are listed in Table 3.4 and 3.5, respectively. As the application continued, sampling points were adjusted depending on previous sampling results.

3.3.2 Field Sampling Methods

Groundwater samples were collected using a manifold sampler (Figure 3.4) and a

Cole-Parmer 7553-70 peristaltic pump with 6 mm OD (outside diameter) × 0.7 mm wall polyethylene tubing (Figure 3.5).

The manifold sampler is designed for 40 ml vials only. As shown in Figure 3.4, it can take samples from six different sampling points simultaneously. Each Teflon tube from the point to be sampled is carefully connected to the appropriate manifold input, and the outlet is connected to the peristaltic pump. The rate of pumping was controlled by the pump controller (Figure 3.5) to avoid generating bubbles during sampling. The desired pressure for sampling is about 10 kPa. The vacuum pressure was read from the barometer on the manifold, and the valves operated to apply and release the vacuum to the vial as required. The syringes on the manifold are designed for retaining purged water that is discarded after sampling.

Before taking a representative sample with the manifold, the first 40 ml of groundwater was discarded in order to purge the sampling tubing. Then, prepared vials contain sodium azide were tightened onto the manifold and pumping restarted. Since both bubbles and headspace may contain VOCs, causing a negative bias in subsequent VOC analyses, the former were minimized during sampling and, if necessary, the vial was filled with sampled groundwater drawn from the sampler tubing and syringe.

The Manifold sampler was not necessary for other types of samples; only the pump was required. The sampling tube was connected to the inlet of the pump and the outlet of the pump discharged water sample into containers. Bubbles and headspace also have to be minimized during this sampling. For the 60 glass bottle samples, a 0.45 μm filter was installed at the outlet tube to filter sediment in the groundwater. To sample the microbial MDNA in the groundwater a pre-sterilized, 0.22 μm screen Sterivex filter was attached to the outlet of the pump and 2.0 L of groundwater passed through. Alternately, if water flow was slow, the volume of water filtered was measured using a volumetric cylinder and recorded. Then, ties were required to secure tubing connections to prevent their bursting by the higher pressure.

3.3.3 Sample Preparation

In both flux and progress sampling, there were six types of samples collected in either a 40 ml glass vial, a 25 ml plastic bottle, a 60 ml glass bottle, a 500 ml amber bottle, 1L amber

bottle, or in a Sterivex filter (Figure 3.6). All samples were aqueous except for the Sterivex filter that retains filterable materials.

Groundwater samples for VOCs, methane, DIC, ^{2}H isotope, and ^{13}C-VOC isotope measurements were collected in 40 ml vials. 0.5 ml of 10% sodium azide was added to the vial for sterilization prior to lab analysis. The vials were finally capped with a Teflon coated septum and a plastic cap (Chen et al, 2008).

Aqueous groundwater samples for ^{13}C-DIC isotope analysis were collected in 60 ml transparent glass bottles to which 0.2 ml of saturated mercuric chloride solution was added for sterilization, and the bottle plugged with a rubber stopper.

Samples for metabolite measurements were collected in two 500 ml sterilized amber bottles. One was acidified to pH < 2, and the other was basified to pH > 8 after sampling.

Aqueous samples were taken immediately in 25 ml plastic bottles for sulfate and EC lab measurements, and in 1L amber bottles for ^{34}S isotope measurements. No additional preparations were required.

Other field measurements were made with instruments shown in Figure 3.7. Geochemical parameters DO, pH, ORP and temperature were measured using the YSI Professional Plus meter with flow-through cell. Although EC can also be measured with the YSI meter, it is more efficient to use the ATI/135 EC meter when EC was the only measurement. Sulfide concentrations were measured with the HACH portable DR/2400 spectrophotometer as per the included instructions (Hach Company, 2004).

3.3.4 Lab Measurements

Samples were shipped from the field to the University of Waterloo in the cooler. When they were stored in the lab, all aqueous samples were stored in a walk-in fridge at about 1 degree Celsius, and Sterivex filters are stored in a Thermal Scientific freezer at -80 degrees Celsius. When aqueous samples were shipped to external labs, they were put in a cooler with ice bags and CFC refrigerant, and Sterivex samples were shipped in a cooler full of dry ice.

For lab measurements, the sulfate concentrations were measured by sulfate ion chromatography ICS-2000 in the Illman Hydrogeology Laboratory at the University of

Waterloo. PHC concentrations were measured by gas chromatography at the Geochemistry Lab, University of Waterloo.

DIC concentration was measured in the Environmental Geochemistry Laboratory and stable isotopes, ^{2}H, ^{18}O, DIC-^{13}C, ^{18}O-SO_4, and ^{34}S-SO_4 were measured in the Environmental Isotope Laboratory, Department of Earth & Environmental Sciences, University of Waterloo. DIC concentration was analyzed after head space equilibration using a Varian 3800 gas chromatograph coupled with a CombiPal autosampler. The concentration of DIC in the original sample was calculated using standard gas laws taking into account changes in temperature and pressure between sample collection and analysis. Samples for DIC-^{13}C analysis were also prepared using a headspace equilibration technique and the resulting CO_2 analyzed using a HP 6890 series GC coupled with an Isochrome (Micromass UK) continuous flow isotope ratio mass spectrometer with ± 0.5‰ uncertainty. ^{2}H was analyzed using a Tekmar 3000 purge and trap system, with Aquatech 70 autosampler, coupled to a Trace Ultra GC and GC-Combustion Furnace III (Thermo) and Delta XL (Thermo Finnigan) continuous flow isotope ratio mass spectrometer (CFIRMS) with uncertainty of ± 5.0‰. Samples for SO_4 isotope measurement were pre-filtered and precipitated with barium bromide to form barium sulfate. Barium sulfate was washed with dilute hydrochloric acid to remove any carbonate, rinsed to neutral pH and freezedried. $BaSO_4$ samples were analyzed for ^{34}S using a 4010 Elemental Analyzer (Costech Instruments) coupled to a Isochrom (Micromass UK) continuous flow isotope ratio mass spectrometer (CFIRMS) (uncertainty of ± 0.3‰). ^{18}O-SO_4 analyses were conducted using a HEKAtech high temperature furnace and Eurovector Elemental Analyzer coupled to an Isoprime (GV Instruments) continuous flow isotope ratio mass spectrometer (CFIRMS) with an uncertainty of ± 0.4‰ (Clark and Fritz, 1997).

The CSIA-^{13}C for benzene, toluene, o-xylene and naphthalene was measured in the Centre for Hydrogeology and Geothermics at University of Neuchatel, and details of measurement method are described in Bouchard and Hunkeler (2014).

3.4 Land Application

As described in Section 2.2.3, a pond contained by a berm and wooden frame was built above the residual hydrocarbon source. A system for supplying groundwater to produce the sulfate solution, and a container to accommodate this water and to dissolve the sodium sulfate powder was required as supporting facilities. The conceptual diagram in Figure 3.8 shows the design for the sulfate application system.

Water was pumped from a groundwater well removed about 50 m from the API gate so that the pumping would not disturb groundwater flow in the gate (Figure 3.9). Pumped water was transported by 2.5 cm diameter rubber hose to the 3.79 m^3 (1000-US gallon) tank placed close to the pond.

The framing of the pond was built by nailing four, 3.25 m long, 0.15 m wide planks in a square and supporting them with soil berms (Figure 3.10). The surface in the pond area was slightly plowed after the construction to flatten and loosen the ground.

Figure 3.1: Geoprobe® 7720DT at Borden field. Another casing would be added to the top of the previous one as the pushing proceeded.

Figure 3.2: The field-view for installed wells.

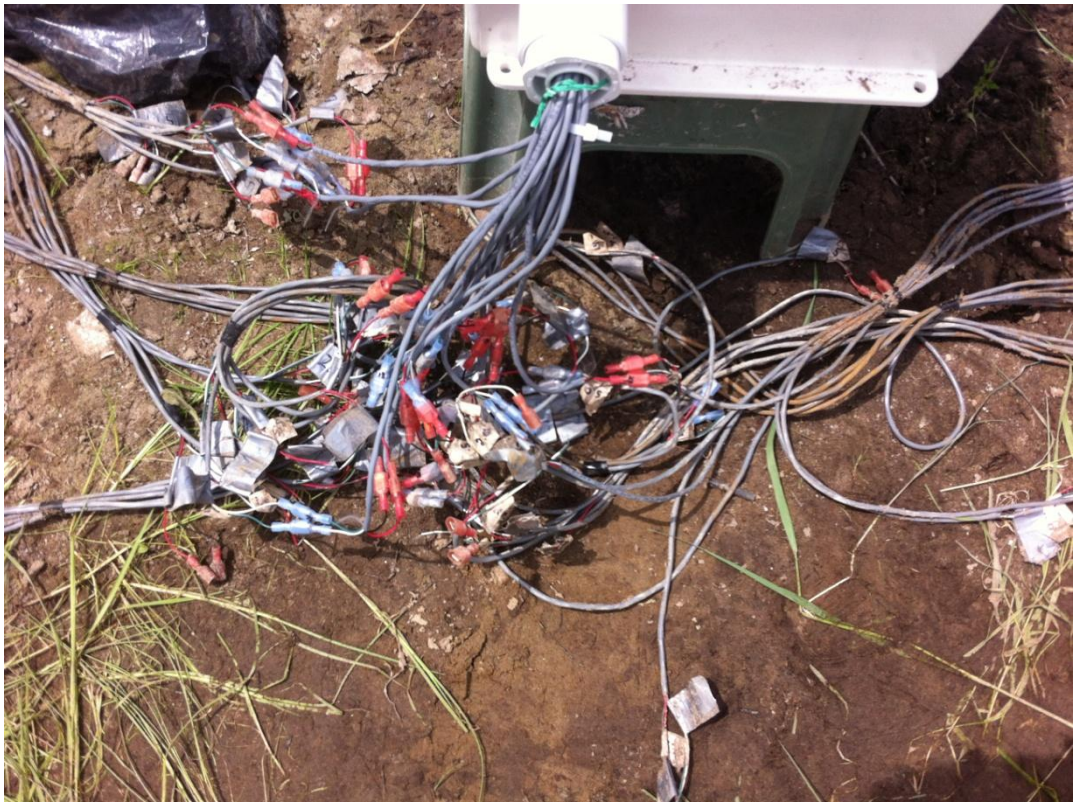

Figure 3.3: Connection between data logger and probe lead extensions at field.

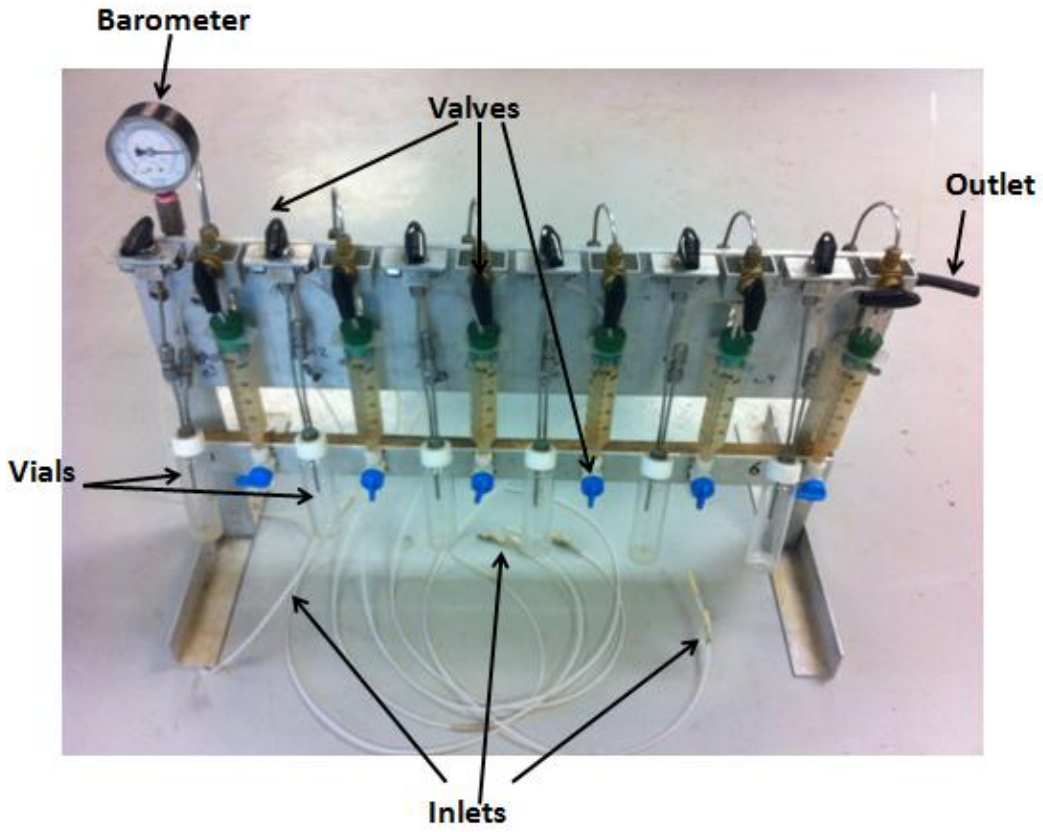

Figure 3.4: Manifold sampler.

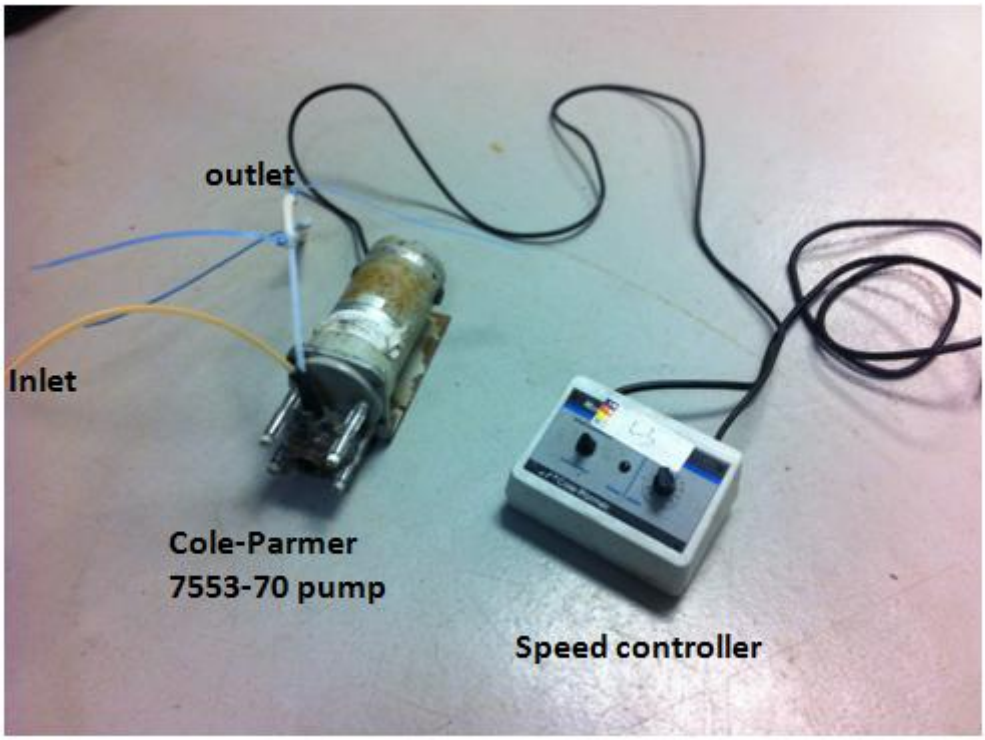

Figure 3.5: Cole-Parmer 7553-70 pump and controller.

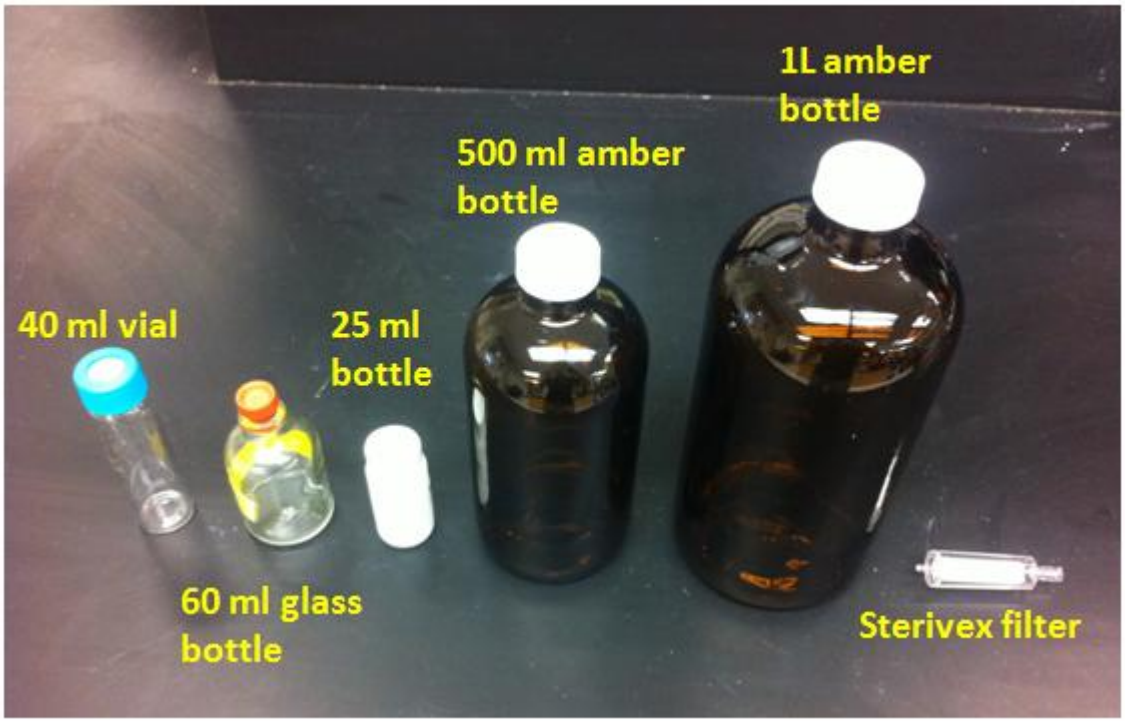

Figure 3.6: Sampling containers.

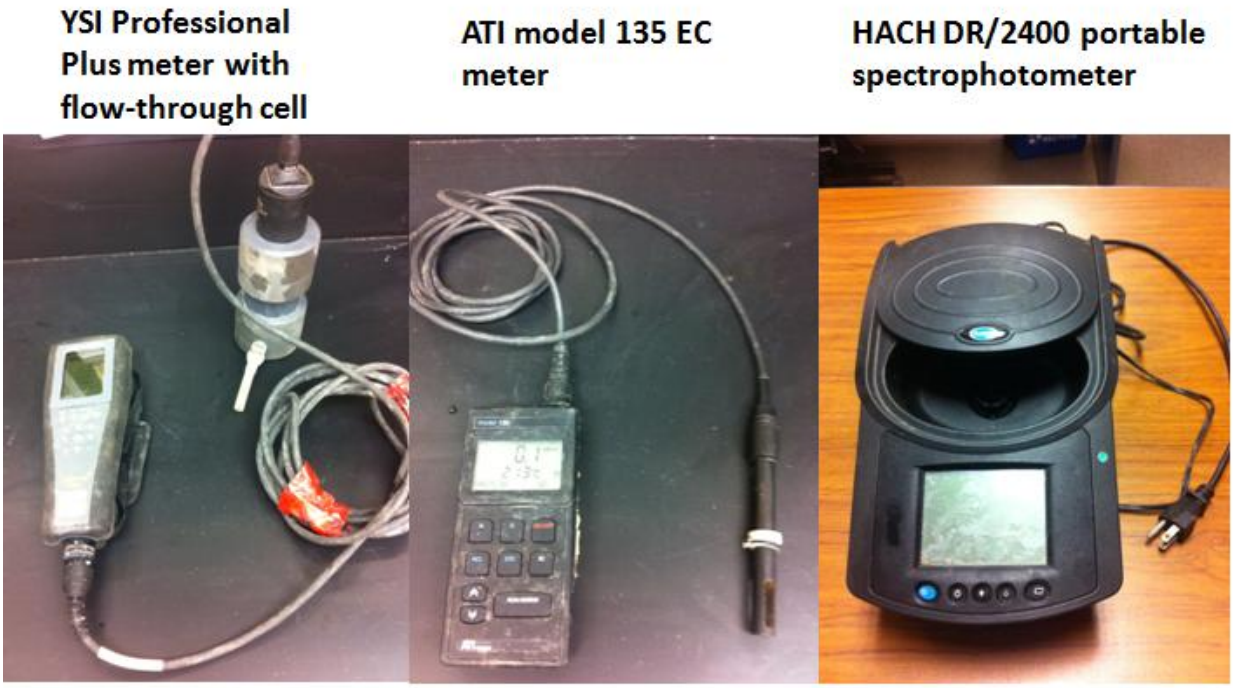

Figure 3.7: Field instruments for parameter measurement

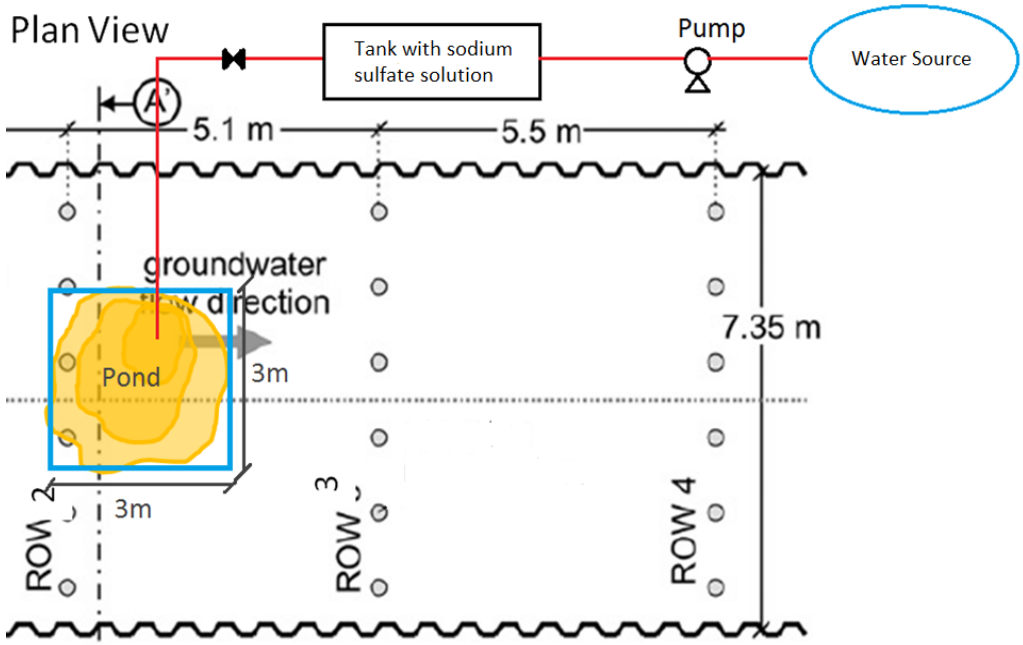

Figure 3.8: Conceptual design for the sulfate application.

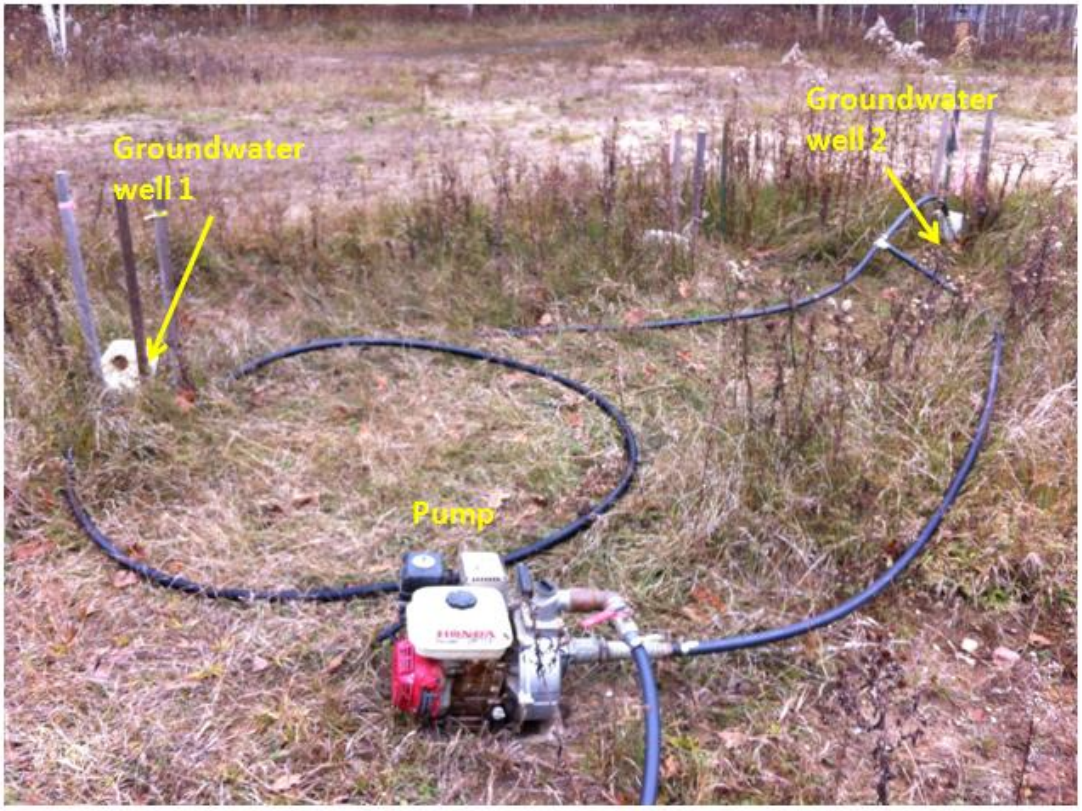

Figure 3.9: Groundwater wells and the pump.

Table 3.1: List of connected EC probes.

Input Port of Multiplexer	EC Probe Code	Depth of the Probe (mbgs)
1	EC1-D1	0.5
2	EC1-D2	1
3	EC1-D3	1.5
4	EC1-D4	2
5	EC1-D5	2.5
6	EC1-D6	3
7	EC2-D1	0.5
8	EC2-D2	1
9	EC2-D3	1.5
10	EC2-D4	2
11	EC2-D5	2.5
12	EC2-D6	3
13	EC3-D1	0.5
14	EC3-D2	1
15	EC3-D3	1.5
16	EC3-D4	2
17	EC3-D5	2.5
18	EC3-D6	3
19	EC4-D1	0.5
20	EC4-D2	1
21	EC4-D3	1.5
22	EC4-D4	2
23	EC4-D5	2.5
24	EC4-D6	3
25	EC5-D1	0.5
26	EC5-D3	1.5
27	EC5-D5	2.5
28	EC6-D1	0.5
29	EC6-D3	1.5
30	EC6-D5	2.5
31	EC7-D3	1.5
32	EC7-D5	2.5

Table 3.2: Flux sampling events schedule.

Flux monitoring, Row B & C: 3 x 3 = 9 cap fringe; 10 X 4 gw = 40 water samples

Weeks	VOCs	sulfate	sulfide	conductivity
0 - initial conditions/before application	100	100	16	98
15 weeks* Row 3 (after some sulfate flush)	52	52	8	52
40 weeks* Row 3	52	52	17	52
40 weeks* Row 4	48	49	3	48
Total samples	**252**	**252**	**44**	**252**

Table 3.3: Schedule for progress sampling events.

Week	VOCs	CSIA	sulfate	sulfide	O18, S34 sulfate	Sodium	conductivity	pH, DO	anions / cations	TDG/C13-DIC	Biomarkers - groundwater or core
-1 (flux, source + Row 3)	8	8	8	8	8		8	8		8	8
3 (Row 3)							36				
5 (Row 3)							60				
6 (source + Row 3)	8	8	8	8	8		8	8		8	8
7 (Row 4 only)	10	10	10	10	10		10	10		10	10
8 (source + Row 3)						80	80				
10 (source + Row 3)							40				
13 (source + Row 3)	8	8	8	8	8	4	75	8		8	8
33 (flux, Row 4)	20	20	20	20	20	95	20	20	6	20	
Total samples	**54**	**54**	**54**	**54**	**54**	**179**	**337**	**54**	**6**	**54**	**21**

Table 3.4: Sampling points selected for flux monitoring.

R3 Wells	Sampling points	Number of Points
M1	D1, D4, D8	
L1	D1, D3	
M2	D1, D2, D4, D6, D8, D10, D12	
L2	D1, D2, D3, D4	
M3	D1, D2, D3, D4, D5, D6, D7, D9, D11, D13	
L3	D1, D2, D3, D4	52
M4	D1, D2, D3, D4, D5, D6, D7, D9, D11, D13	
L4	D1, D2, D3, D4	
M5	D1, D3, D5, D8, D11	
L5	D1	
M6	D4, D10	
R4 Wells		
M1	D1, D4, D8	
L1	D1, D3	
M2	D1, D2, D4, D6, D8, D10, D12	
L2	D1, D2, D3, D4	
M3	D1, D2, D4, D5, D7, D9, D11, D13	
L3	D1, D2, D3, D4	48
M4	D1, D2, D4, D5, D7, D9, D11, D13	
L4	D1, D2, D3, D4	
M5	D1, D3, D5, D8, D11	
L5	D4	
M6	D4, D10	
	Total	**100**

Table 3.5: Sampling points selected for progress monitoring.

Source	Sampling points	Number of Points
S3	D2, D3	5
S5	D2, D3, D6	
Row 3		
R3-M3	D1, D3	5
R3-M4	D1, D3, D11	
Row4		
R4-M2	D13	
R4-M3	D1, D2, D5, D13	10
R4-M4	D1, D2, D3, D4, D14	
	Total	**20**

4. Result and Discussion

In this Borden sulfate land application project, three sulfate applications and sixteen sampling events were conducted as listed in Table 4.1. The day of first application on September 7, 2013 is set as Day 0. Before that date days are negative and after that days are positive. Sulfate applications were conducted on Days 0, 59 and 262.

Before each application, a calculated volume of water was pumped into the storage tank, and a specific amount of sodium sulfate and ammonium sulfate were added. As the capacity of the tank is 3780 L, while the total volume of sulfate water for each application is 5000 L, it required the preparation of the sulfate solution in two steps. Approximately 3500 L of groundwater was pumped into the tank on the preparation day, chemicals were added, and a submersible pump was put in the tank for stirring the solution overnight (Figure 4.1). The other 1500 L of sulfate water was recharged immediately when the space in the tank became available during the application on the next day (application day). The application was shut down briefly during the tank recharge.

When the sulfate water was well mixed, it was applied onto the bermed area creating ponding. The flow rate was controlled by a valve installed at the outlet of the tank to maintain a constant water level in the pond, and the water was infiltrated into the subsurface passively by the action of gravity (Figure 4.2). During the application, the position of the drainage outlet was changed every 20 minutes to evenly distribute sulfate water in the bermed pond. Water tables were measured around the pond, and ECs were also measured by the data logger at selected points in real-time. A summary of applications is shown in Table 4.2.

For sampling events, mass discharge sampling was conducted on Day -9, 86, 277 and 394; and progress sampling was conducted on Day -1, 44, 50, 103 and 233.

4.1 Sulfate Application and Migration

4.1.1 EC Manual Measurement

The main objective of this research activity is to monitor the track of sulfate water after the application. As the background EC of groundwater at the Borden site is very low (ranging from 280 to 400 microsiemens per centimeter, μS/cm) compared to the EC of applied sulfate water (6800, 23500, and 17700 uS/cm for three applications, respectively), EC was used as an semi-quantitative indicator of sulfate concentration. Therefore, a resistivity data logger system was designed for real-time groundwater monitoring of EC changes in the subsurface. However, due to various technical problems, the data logger system was not reliable in the first two applications, so EC measurements were only taken manually before the third application.

4.1.1.1 Application I

Groundwater was sampled with the manifold sampler (Figure 2.18) at sampling ports where sulfate was anticipated to pass through. Special focuses were given to monitoring fences Row 3 and Row 4. Sampling extended from the top sampling port of each well down until the point where EC values had declined to the background values. In order to facilitate discussion, EC results from the source area are listed in Tables 4.3 – 4.9 for reference, and those at Row 3 and Row 4 are contoured in cross-section views (Figures 4.3 – 4.8; selected monitoring points are provided in Appendix A).

The background EC values measured at Row 3 and Row 4 during the first mass discharge sampling on Day -9 are shown in Figure 4.3. EC values had a small range (300-400 μS/cm) prior to the sulfate application.

The EC of the first applied sulfate solution was around 6800 μS/cm. After the first application, ECs were measured at Day 10 and results are listed in Table 4.3. It appears that the bottom of the sulfate plume at that time was at approximately 1.5 mbgs, which is quite shallow compared to the maximum depth of PHC residual source (3 mbgs). No elevated EC values were detected at Row 3 at Day 10.

On Day 23, although ECs showed no change in infiltration depth (Table 4.4), elevated EC

obviously moved forward and was now detected at Row 3 (Figure 4.4). The depth of the sulfate plume at Row 3 was about 2 - 2.5 mbgs. This is slightly deeper than the elevated EC measured in the source, which suggests the sulfate plume had a slight downward flow component.

ECs on Day 37 shows that the majority of sulfate had left the source area; some moderate ECs were measured at the downgradient margin of the source area at S5 (Table 4.5). At Row 3, the distribution of elevated EC expanded both horizontally and vertically, compared to Day 23. The core of the EC contours also had higher values and extended over a larger area (Figure 4.5).

On Day 58, one day before the second application, scattered moderate ECs readings (1000 – 2000 μS/cm) were measured in the source area, mostly at 1.5 mbgs. These indicate the tail of the sulfate plume still remained in the source zone. The contour of EC at Row 3 for Day 58 is shown in Figure 4.6. The EC contours indicate that the sulfate concentrations at Row 3 generally increased and the plume sank further than on Day 37. No elevated EC was observed at Row 4 by Day 58.

4.1.1.2 Application II

The second application was conducted on December 5th, 2014 (Day 59). Because of the limited depth penetration in the first application, the density of the applied water was increased by adding 20 g sodium sulfate/L, four times higher than in first application, in order to enhance the sulfate infiltration depth in the source zone. The EC of this applied water was about 23500 μS/cm.

The first EC mapping was conducted on Day 68, 9 days after the second application. Results in Table 4.6 show that the infiltration depth of sulfate water increased to 2.5 mbgs, which is 1 meter deeper than the first application at the same measuring period. Based on the measurement from the well R3-M4 (Table 4.6), the core of the sulfate plume from the first application had already left Row 3, while the sulfate from the second application had not arrived. At Row 4, no high EC was measured indicating no significant sulfate arrival at day 68.

The next EC mapping was conducted on Day 86, 27 days after the second application. The infiltration depth of sulfate was similar to Day 68, while EC values in the source area were significantly reduced, indicating the main body of the sulfate plume had already left the source zone (Table 4.7). As suggested by the EC measurements, sulfate from the second application had arrived at Row 3 on Day 86. ECs at R3-M1 and R3-M6 were not measured due to cold winter conditions. The enhanced EC values spread deeper than those from application one, showing that the sinking was increased with a more concentrated sulfate water (Figure 4.7). Values of ECs were much lower than those measured in the source area on Day 68; suggesting that only the dispersed front of the sulfate plume arrived at Row 3 on Day 86. No elevated EC was found at Row 4.

The last EC mapping in 2013 was done on Day 103. Samples could not be collected from most of the source area because of snow accumulation. ECs were only measured at well EC2 at the downgradient corner of the pond (Figure 2.8). Sulfate had infiltrated deeper than 3.5 mbgs here (Table 4.8). At Row 3, ECs at wells R3-M1, R3-M6 and lysimeters were also not measured because of freezing. Results from the other four wells were contoured in Figure 3.6. Elevated ECs spread across almost the entire Row 3, likely even below the monitored depth (~5 mbgs). This illustrates that the dense sulfate plume probably sank below the design monitoring depth.

No EC was measured through the winter. Another measurement was conducted before the third application on Day 197 on March 23, 2014. Results in Table 4.9 indicate that only scattered and low EC remained in the source and at Row 3. At Row 4, EC values higher than baseline measurements (~300 uS/cm) were found at every depth. ECs at depth were higher than at shallow points, indicating the core of sulfate plume had migrated downward. Since the highest EC was measured in the deepest monitoring point, it is difficult to determine the maximum depth of the sulfate core from Application II, but it extends deeper than 5 mbgs. These results also suggest that the movement of the core of sulfate trended downward from Row 3 to Row 4 (Table 4.9).

4.1.1.3 Application III

The third sulfate application was conducted on Day 262 (June 11th, 2014). The concentration of applied sodium sulfate water was 15 g/L to avoid a strong density-dependent flow that may have happened in the second application. The EC of the applied sulfate water was about 18000 uS/cm.

The EC data logger system was fixed before the third application and so resistivity coefficient reflects the magnitude of ECs was measured in real time with the data logger after the third application. Results for the data logger measurements are discussed in detail in the following section.

4.1.2 Resistivity Data Logger System Measurement

The background EC of groundwater at the site ranged from 280 to 560 μS/cm, and EC of the applied sulfate water ranged from 6.8 to 23.5 mS/cm at room temperature in the lab. So, the resistivity data logger system was required to span most of this range with significant accuracy (±5%，Stevenson, 2013) to adequately monitor the migration and dispersion of the applied sulfate solution.

However, at the initial stage of EC monitoring, the data was incomprehensible and so several adjustments were made successively as described in Appendix B.

The repaired data logger was installed in the field and tested prior to the third application. Readings from the data logger were compared with meter-measured ECs at the same sampling points on EC wells, and they were plotted as shown on Figure 4.9. Their relationship indicates that the data logger reading and field-measured EC were correlated. It should be noted that for the selected resistor setting, it was difficult to distinguish EC values when they are larger than 8 mS/cm. Readings ("X") range only from 0.75 to 0.83 when solution ECs are between 8 to 18 mS/cm. It is possible to develop a data logger system that provides precise reading in a desired range, but it is at the cost of the precision at other ranges.

Resistivity data were monitored at selected points at real time from the beginning of the third application (Day 262) to 78 days after the third application (Day 335). Plots for

representative datalogger readings are shown in Figure 4.10 a-c. Plots show the data logger readings at well EC1, EC2 and EC5, respectively. These three wells represent the source zone, downgradient of the source zone and at monitoring fence Row 3 (see Figure 2.8). Figure 3.11 (a) shows results for EC1, which is the only EC well located in the ponding area and is in the upgradient/west quadrant of the pond. During the sulfate application, the shallowest monitoring point at 0.5 mbgs detected the arrival of sulfate within 30 minutes (Figure 4.10 a). The data logger reading increased sharply and reached a plateau, indicating the arrival of sulfate water. The plateau value was about 0.8, and the EC measured by meter was about 17 mS/cm. Then, the reading decreased over time, illustrating the migration and eventual departure of the sulfate plume. At about 12 hours, sulfate water arrived at EC1-D2 and the EC was measured as 15 mS/cm. Sulfate water arrived at EC1-D3 about 2 days after the application. The estimated apparent vertical groundwater velocity by Darcy's Law is 0.64 m/day ($K_z = 4.88\times10^{-5}$ m/s, n = 0.33, Table 2.3; $i = \Delta h/\Delta l = -0.05$), which is consistent with data logger measurement of ~ 0.75 m/day. No elevated resistivity data was detected at points lower than D3 (1.5 mbgs). Sulfate left the monitoring points 1 and 1.5 mbgs at EC1 in less than 30 days, while sodium sulfate remaining at 0.5 mbgs provided continuous elevated data logger values to the end of the monitoring period (Day 355).

Figure 4.10 (b) shows results from EC2, which is located outside of a downgradient corner of the pond (see Figure 2.8). It shows the first arrival of sulfate water at EC2-D1 was about 8 hours after the application. EC was measured as 17 mS/cm at that time. Sulfate water arrived at D2 and D3 of EC2 in one day.

Unlike at EC1, the sodium sulfate plume was detected up to 3 mbgs at EC 2. It indicates the sulfate infiltration downgradient of the source zone is deeper than directly under the application pond. This was anticipated in the numerical modeling (Figure 2.4 and 2.5). The longevity of the sodium sulfate in the source zone at 1.5 mbgs is >70 day and so meets the design requirements. However, sodium sulfate residence time was less than 40 days at other depths and that is less than the design.

Results from EC 5, immediately downgradient of Row 3, are shown in Figure 4.10 (c). Only the probe at 2.5 mbgs detected the arrival of the applied sulfate. No sulfate was observed at 0.5 and 1.5 mbgs for the whole monitoring period. This suggests the sinking of

the sulfate plume. Overall, the EC probe results show that at EC 1, no applied sulfate lower than 2 mbgs; at EC 2, all probes from 0.5 to 3 mbgs found the applied sulfate; while at EC 5, no applied sulfate was found at shallow depths, but only at deeper depths. This set of result suggests that at a concentration of 15 g sodium sulfate per liter, the sulfate plume has a downward trajectory.

4.1.3 Comparison between SALTFLOW and Actual Sulfate Migration

Based on the field monitoring and SALTFLOW modeling results from each application, a comparison of sulfate migration pathways between modeling and field results can be made (Figure 4.11 A-C). SALTFLOW precisely predicted the sulfate transport in the first and third applications, but it underestimated the sinking effect of the sulfate plume in the second application.

The complexity of flow and heterogeneity of the aquifer can be observed in Figure 4.8. Figure 4.8 shows that elevated EC were measured at the bottom of all Row 3 wells, while some baseline EC were found in the at middle depth at R3-M2, R3-M4 and R3-M5. It suggests the sulfate solution flowed through some preferential pathway to depth in the source area, before the horizontal transport in the upper plume took the high EC water to the upper points in Row 3. The high density of the second applied solution may have facilitated this rapid migration to depth.

Although the SALTFLOW simulation in the second application did not match the deeper migration of the sulfate plume, it is still a useful tool to predict the salt flow in future land applications, especially when the model can be conditioned for the porous media properties.

4.1.4 Water Table Fluctuation during Sulfate Application

The fluctuation of the water table during and after each sulfate application was also monitored manually. The purpose of this monitoring was to evaluate the distribution of applied sulfate solution around the application area.

Existing wells (76.2 mm OD, 2 m deep, screened 1.5 to 2 mbgs; Kovacik, 2013) were

used as water table monitoring wells and their layout is shown in Figure 4.11. One monitoring well was assigned to each side of the pond at slightly different distance from the pond boundary.

Water table elevations were measured occasionally only at MW4 during the first application. Results (Table 4.10) indicate that the water table at 0.5 m downgradient of the pond increased 6 cm after the first application and stabilized within 40 min. However, results from the first application are not detailed enough to define the water table change in the first 30 minutes and beyond 5 hours of the application. The total infiltration time was about 12 hours in the first application, consistent with the modeling result.

More data were collected during the second application at all four monitoring wells (Table 4.11). Results show that the water table around the ponding area increased rapidly in the first 20 minutes of application and the rate slowed after that. Twenty-four hours after the application began, although no water remained in the pond, the water table at each monitoring well had not returned to the original level, indicating the water table was still mounded in the source area and infiltration of sulfate water was on going. Therefore, the actual infiltration time (18 h) is significantly larger than modeling result (12 h).

In the third application, the initial water table was higher than in the first two applications, because of the snow melting and high recharge in the spring. Results in Table 4.12 show that the fluctuations of the water table are also lower than previous. The mounded water table was again stable in less than one hour. Due to the high water table, it required twice as long to infiltrate the third application (~24h), so no water table levels were measured for the recovery period.

4. 2 Mass Discharge Monitoring

Sampling to define the mass discharge of sulfate and PHCs through Row 3 and Row 4 were taken on Days -9, 86, 277 and 394. EC was also measured, but it has already been presented in the previous section that depicted the migration of the applied sodium sulfate solutions. This section presents results of the distribution of sulfate at Row 3 and Row 4, and

partly reveals the stimulation of SRB based on sulfide formation as well as the apparent attenuation of BTX.

4.2.1 Sulfate

The first sulfate sampling of Rows 3 and 4 on Day -9 was the baseline sampling that defined the background concentrations. The baseline for sulfate is shown in Figure 4.12. Sulfate generally ranged from 2 to 10 mg/L before the application. The sulfate concentration is relatively high at the bottom of Row 3, while it is relatively high at the top of Row 4.

On Day 58, sulfate was sampled where EC was larger than 350 μS/cm. The purpose was to establish a correlation between them. The curve in Figure 4.13 shows that EC is linearly correlated with sulfate concentration (correlation coefficient R^2 = 0.8625), which demonstrated that the use of EC as an indicator for the sulfate arrival is reasonable. However, since sulfate could undergo biological sulfate reduction and both sodium and sulfate contribute to EC, defining the sulfate concentration via EC measurements throughout the experiment was deemed inappropriate.

The second sulfate sampling was taken on Day 86, 27 days after the second application. The distribution of sulfate at Row 3, showed in Figure 4.14, is very similar to the EC distribution in Figure 4.7, which confirms the observations based on EC. Sodium sulfate from the second application sank deeply by Day 86, and more of the sulfate flows through the east side of the monitoring fence rather than the west side (Figure 4.14).

Results at Row 3 for the third sulfate sampling on Day 277, 15 days after the third application, are shown in Figure 4.15. The arrival of the third sulfate plume was also indicated in the resistivity data logger monitoring result (Figure 4.10). The arrival of sulfate was earlier than expected, yielding an apparent groundwater velocity of 14 cm/day, faster than the velocity of 9 cm/day given by Fraser (2007). This likely reflects the higher gradient induced by mounding in the pond area. The apparent groundwater velocity during mounding as estimated by Darcy's Law is about 25 cm/day ($K_x = 9.75\times10^{-5}$ m/s, n = 0.33, Table 2.3; $\Delta x/\Delta l = -0.01$), which is even faster than field observation. At Row 4, the shallow depths had no sulfate flow, while with the highest concentrations found at about 3 mbgs. This is more

evidence that the sulfate plume had a significant vertical flow component when the salt concentration was high.

4.2.2 Hydrocarbons

4.2.2.1 Residual NAPL and Initial Mass Discharge

As discussed in Section 1.4, about 110 L of PHCs were emplaced at Borden site in August 13, 2012 (Day -390) as the source. The NAPL distribution was characterized by a ultra-violet optical scanning tool (UVOST) on August 15, 2012 (Day -388) (Kovacik, 2013). UVOST recorded photo emission data by laser induced fluorescence along 13 boreholes (Figure 4.16) to examine the presence of the NAPL (Kovacik, 2013). The UVOST logs are provided in Appendix C.

Based on the UVOST results, the dimension and relative concentration of NAPL are depicted in Figure 4.17 a and b.

Two sampling events examined the PHC concentrations at Row 3 on September 6, 2012 (Day -366) and November 6, 2012 (Day -305) (Kovacik, 2013, data are shown in Appendix D). Mass discharge for selected compounds at Row 3 then can be computed according to these data and they will be considered as pre-sulfate application PHC mass discharge from the source.

Mass discharge (MT^{-1}) can be expressed by Equation 4.1 (ITRC, 2010):

$$M = \int_A J \, dA \tag{4.1}$$

where J ($ML^{-2}T^{-1}$) is mass flux which equals the Darcy flux q (LT^{-1}) times flux sampling concentration C (ML^{-3}). dA is the representative area of each sampling point. Darcy flux q is the product of groundwater velocity (LT^{-1}) and porosity (-), which is 0.09 × 0.33 = 0.03 at Borden (Fraser, 2007). Therefore, Formula 3.1 can also be written as:

$$M = \int_A 0.03C \, dA \tag{4.2}$$

The boundary of the representative area (dA) of a sampling point is set half way to the adjacent point, and the boundary of NAPL projection at Row 3 is also considered. The representative area block setting for the sampling points in Kovacik 2013 is shown in Figure 4.18. Only results from four compounds are illustrated here: benzene, toluene, o-xylene and naphthalene (BTXN). Based on the block setting in Figure 3.16, the mass discharges for BTXN on Day -366 are 2.75 ± 0.82, 0.394 ± 0.12, 0.045 ± 0.01 and 0 g/day, respectively. They are 6.52 ± 1.96, 1.0 ± 0.3, 0.13 ± 0.04 and 0.163 ± 0.05 g/day on Day -305. Uncertainty for mass discharge is estimated based on the calculation of relative standard deviation by Beland-Pelletier et al. (2011). It is about 30% for our sampling density of 2.2 points/m^2 and the same uncertainty will be carried through the following mass discharge calculation.

4.2.2.2 PHC Mass Discharge Monitoring Results, Sulfate Application Phase

The PHC concentration contours at Row 3 and Row 4 on Day -9 are shown in Figure 4.19. The plumes for BTXN were well developed at both monitoring fences since the NAPL was emplaced one year previously. Sampling points are shown as red dots in Figure 4.19 and following figures, and the representative area boundary for each point is set as halfway to the next point. At Row 3, the mass discharges for BTXN are 0.72 ± 0.22, 0.56 ± 0.17, 0.09 ± 0.03, and 0.59 ± 0.18 g/day, respectively, and they are 2.21 ± 0.66, 0.67 ± 0.2, 0.15 ± 0.04 and 0.37 ± 0.11 g/day at Row 4.

When the applied sodium sulfate solution flowed through the hydrocarbon source, two conceptual models should be considered. The first model is that the applied water dissolved PHCs the same as the groundwater (i.e. at the dissolution equilibrium). The second model assumes the applied sulfate solution passed the PHC source zone rapidly due to mounding and density-dependent flow so that PHC dissolution did not reach equilibrium. For the first conceptual model, the PHC concentration monitored downgradient is not affected by the applied solution. However, for the second model, PHC concentration in the downgradient sample could be diluted and, in the following, it is assumed that the applied water dissolves no PHCs as it moves through the source NAPL. This is one conceptual extreme; the other is that the groundwater leaving the source has attained aqueous concentrations in equilibrium

with residual NAPL.

To evaluate the dilution effect, EC was used to estimate the dilution effect and "correct" the hydrocarbon concentrations. The dilution coefficient D_c is defined as:

$$D_c = \frac{EC_i - EC_0}{EC_{measured} - EC_0} \quad (4.3)$$

where EC_i is the EC of the applied sodium sulfate solution, EC_0 is the baseline EC (use 300 μS/cm), and $EC_{measured}$ is field-measured EC. D_c represents the fraction of pre-existing groundwater which has been diluted by the applied water.

Then, the diluted hydrocarbon concentration can be corrected as:

$$C = \frac{C_{measu}}{D_c} \quad (4.4)$$

where C is the corrected hydrocarbon concentration excluding the dilution effect and $C_{meaured}$ is the measured hydrocarbon concentration at Row 3 and Row 4.

Therefore, in the following discussion of the PHC mass discharge results, dilution effect (corrected results) will be considered, with the presented PHC concentrations will be corrected by using Formula 4.3 and 4.4. Meanwhile, non-corrected PHC results are also provided for comparison and discussion. When calculating hydrocarbon mass discharge, those points which have non-detected PHC concentrations are consider to be diluted to concentrations lower than lab detection limit. So, instead of 0 μg/L, about ½ the method detection limit, 0.5 μg/L, was used in the mass flux calculation at those points.

On Day 86, only Row 3 was sampled as sulfate was still not present at Row 4. As the sodium sulfate water from the second application also arrived at Row 3 on Day 86, dilution from both the first and the second application were considered. Based on SALTFLOW modeling and advection calculations, a 50%/50% dilution from each application is reasonable and provided EC_{12} = (50%×6800) + (50%×23500) = 15150 μS/cm. The hydrocarbon concentration contours are shown in Figure 4.20. The dilution corrected mass discharge for

BTXN on Day 86 are 0.23 ± 0.07, 0.10 ± 0.03, 0.03 ± 0.01 and 0.49 ± 0.15g/day, respectively.

For the PHC flux sampling on Day 277, contours for PHC concentrations are shown in Figure 4.21. The sodium sulfate water from the third application just arrived at Row 3. So, at Row 3, only the dilution from the third application is considered in the correction of PHC results; for Day 277 dilution at Row 4 is estimated 50%/50% from the first two sulfate applications. In this case, EC_3 = 18000 uS/cm and EC_{12} = 15150 μS/cm. A significant reduction of mass discharge for benzene (0.03 ± 0.008 g/day) was observed. However, mass discharge for toluene and o-xylene (0.27 ± 0.08 and 0.1 ± 0.03 g/day) were even higher than that from Day 86. Naphthalene still showed little change (0.56 ± 0.17 g/day). At Row 4, all BTX mass fluxes were reduced significantly (0.1 ± 0.03, 0.01 ± 0.003 and 0.017 ± 0.005 g/day), while naphthalene showed no change from pre-application results (0.394 ± 0.12 g/day).

At the end of the monitoring period on Day 394, only dilution by the third application at both Row 3 and Row 4 is considered. Significant decrease of benzene, toluene and o-xylene mass discharge was observed at both Row 3 (0.02 ± 0.005, 0.06 ± 0.02 and 0.02 ± 0.007 g/day) and Row 4 (0.016 ± 0.005, ~0, ~0 g/day) (Figure 4.22). Toluene and xylene were highly attenuated compared to results from Day 277, especially at Row 4, where no toluene and xylene was detected. Naphthalene did not show apparent attenuation during the whole flux sampling period. The overall mass discharge results are summarized in Table 4.15 and plotted in Figure 4.24. Both corrected and non-corrected mass discharges are shown, as the actual mass discharge should be between these two value sets.

4.2.2.3 Source Depletion and Natural Attenuation

While dilution of groundwater by applied sulfate water should be considered, PHC concentrations emanating from the NAPL will naturally decline over time as these components become depleted in the NAPL. So, the reduction of PHC concentrations and mass discharge due to the depletion of these components in the NAPL during the 782 days since the source emplacement is also considered using a Raoult's Law model developed by

Fraser (2007). Essentially, the groundwater within the source area is assumed to equilibrate with the bulk NAPL in accordance with Raoult's law:

$$C_i^{sat} = x_{i-NAPL} C^{sat}_w \quad (4.5)$$

where C_i^{sat} is the concentration of i in equilibrium with a NAPL containing a mole fraction of i, x_{i-NAPL} and C^{sat}_w is the reported solubility of pure i (Fraser, 2007). Water is removed from the source area, the remaining masses of PHCs in the NAPL are recalculated, and the next batch of groundwater moving into the source area is equilibrated with the new NAPL. This continuing process is incorporated into a spread sheet which provides the mass discharge of each PHC over time.

The predicted mass discharge relative to the initial value (M/M_0) over time using this Raoult's Law model is shown for BTXN in Figure 4.23. M_0 is the initial PHC mass discharge during the first modeling time step divided by 33, the number of days in the first time step, and M is the PHC mass discharge in each subsequent modeling time step divided by the 3 days of each time step (Fraser, 2007).

M/M_0 for all of BTXN were larger than 1 after the source emplacement due to the rapid dissolution of more soluble compounds (MTBE) and the resultant increase of the mole fraction of BTXN (Fraser, 2007). In Figure 4.23, modeling results show that the dissolution of benzene is fast and its mass discharge naturally decreased to a very low level by Day 800, while the mass discharges of toluene, o-xylene and naphthalene remained higher.

The comparison between modeling and field BTXN mass discharges are shown in Figure 4.24 A-D. Before the sulfate application, the correlation of field and predicted or modeled curves are good for benzene, toluene and o-xylene, while the agreement between naphthalene field and model results is poor. The naphthalene solubility used in the model was 151 mg/L from King and Barker (1999). A higher effective solubility (350 mg/L) for naphthalene would create better agreement, but there is no reason for such an elevated effective solubility. The presence of naphthalene from a previous gasoline injection at this site (Mocanu, 2006; Fraser, 2007) could have enhanced the initial mole fraction of naphthalene, but Kovacik (2013) found no evidence for this.

Although the general correlation between model and field BTX results are good, it should be noted that their initial mass discharges all deviate significantly from the model prediction. This is because the Raoult's Law model simulates the mass discharge at the source zone, while the field data were sampled at 2.5 m downgradient of the source. Therefore, the sorptive retardation of PHCs should be considered to discuss the correlation between field and model data.

Retardation factors, R, for BTX at Borden are 1.1, 1.2 and 1.4, respectively (Patrick and Barker 1985). The calculated naphthalene R based on Borden parameters is 2.2 (Patrick and Barker, 1985). These R values make the first arrival of BTXN at Row 3 in about 24, 26, 31 and 48 days respectively, with the peak concentrations reaching Row 3 in 41, 44, 52 and 81 days, respectively. The first sampling taken on Day -366 was 22 days after the source emplacement, and the second was 83 days after (Day -305). Therefore, it is reasonable to see low BTX concentrations and almost zero naphthalene concentration on Day -366 at Row 3. On Day -305, peak concentrations for BTX should have arrived, while naphthalene's peak concentration may have not yet come.

Further, it should be noted that Raoult's Law model only considers the depletion of the source, while the natural biodegradation process is not considered. As Fraser et al. (2007), Freitas et al. (2011) and others have shown, natural biodegradation of BTEXN is a major factor in the formation of plumes from residual PHC sources. Mass removal from the dissolved plumes by biodegradation is likely the dominant reason that the modeled curve and field curve show disagreement on Day -9 (Day 379 on the plots) before the first application. To adjust the model to account for the ongoing natural biodegradation all Raoult's Law model curves in Figure 3.24 A-D were adjusted to intersect the field mass discharge points on day -9. The adjusted model curves are parallel to the unadjusted curves, assuming the natural biodegradation continues in addition to any biodegradation enhanced by the sulfate application. The comparison between field and model mass discharge plots for the other compounds are provided in Appendix E.

The comparison between adjusted model and field mass discharge suggested that natural attenuation for benzene occurred at the Borden site. Benzene mass discharge declined significantly prior to the first application and was not obviously affected by applied sulfate

(Figure 4.24 A). Additional toluene attenuation following sulfate application was evident (Figure 4.24, B), while o-xylene may or may not have additional attenuation (Figure 4.24, C) with sulfate application. Naphthalene mass discharge apparently remained unenhanced and consistent with the modeled source depletion scenario.

4.2.2.4 Sulfate Consumption

To demonstrate that sufficient sulfate had been applied to provide the required electron acceptor to support sulfate reduction, the mass of sodium sulfate consumed by toluene was calculated and compared with the mass of sodium sulfate actually applied, because toluene is most evidently consumed after sulfate application.

Toluene consumed by sulfate reduction can be estimated by calculating the area between the modeling discharge curve and actual or field mass discharge curve over the time when additional sulfate had been available (Day 388 to 782 on Figure 3.24 B).

The mass of toluene consumed by sulfate reduction is estimated to be 700 g. Table 4.16 summarizes the physical properties of the emplaced NAPL chemicals and stoichiometric mineralization by sulfate reduction of each unit mol of PHC. The total mass of sodium sulfate required for toluene mineralization totaled about 4.9 kg, which is much less than the 200 kg sodium sulfate that was applied. Clearly, the apparent mass decline could be easily supported by the mass of sulfate applied.

4.2.3 Sulfide

Sampling at Row 3 and Row 4 assessed sulfide production via sulfate reduction at Day -9 (Table 4.13). This sampling focused on the area shallower than 2.5 mbgs where the sulfate water was anticipated to flow through. Sulfide concentrations at Row 3 ranged from 10 to 90 μg/L and at Row 4 ranged from 0 to 55 μg/L.

Another sulfide sampling was taken on Day 197, the first fieldwork after winter in 2014. Sulfide concentrations at both Row 3 and Row 4 (100-500 μg/L) were much higher than that on Day -9 (10-90 μg/L) (Table 4.14). At Row 3, high sulfide concentrations were detected at

every depth. Sulfate and EC results from Day 86 and 102 demonstrated sodium sulfate occurred over the whole Row 3, suggested the generation of sulfide originated from the applied sodium sulfate.

The other sulfide concentrations were measured for progress monitoring and will be discussed in the following section.

4. 3 Progress Monitoring

The purpose of progress monitoring was to identify the processes responsible for reactions that caused the PHC concentrations to be lower than expected based on the source depletion calculated in 4.2.2.3. Results of the progress monitoring should demonstrate if the redox condition were correct for sulfate reduction (Eh); whether sulfate reduction occurred (sulfide, $\delta^{34}S$); whether PHCs underwent biodegradation (dual isotope, biochemistry); and if biodegradation occurred, progress monitoring can identify if the biodegradation process was dominantly sulfate reduction, methanogenesis, or aerobic biodegradation (methane, DO, dual isotope, DIC and DIC-$\delta^{13}C$).

Four progress samplings were taken on Days -1, 44 (Row 3 only), 50 (Row 4 only), 103 (Row 3 only), and 233. As described in section 2.3, progress sampling points were in three areas: the source, Row 3 and Row 4. As the pattern of data changes at Row 4 remains unclear by the thesis writing, only representative progress results from the source and Row 3 are shown and discussed here. One point was assigned at the source (S5-D3) and another at Row 3 (R3-M4-D1) for frequent monitoring. These sampling points are at the same depth and were in areas where the applied sulfate water flowed through.

Results for each parameter at each sampling point will be considered chronologically, from Day -1 to Day 233. Geochemical parameters measured and analyzed include oxidation reduction potential (Eh), sulfide concentration, methane concentration, sulfate concentration and $\delta^{34}S$ in sulfate, $\delta^{2}H$ and $\delta^{13}C$ in benzene, toluene, o-xylene for dual isotope analysis (other hydrocarbon concentration are provided in Appendix F), dissolved inorganic carbon (DIC) concentration, and DIC-$\delta^{13}C$, and. These parameters will be presented and discussed

for S5-D3 and R3-M4-D1. They are categorized and plotted into four groups: Redox, SO_4, CSIA and DIC (Figure 4.25 and 4.26).

4.3.1 Source Area (S5-D3)

Figure 4.25 A shows results for Eh, sulfide concentrations and methane concentrations, all related to the in situ redox conditions. The low Eh illustrates that a strong reducing environment was created when sulfate was applied. The increased concentration of methane and sulfide, indicate that both sulfate reduction and methanogenesis were enhanced after sulfate application. By Day 230, the methane concentration reduced to about the baseline value while sulfide concentration remained high, suggested sulfate reduction became dominant.

The application of environmental isotopes in biodegradation studies is based on the isotopic fractionation in affected compounds involved in biogeochemical processes (Aravena and Hunkeler, 2009). In case of sulfate, during sulfate reduction the remaining sulfate gets enriched in the ^{34}S as the concentration of sulfate decreases (Strebel et al., 1990). Similarly, for benzene, toluene and xylene, the remaining compounds get enriched in ^{13}C and ^{2}H as the concentration of these compounds decreases due to biodegradation (Hunkeler et al., 2001, Mancini et al., 2003; Meckenstock, et al, 2004).

Figure 4.25 B shows $\delta^{34}S$ in sulfate and sulfate concentrations. The major change of sulfate concentration is related to the three applications of sodium sulfate. It increased quickly after the first sulfate dosage on Day 0 and reached the peak concentration of about 1600 mg/L after the second application on Day 57. The $\delta^{34}S$ showed values around 10 ‰ even in the high concentration sample. The $\delta^{34}S$ value for the added Na_2SO_4 was 3.2 ‰. Therefore the ^{34}S enrichment indicated that sulfate reduction was active in the source area. In the CSIA diagram (Figure 4.25 C), benzene, toluene and o-xylene $\delta^{13}C$ and concentration results were plotted to evaluate the process(es) resulting in changing hydrocarbon concentrations. As a reference, the $\delta^{13}C$ values for benzene, toluene and xylene in the source material were -27, -26 and -26 ‰, respectively. Each hydrocarbon concentration has been `corrected for the dilution by the applied sulfate solution (see 4.2.2.2 for explanation).

Toluene results are highlighted in the CSIA plot.

Toluene concentrations at S5-D3 decreased from 7000 ug/L to < 10 ug/L on Day 103. The $\delta^{13}C$ value was about -25.7‰ on Day -1 and it reached a value of -21.7‰) on Day 103, 46 days after the second application. The large ^{13}C enrichment which is correlated with the application of sodium sulfate, is a clear indication of biodegradation of toluene. Similar decreasing concentration trends are also observed for benzene and o-xylene. The $\delta^{13}C$ data for o-xylene showed a value of -25.7 ‰ during baseline condition changing to a value of -24.2 ‰ during Day 103. This appreciable ^{13}C enrichment is consistent with biodegradation of o-xylene. However, no distinctive $\delta^{13}C$ pattern was observed for benzene; the $\delta^{13}C$ values fluctuate from -25.1 ‰ during baseline condition to -25.7 ‰ during the experiment. Based on a $\delta^{13}C$ value of -27 ‰ for benzene in the source material, the isotope data showed that benzene was affected by biodegradation before the injection of the sulfate solution. The fact that the $\delta^{13}C$ value of the benzene never moved back towards the original benzene value indicates that benzene was similarly affected by biodegradation during the sulfate application period.

The role of biodegradation can be further analyzed using a dual isotope graph by plotting $\delta^{2}H$ on y-axis and $\delta^{13}C$ on x-axis (Figure 4.27 and 4.28). The red and green areas represent the trajectory of the isotopic values in BTX residual after increasing degrees of aerobic and anaerobic biodegradation, respectively (Aelion et al, 2009). The dual isotope plots for BTX at S5 are shown in Figure 4.27 A-C. Numbers beside each data point is the day of sampling relative to the first application. The dual isotope results suggest toluene, o-xylene and benzene underwent anaerobic biodegradation, and some aerobic biodegradation may have also occurred for benzene.

DIC concentration increased from 50 mg/L before the sulfate application to 70 mg/L during and after sulfate dosage (Figure 4.25 D). These results showed that the formation of inorganic carbon from mineralization of organics was persisting even when the sulfate left the source zone. The DIC-$\delta^{13}C$ values decreased since the beginning of sulfate application, indicating the input of a ^{13}C depleted carbon from biodegradation of BTX. Although the isotopic depletion declined after 100 days of application, the DIC-$\delta^{13}C$ value was still more depleted (more negative) than the original value documenting the continuing mineralization

of PHCs.

This geochemistry data support the occurrence of microbial sulfate reduction at S5-D3 after the sodium sulfate water application, ongoing anaerobic biodegradation of toluene, o-xylene and benzene and perhaps some aerobic biodegradation of benzene.

4.3.2 Row 3 (R3-M4-D1)

R3-M4-D1 is located at the same depth but downgradient of S5-D3 (Figure 2.8). Progress monitoring results from this point provides some insight into the cumulative reactions in the source zone and in the dissolved plume just beyond the source zone.

Redox results at R3-M4-D1 are similar to S5-D3 (Figure 4.26 A). The applied sodium sulfate created anaerobic, sulfate reduction/methanogenesis at first with sulfate reduction dominating by Day 240.

The SO_4 concentration clearly indicates the presence of the applied sulfate solution on days 40 and 100 (Figure 4.26 B). The peak value was also found after the sulfate arrival from the second application around Day 70. A strong ^{34}S enrichment from 5‰ to 14‰ was observed after Day 100, which provided clear evidence of sulfate reduction (Strebel, et al., 1990).

BTX concentration changes are complex at Row 3 (Figure 4.26 C), in contrast to the continuously decreasing trends at S5-D3 located near the source. The toluene and xylene concentration increased after the second sulfate application and tend to decrease after. This trend is more pronounced for toluene. Benzene concentration tends to increase after application I and decreases after applications I and II. The BTX concentration patterns are related to transport of mass associated to the sulfate applications from the source to the Row 3 line. It is important to remember that sulfate plume got deeper in the aquifer than the first application, which may also influence the concentration pattern.

The $\delta^{13}C$ values of toluene (-25.5 to -25.1 ‰) after the second sulfate application are more depleted than the initial baseline values of –0.4 ‰. Considering the isotope composition of the toluene at the source material, these data showed the toluene before the sulfate application was affected by biodegradation. The o-xylene $\delta^{13}C$ became somewhat enriched from -26.5 ‰ to values of -25.6 and -25.1 ‰ after the second sulfate application. In the case

of benzene, the $\delta^{13}C$ values decreased from -23.8 to -24.8 ‰ and then increased to a value of -24.2 ‰ during the sulfate applications. In general the enriched pattern observed in the isotope data indicated that toluene, xylene and benzene have undergone significant biodegradation before and during the sulfate application.

The dual isotope results at R3-M4 (Figure 3.28 A-C) showed toluene and o-xylene have been biodegraded under anaerobic conditions, while benzene, surprisingly, seems to be biodegraded mainly under aerobic condition.

Similar to S5-D3, DIC concentration at R3-M4-D1 also increased from 40 mg/L to 110 mg/L once sodium sulfate arrived which is likely associated with mineralization of organic carbon (Figure 3.26 D). The DIC $\delta^{13}C$ values decreased in response to the sulfate arrival, demonstrating ongoing and perhaps enhanced mineralization of PHCs related to the sulfate dosage.

Progress monitoring results at R3-M4-D1 are supportive of sulfate reducing persisting into the hydrocarbon plume, with the attenuation of toluene and o-xylene likely related to microbial sulfate reduction. Again benzene degradation appears minor, but under aerobic conditions.

4.3.3 Biomarkers

The last lines of evidence to support BTX biodegradation are to use microbial and gene tools (i.e. biomarkers) that directly measure the microbial metabolites and message RNA (mRNA) associated with specific biodegradation mechanisms. The microbial metabolite created during biodegradation indicates the intensity of degradation, and the mRNA indicates the transcription of the functional genes directing that degradation. Biomarker results indicative of aerobic toluene degradation and anaerobic degradation of toluene and of benzene anaerobic were measured. Results are provided in Appendix G. Diagrams compare the metabolite and mRNA concentrations before (Day 0) and after (Day 44) the first sulfate application.

Aerobic toluene activity was indicated by the aerobic metabolite Toluene-*cis*-dihydrodiol concentration and related mRNA $todC_{mRNA}$. The aerobic toluene metabolite consistently

decreased below the detection limit after the sulfate application. Ten out of twelve points showed zero todC_{mRNA} after the application on Day 103, suggested the applied sulfate has enhanced anaerobic conditions, thus inhibiting aerobic toluene biodegradation.

The anaerobic toluene activity was demonstrated by benzylsuccinate (metabolite) and bssA-SRB_{mRNA} (mRNA) concentrations. Significant increase of benzylsuccinate was observed at source monitoring points after the application on Day 44, indicating the establishment of an anaerobic metabolic environment in the source. On the other hand, a benzylsuccinate decreasing trend at Row 3 suggests less anaerobic activity occurred at Row 3 on Day 44. As the anaerobic biodegradation enhanced by applied sulfate requires a stimulation time (Suthersan, 2011), it is reasonable to see less anaerobic biodegradation when the sulfate was just arrived at Row 3 less than 20 days on Day 44.

The benzene anaerobic mRNA ancA_{mRNA} did not show a consistent pattern. As indicated by benzene dual-isotope results (Section 4.3.1 and 4.3.2), benzene biodegradation was likely under both aerobic and anaerobic conditions.

While there is certainly compelling evidence that sulfate application enhanced anaerobic conditions, there is no direct evidence of sulfate enhancement of PHC biodegradation The metabolites specific for toluene and o-xylene biodegradation by sulfate reducing bacteria (benzylsuccinate and 2-methylbenzylsuccinate) (Shayan, 2015) were not found to date and so enhanced biodegradation of PHCs has not yet been tied directly to reduction of the applied sulfate. Additional samples are currently being analyzed and may provide a direct linkage of sulfate application to enhanced PHC biodegradation by sulfate reducers.

Figure 4.1: The pond created by planks and bermed sand. Prepared sulfate water stored in the tank to the right of the pond area.

Figure 4.2: Bermed pond at constant water level during the first application.

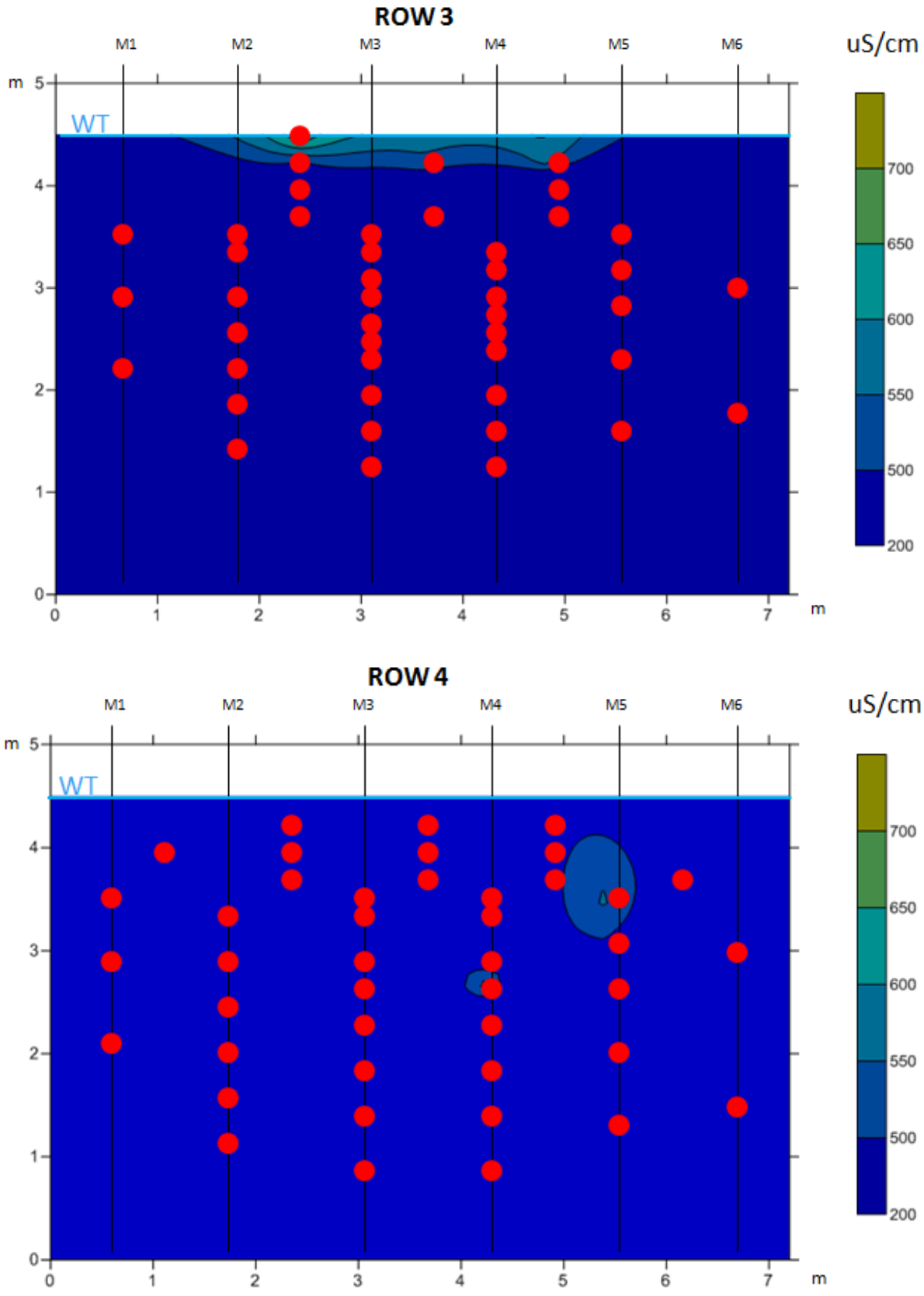

Figure 4.3: Background EC contours on Day -9. Top diagram, EC distribution at Row 3; bottom, EC distribution at Row 4. Red dots represent sampling points reported. Red dots represent points where EC was measured.

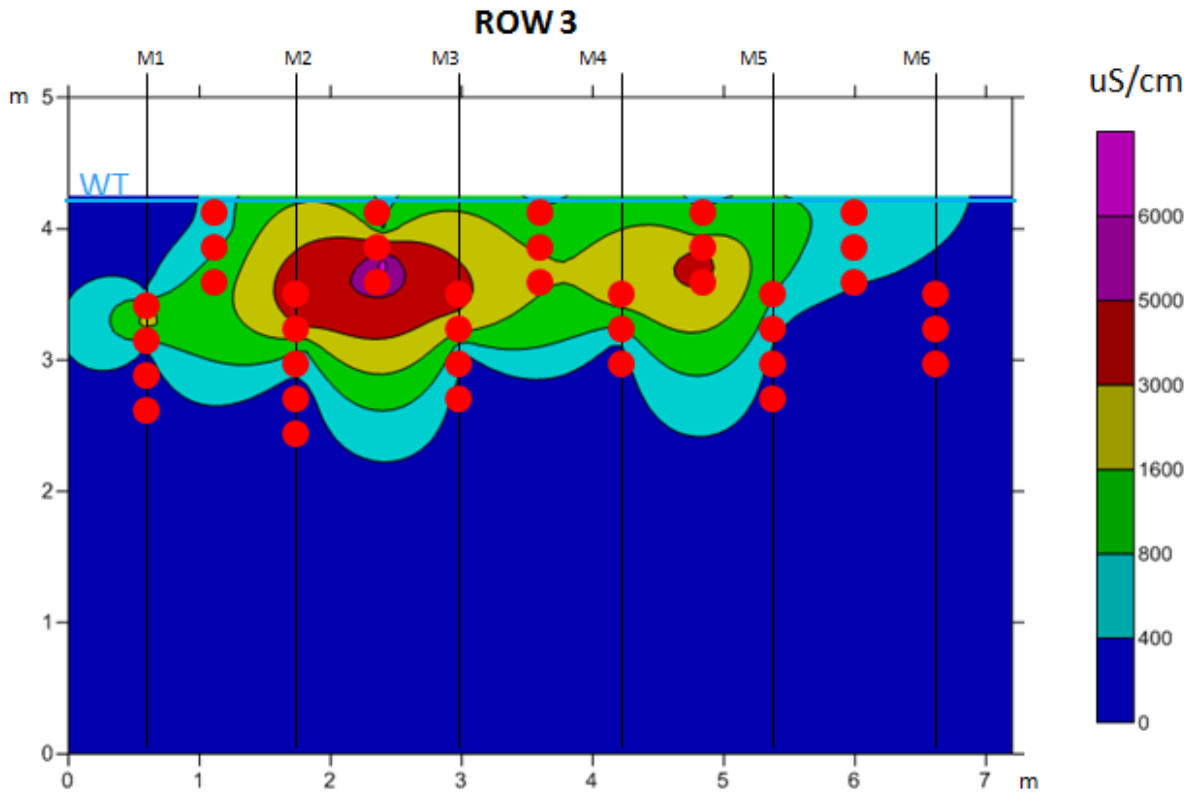

Figure 4.4: EC contour at Row 3 on Day 23. Red dots represent EC measurement points.

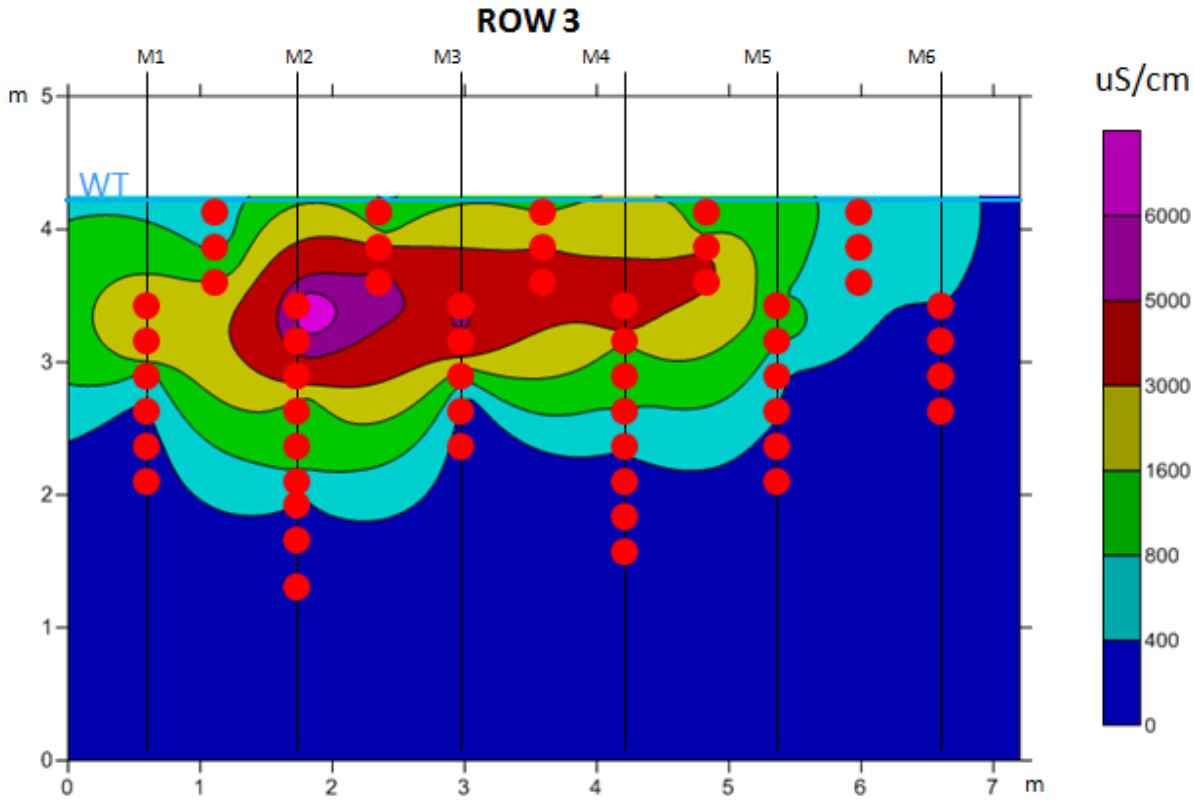

Figure 4.5: EC contour at Row 3 on Day 37. Red dots represent EC measurement points.

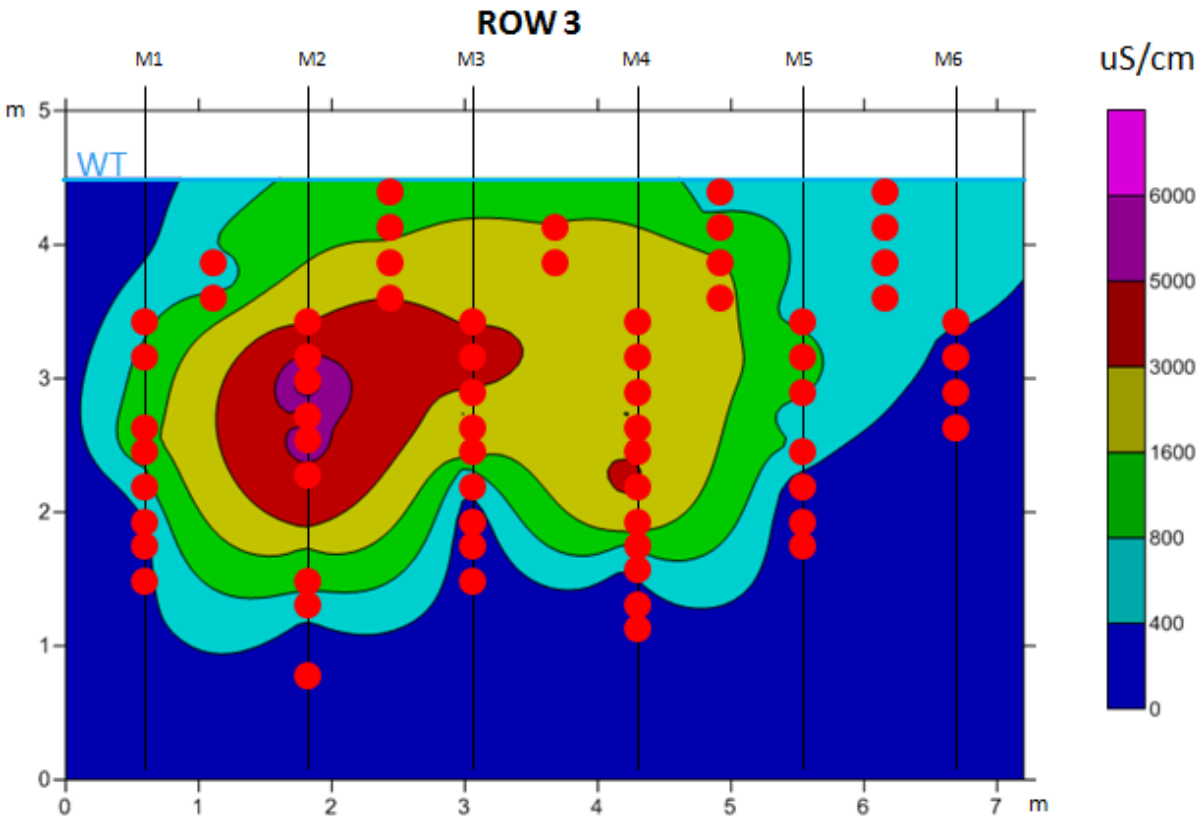

Figure 4.6: EC contour at Row 3 on Day 58. Red dots represent EC measurement points.

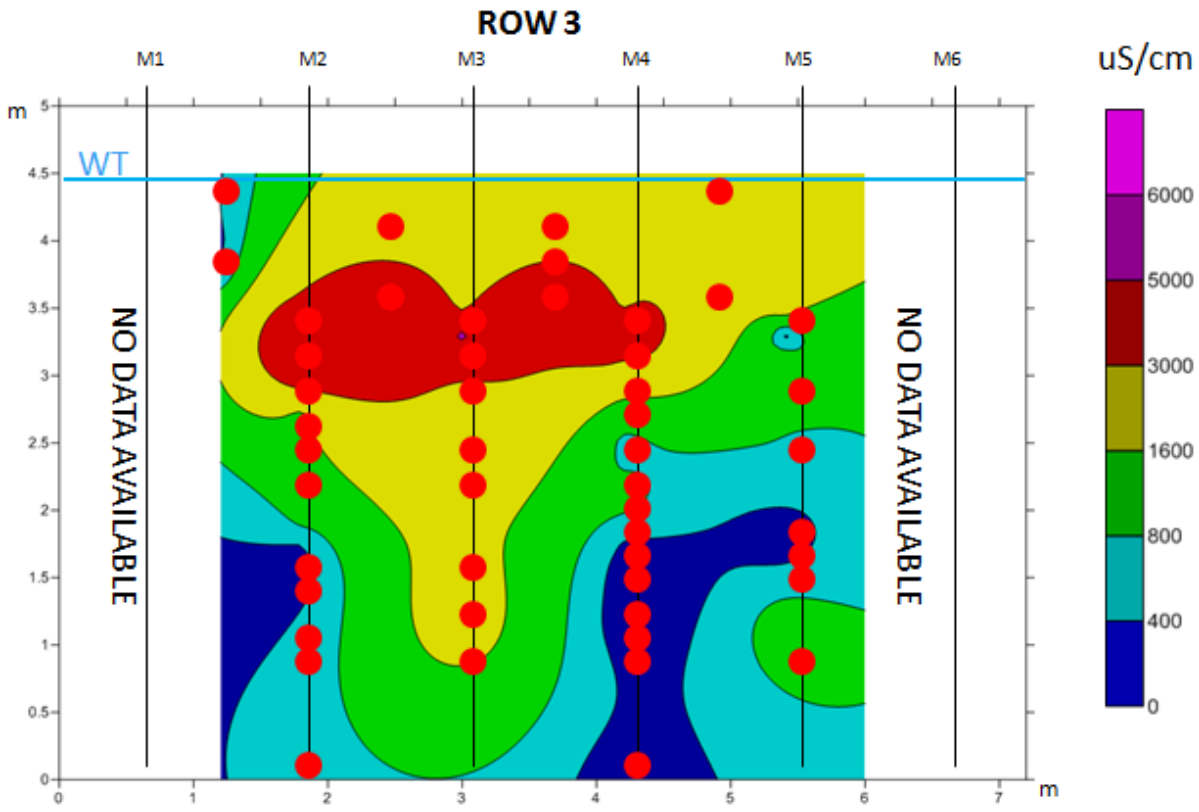

Figure 4.7: EC contour at Row 3 on Day 86. Red dots represent EC measurement points. No data available at R3-M1 and R3-M6 due to winter conditions.

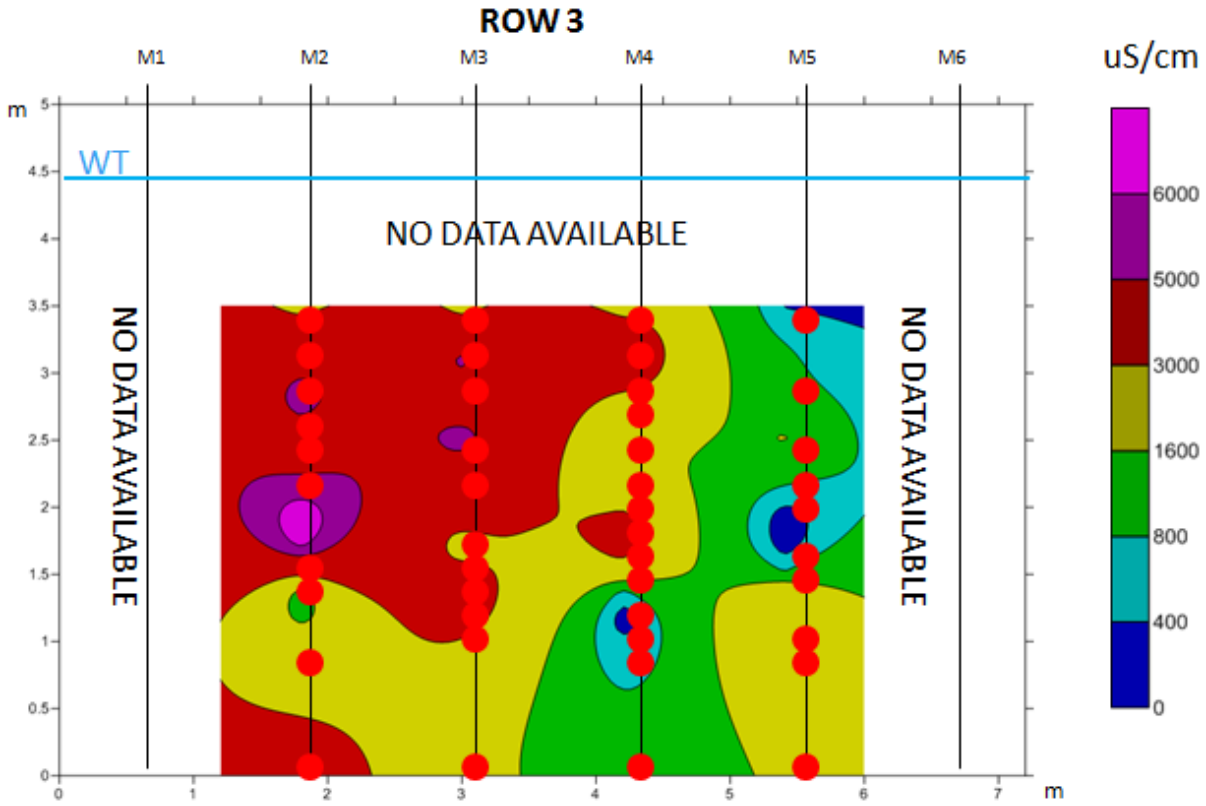

Figure 4.8: EC contour at Row 3 on Day 103. Red dots represent EC measurement points. No data available at R3-M1 and R3-M6 due to winter condition.

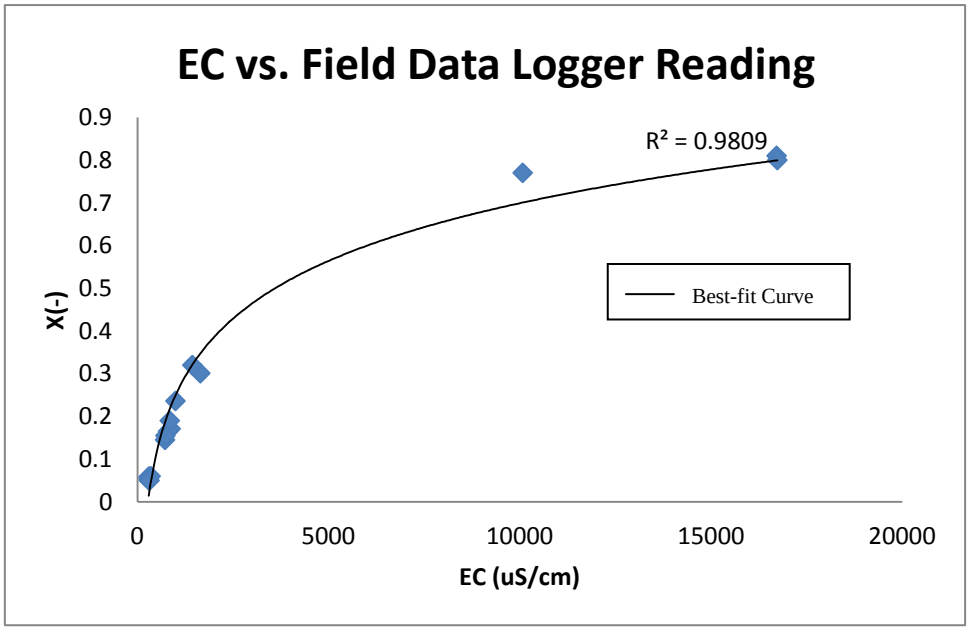

Figure 4.9: Relationship between EC and datalogger reading for field test.

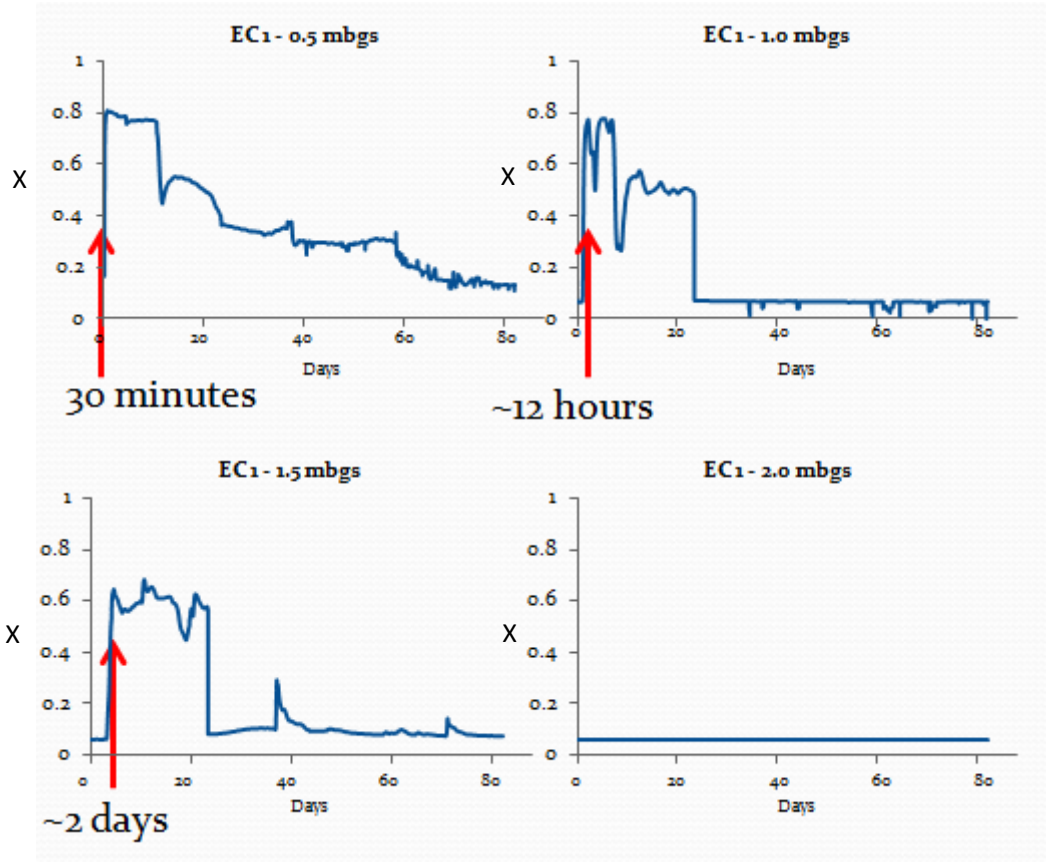

A

Figure 4.10: Resistivity data logger readings (X) at A) EC1, B) EC2, C) EC5 for a period of 78 days after the third application. The red arrow indicates the estimated arrival of sodium sulfate.

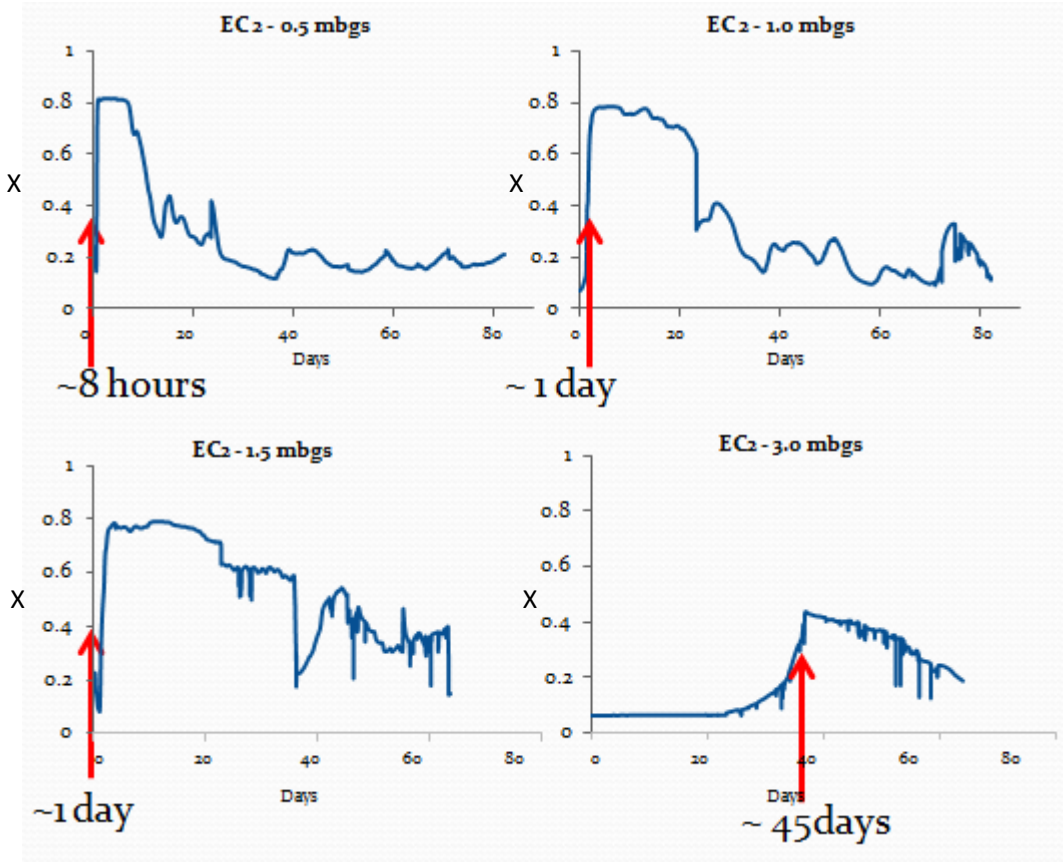
EC2 - 0.5 mbgs
EC2 - 1.0 mbgs
EC2 - 1.5 mbgs
EC2 - 3.0 mbgs
X
Days
~8 hours
~ 1 day
~1 day
~ 45days

B

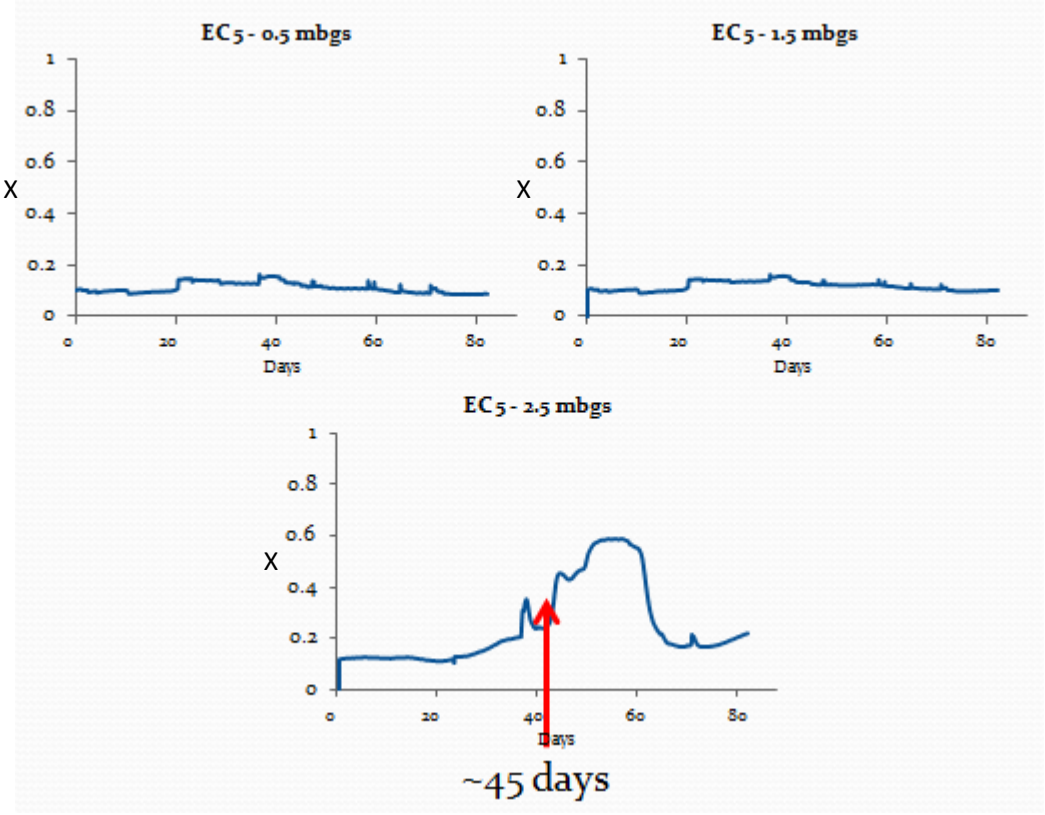

C

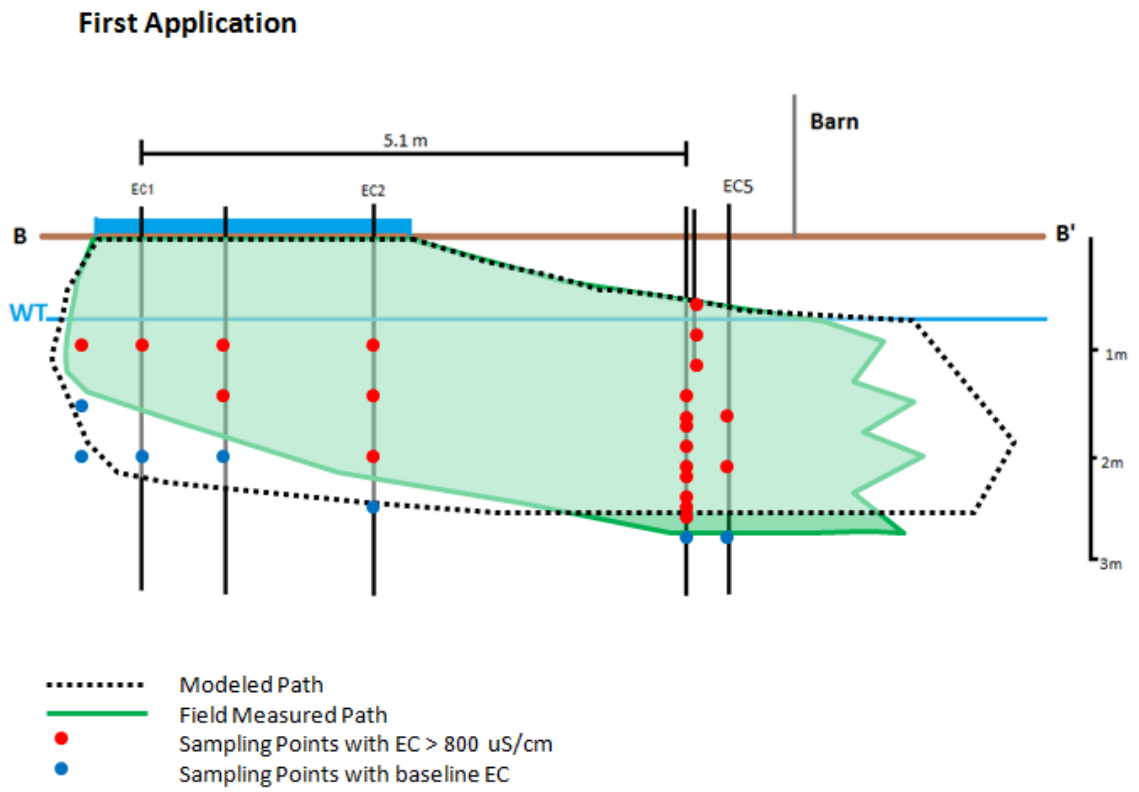

A

Figure 4.11: Comparison of sulfate migration track between SALTFLOW and field monitoring for each sulfate application. A) First application; B) second application; C) third application.

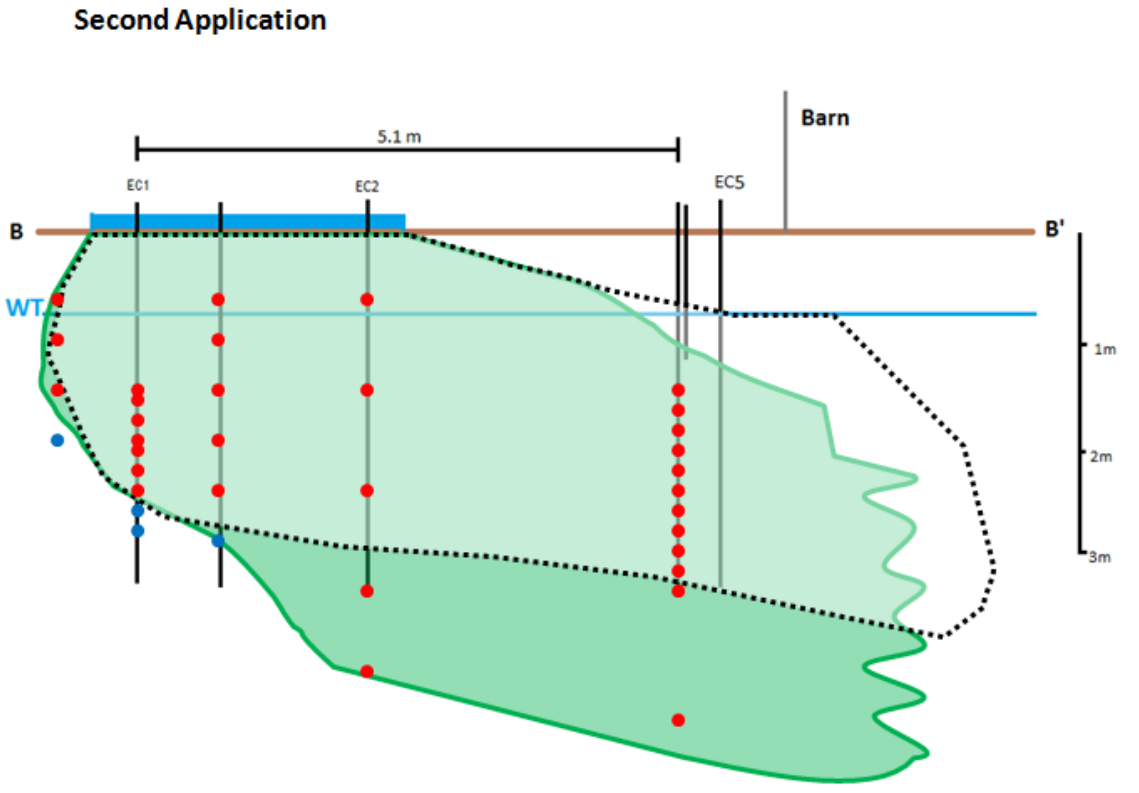

B

Third Application

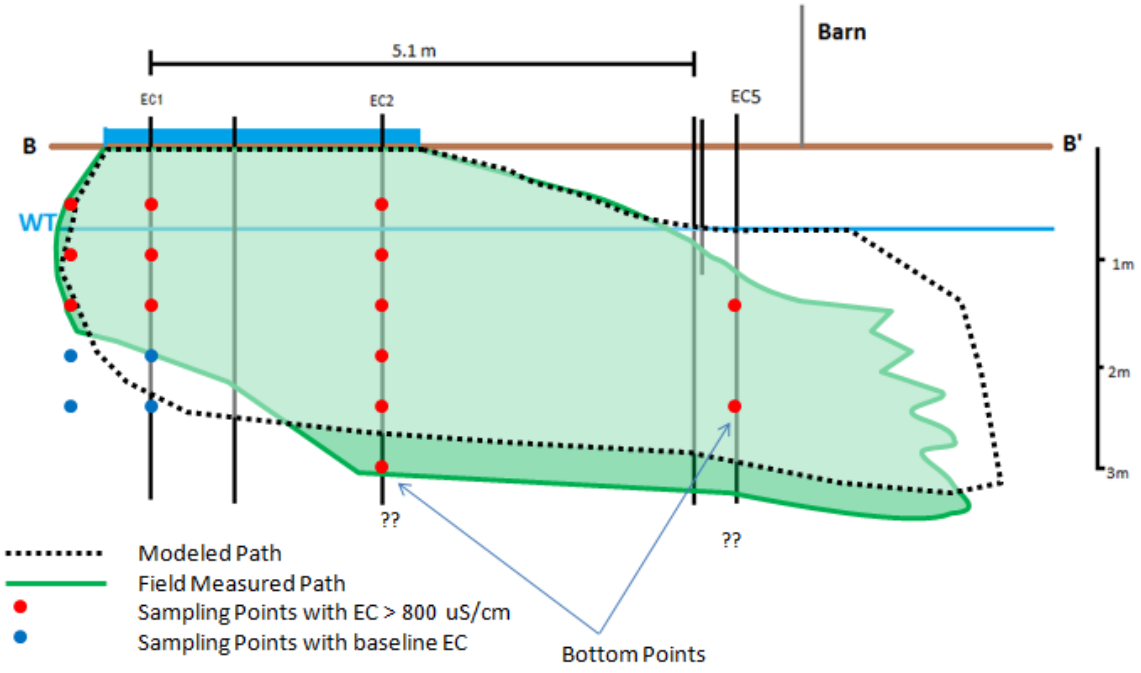

C

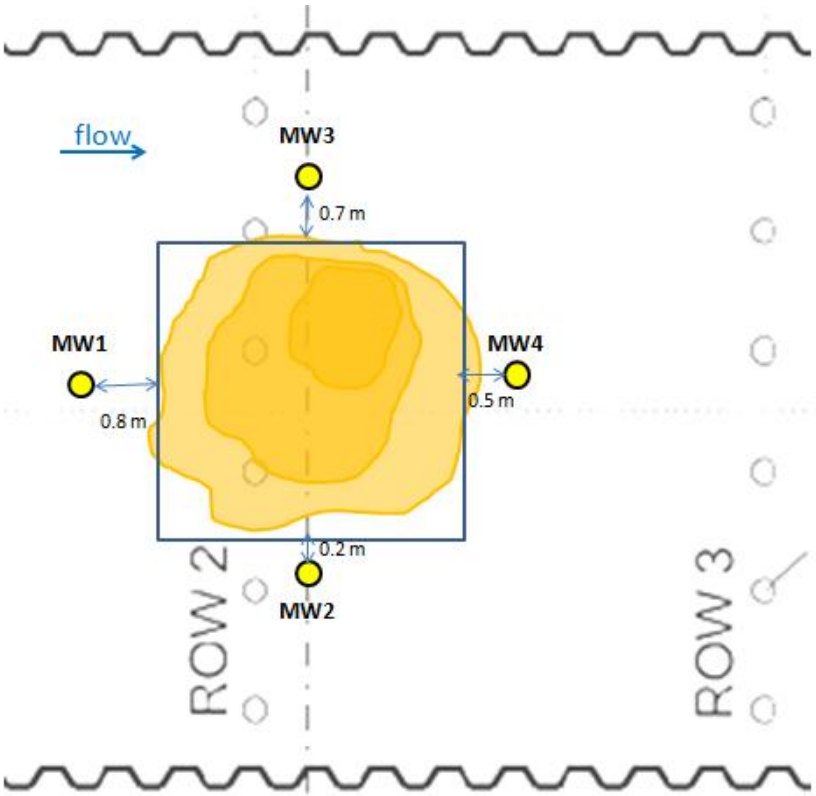

Figure 4.11: The layout of water table monitoring wells.

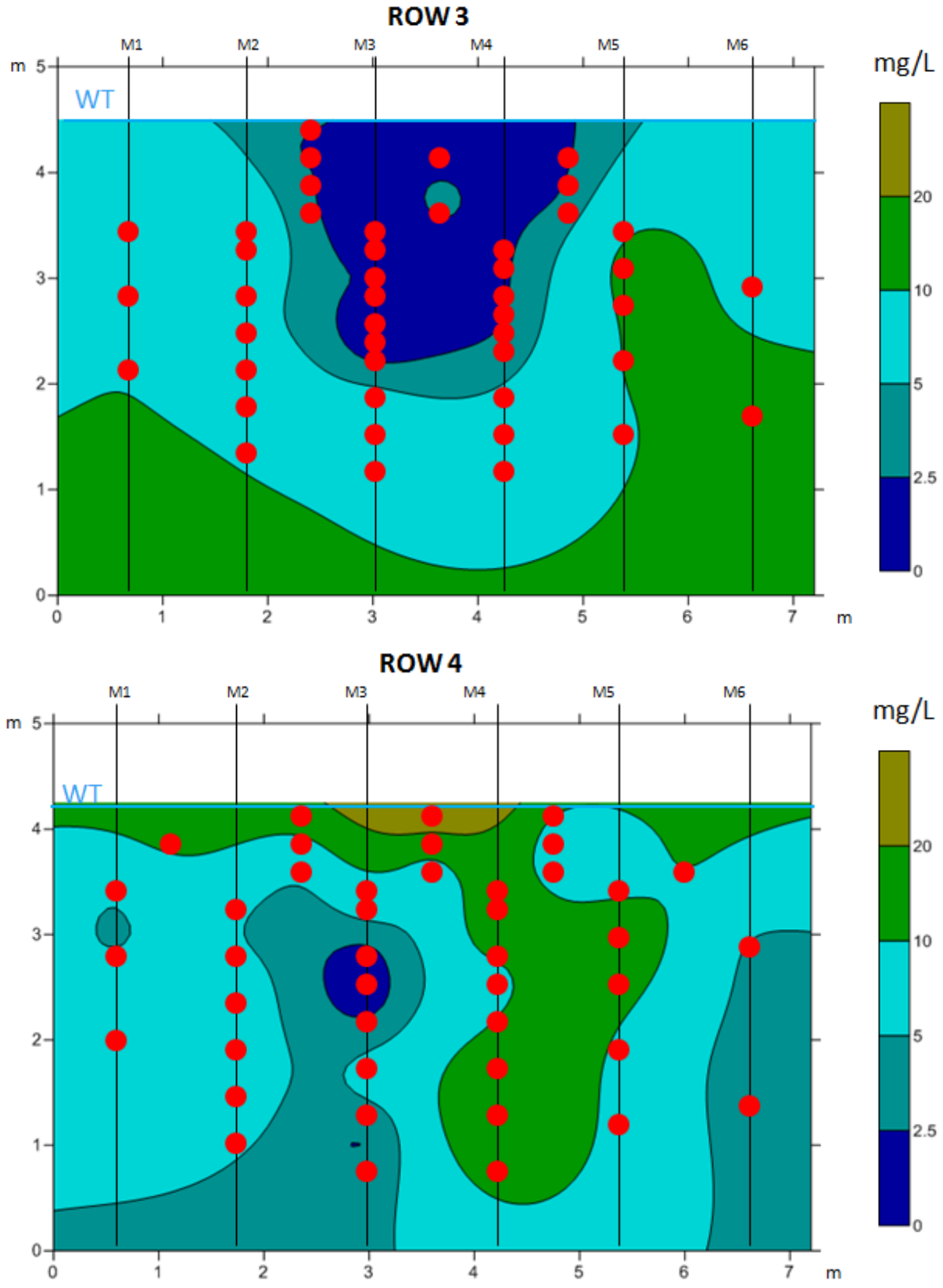

Figure 4.12: Sulfate concentration at Row 3 and Row 4 on Day -9. Red dots are EC data points.

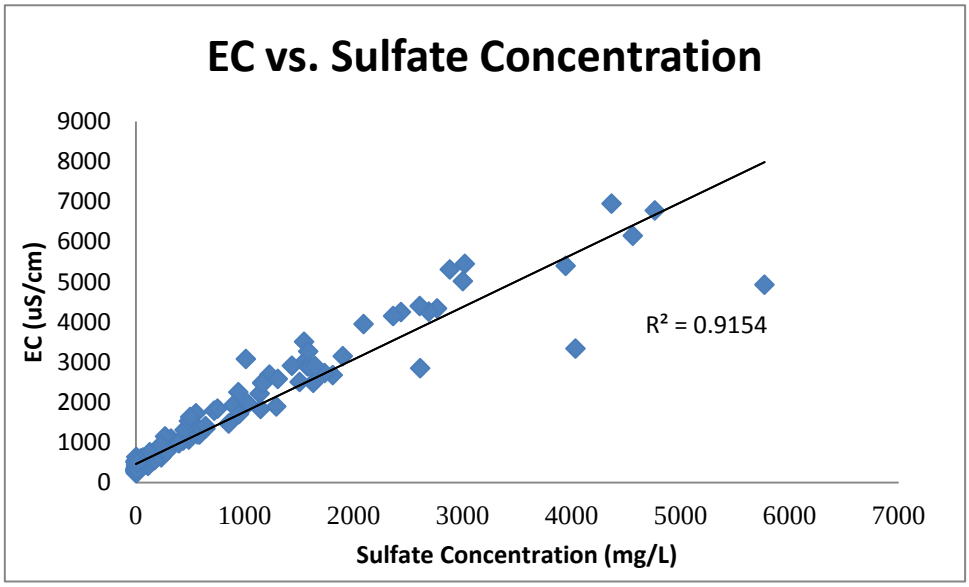

Figure 4.13: Relationship between EC and sulfate on Day 58.

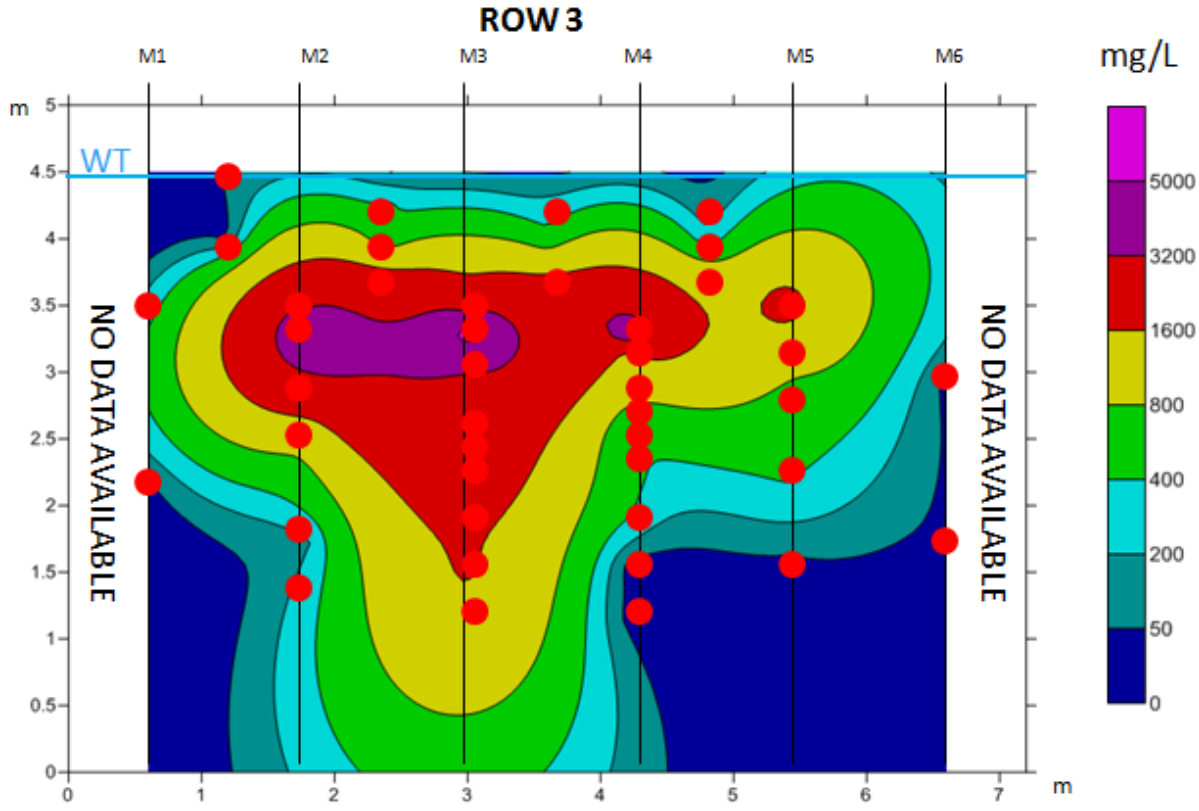

Figure 4.14: Sulfate concentration at Row 3 on Day 86. Red dots are sampled points.

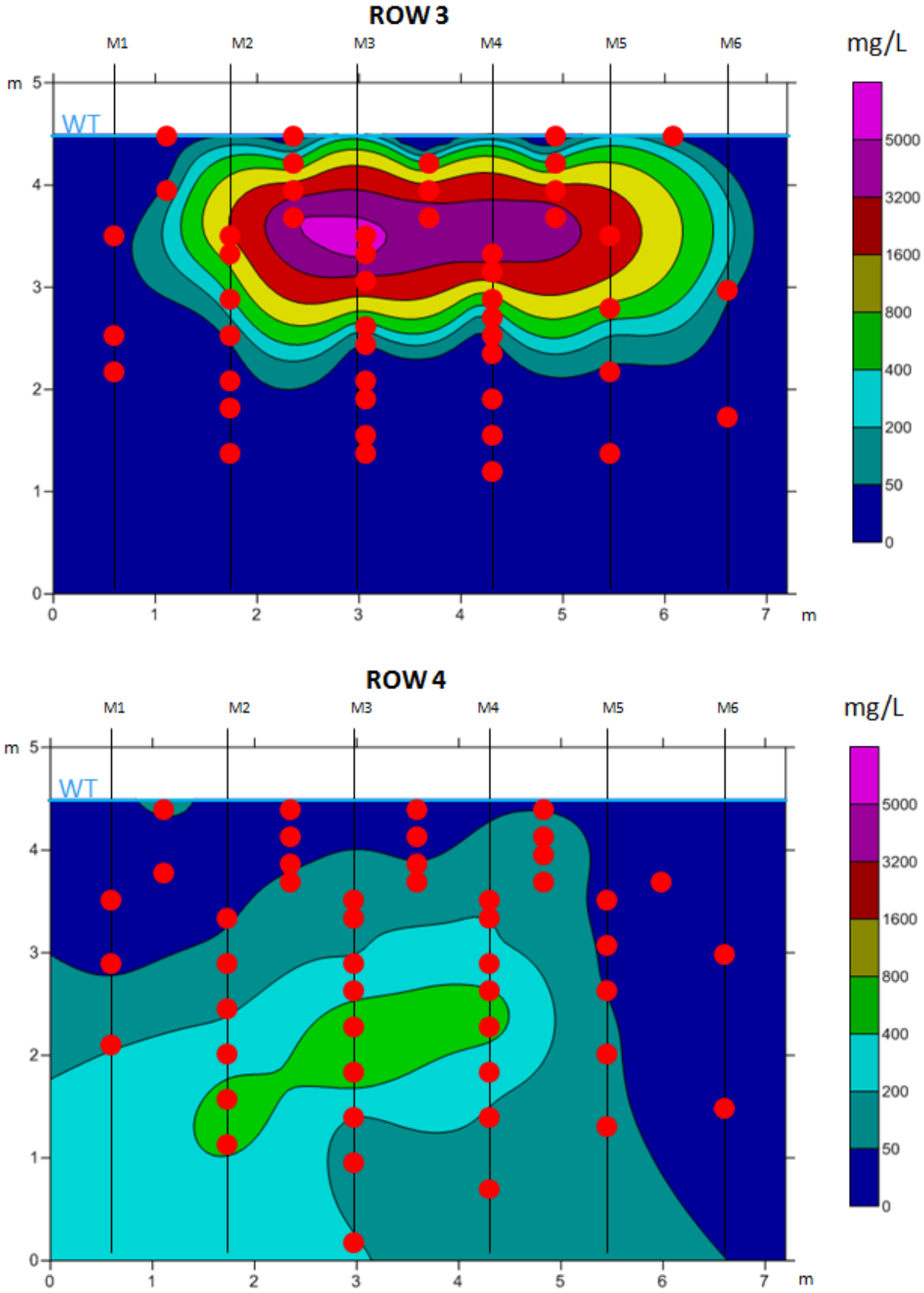

Figure 4.15: Sulfate concentrations at Row 3 and Row 4 on Day 277. Red dots are sampled points

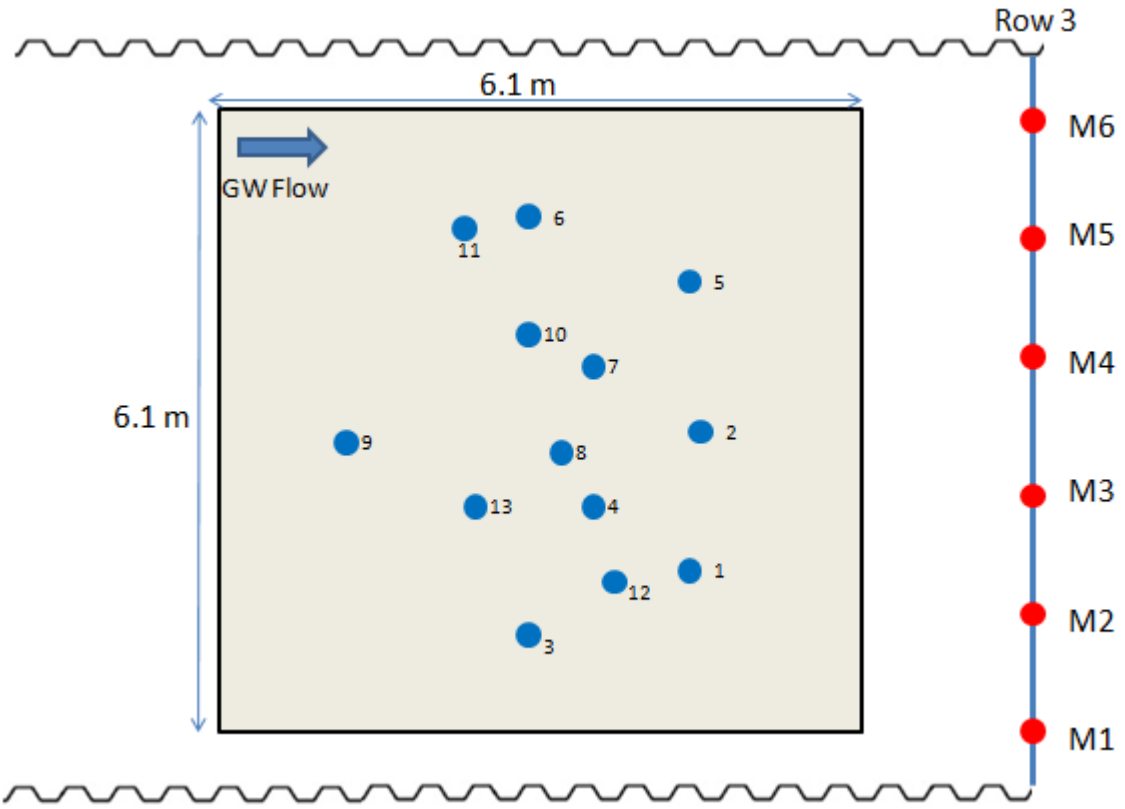

Figure 4.16: UVOST survey boreholes 1-13.

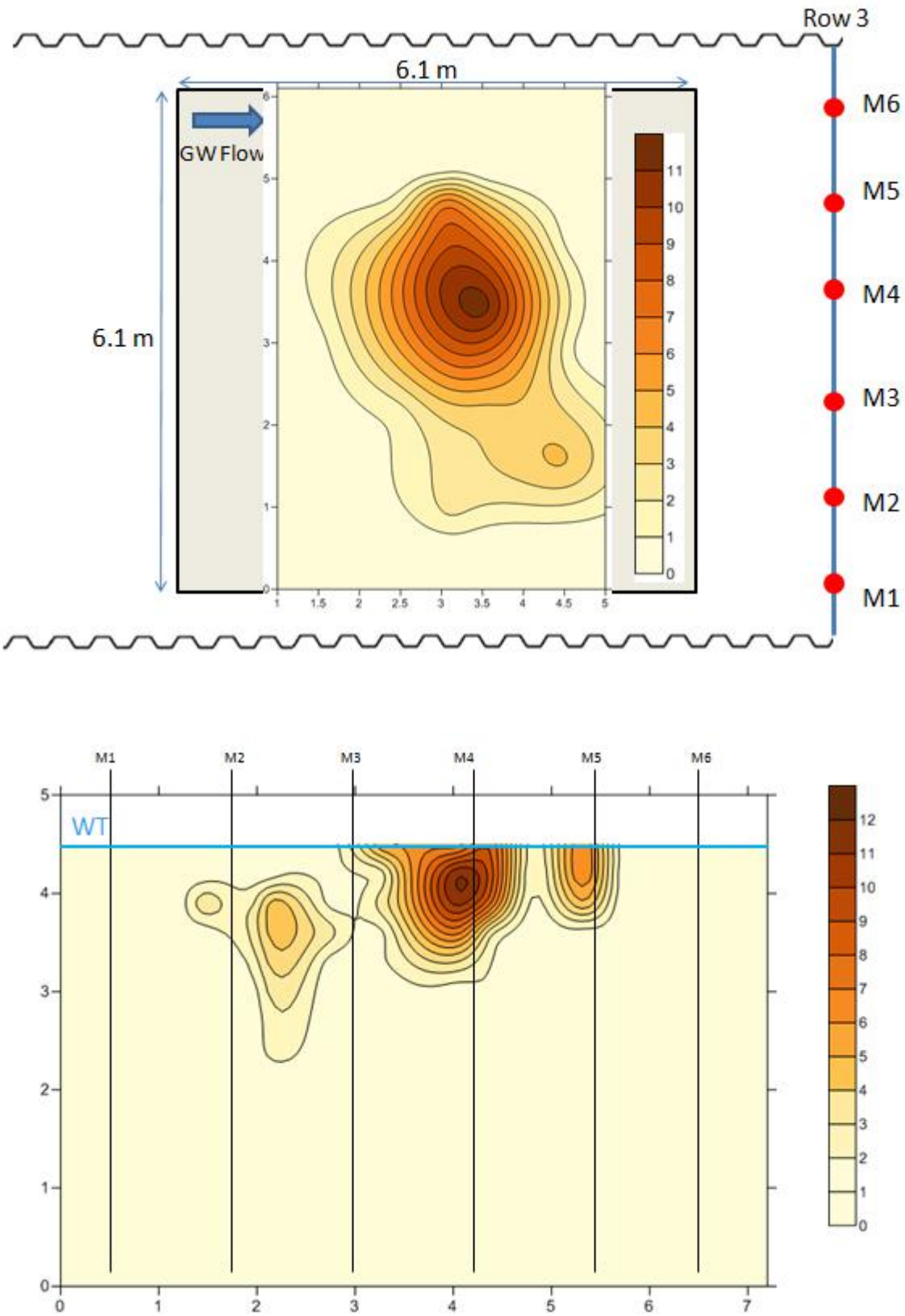

Figure 4.17: NAPL distribution. A) top, plan-view; B) bottom, cross-section view relative to Row 3.

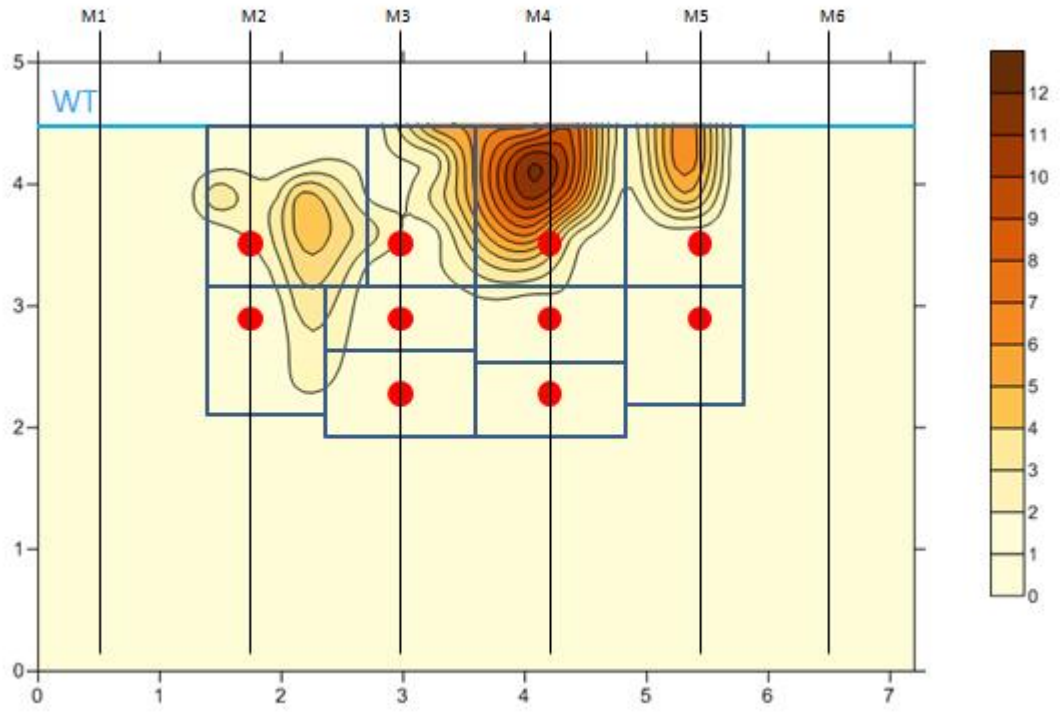

Figure 4.18: Representative area blocks and sampling points (red dots) from Kovacik, 2013. Contour is the NAPL cross-section projected onto Row 3.

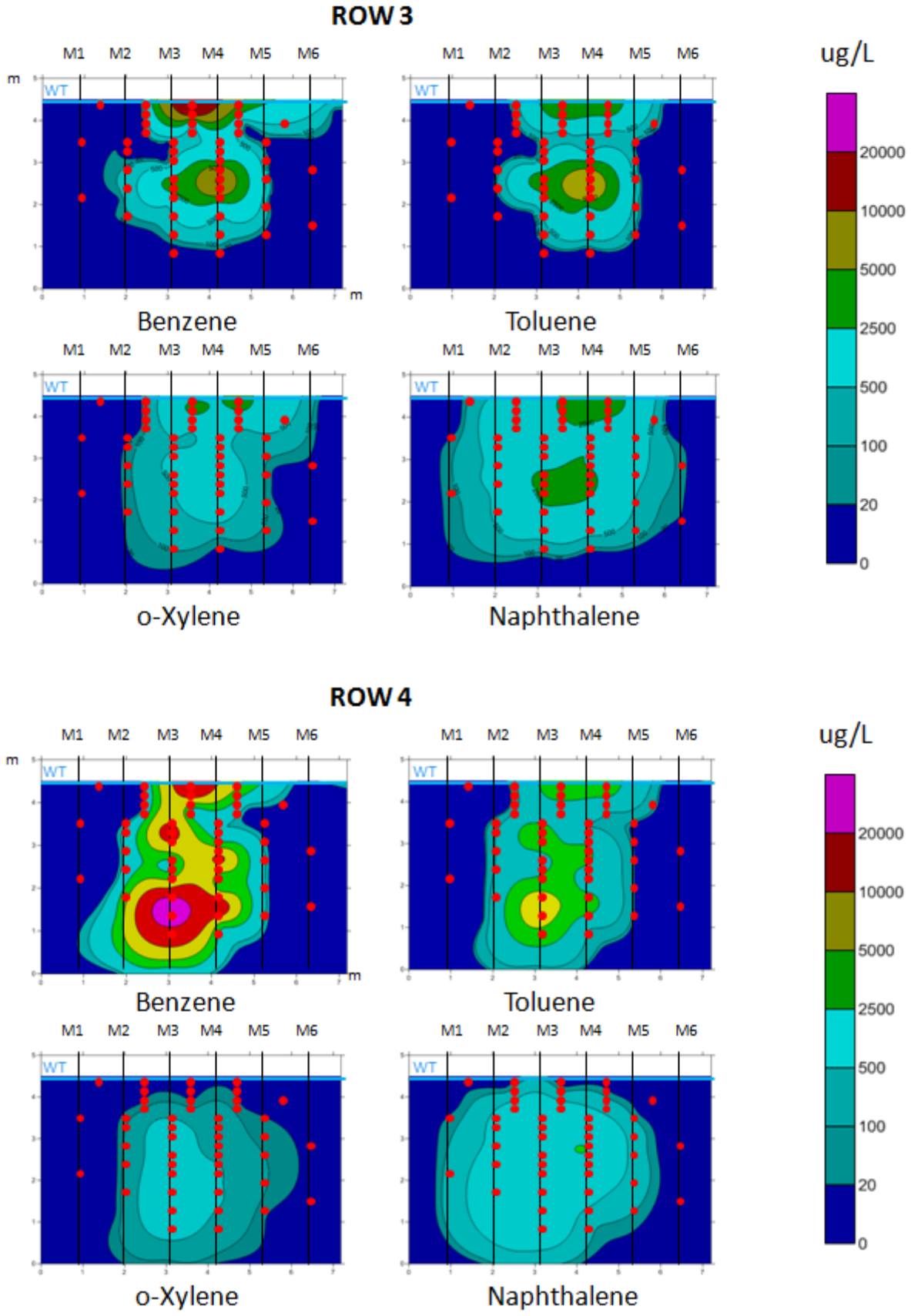

Figure 4.19: Distribution of BTXN on Day -9 at Row 3 and Row 4. Red dots are sampled points.

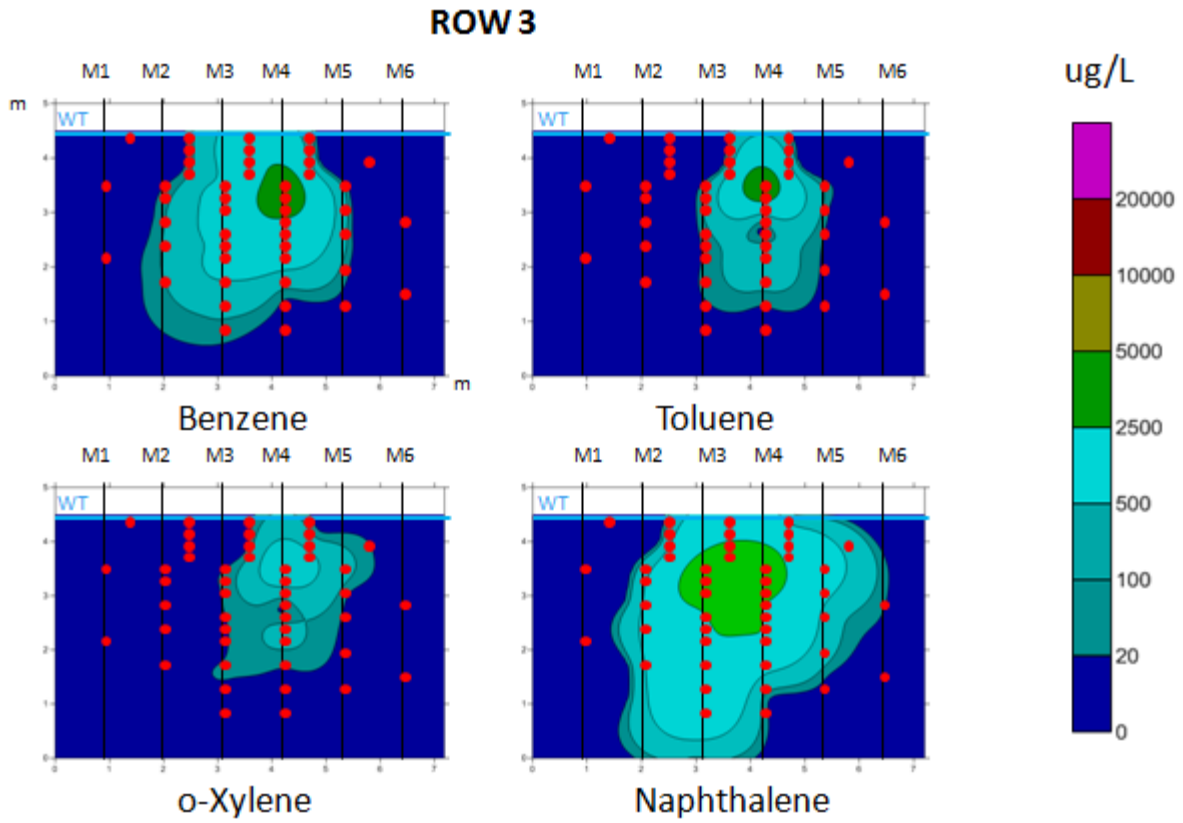

Figure 4.20: Distribution of BTXN on Day 86 at Row 3.

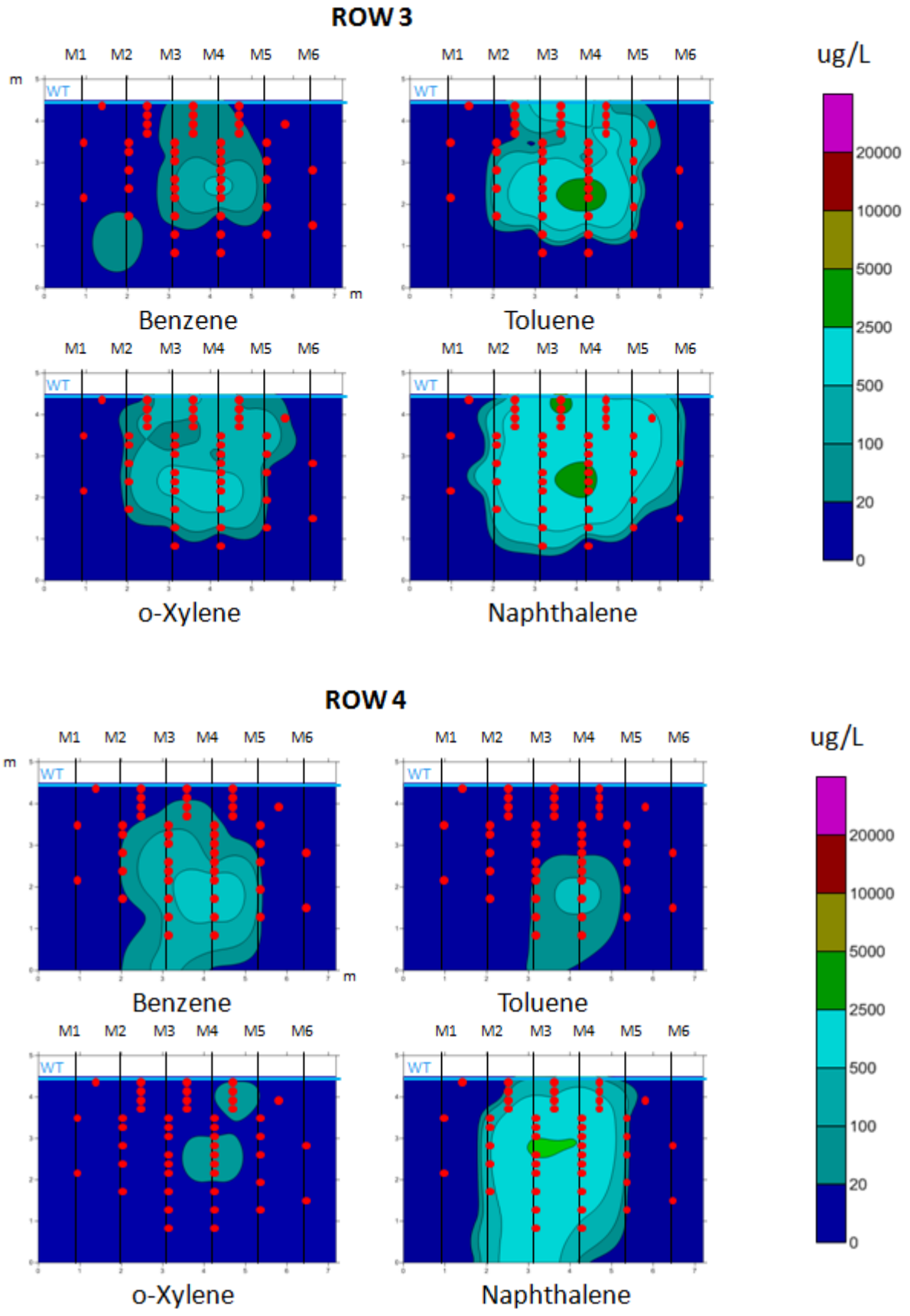

Figure 4.21: Distribution of BTXN on Day 277 at Row 3 and Row 4.

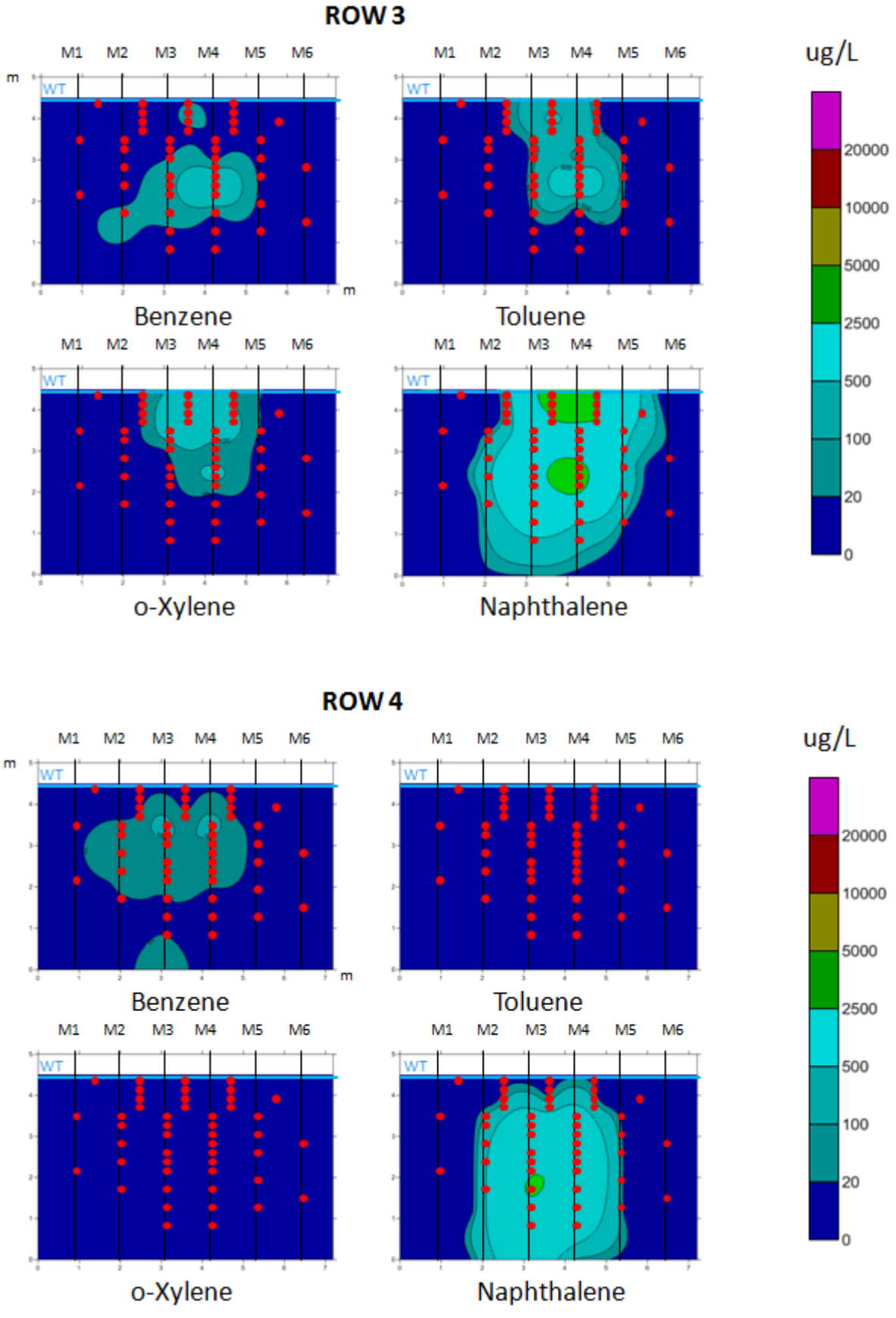

Figure 4.22: Distribution of BTXN on Day 394 at Row 3 and Row 4.

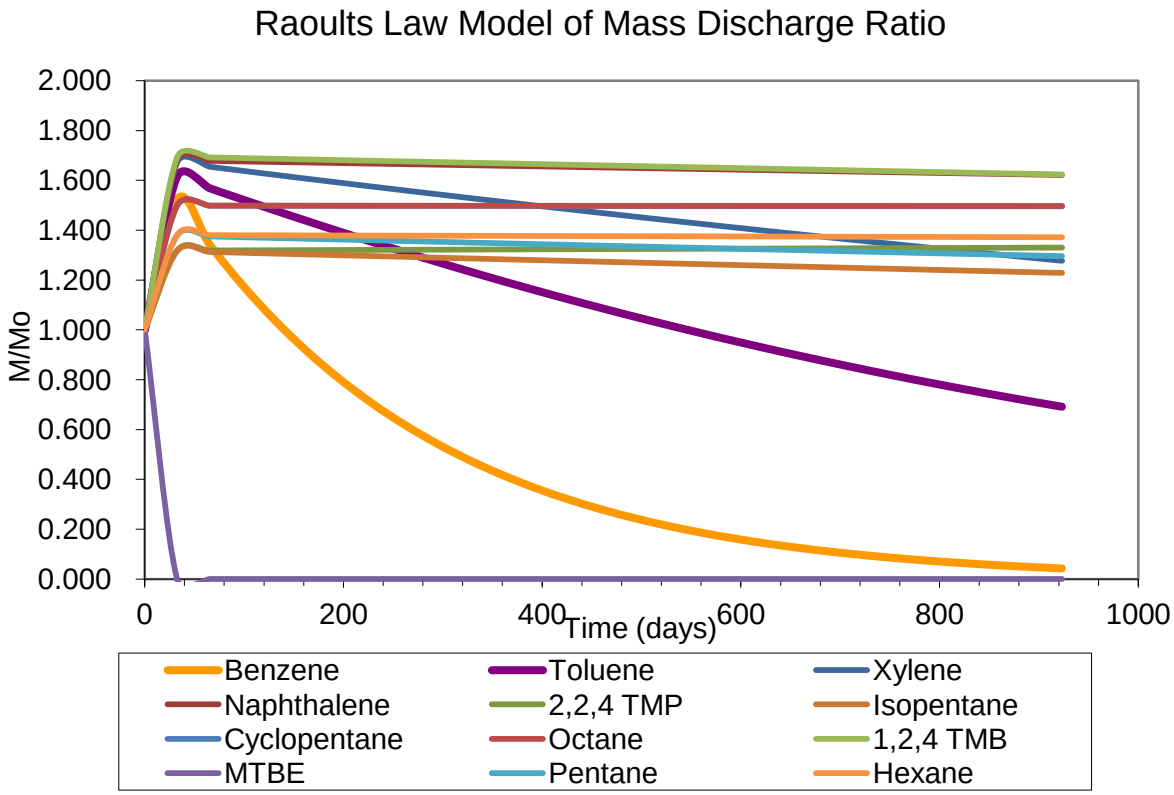

Figure 4.23: Raoult's Law model of mass discharge ratio for BTXN

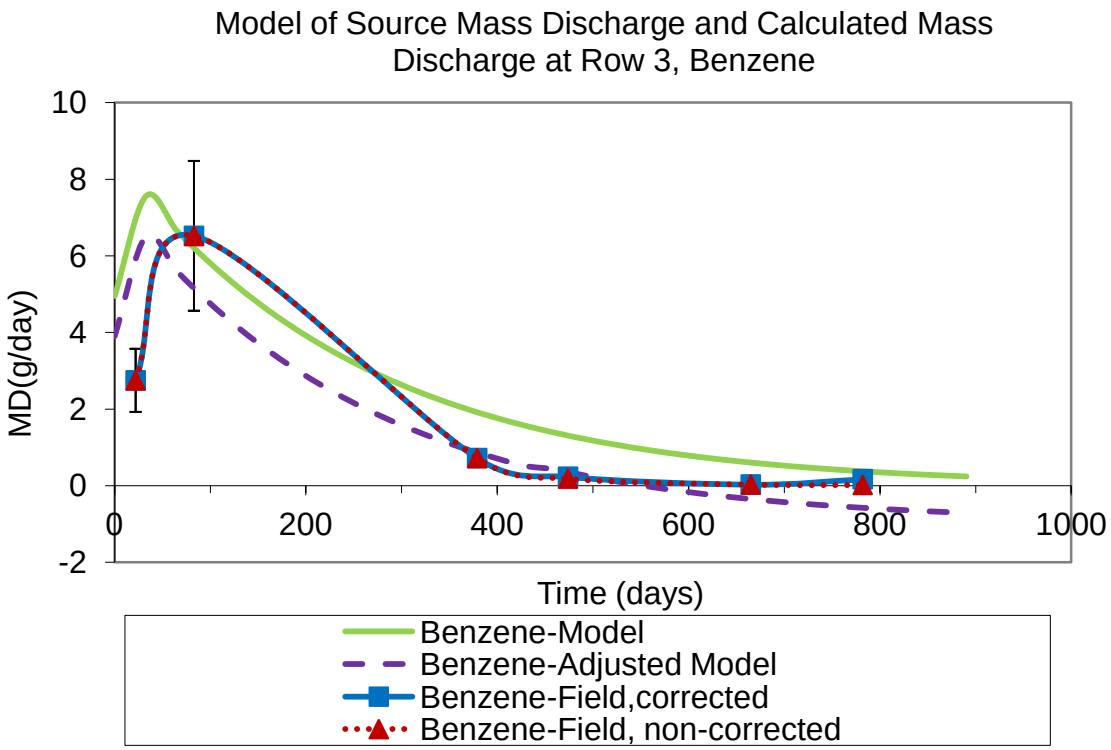
Model of Source Mass Discharge and Calculated Mass Discharge at Row 3, Benzene
MD(g/day)
Time (days)
Benzene-Model
Benzene-Adjusted Model
Benzene-Field,corrected
Benzene-Field, non-corrected

A

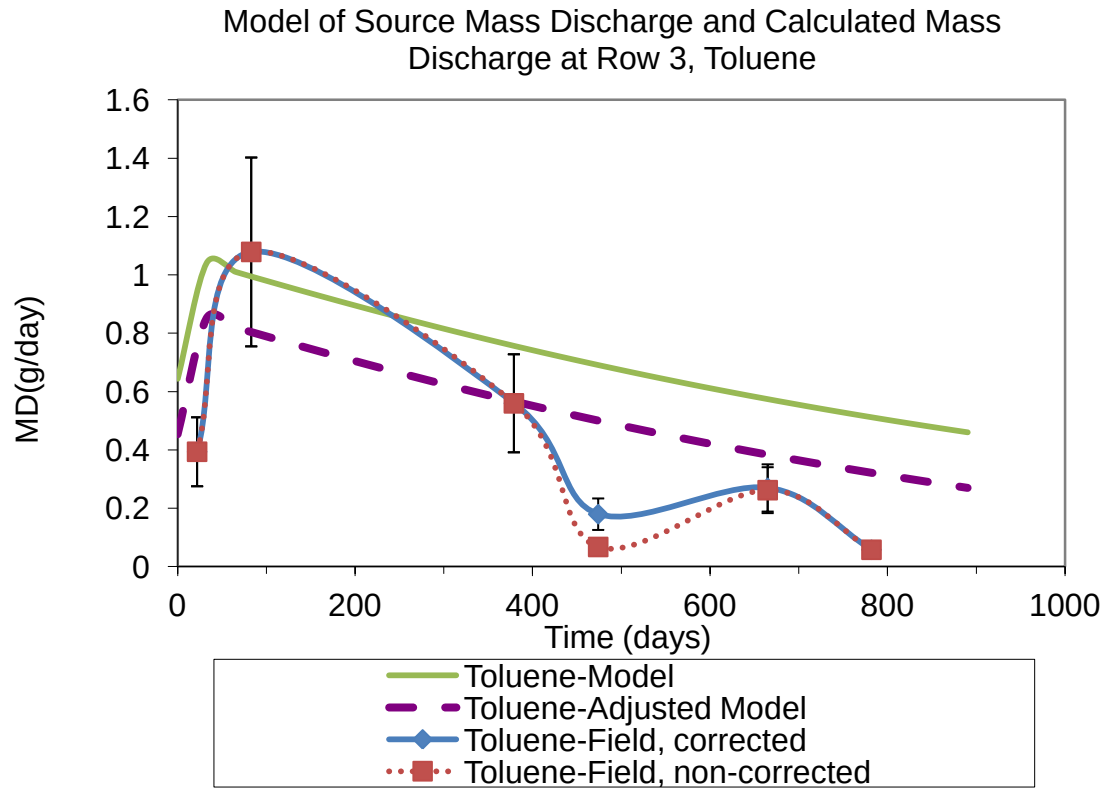
Model of Source Mass Discharge and Calculated Mass Discharge at Row 3, Toluene
MD(g/day)
Time (days)
Toluene-Model
Toluene-Adjusted Model
Toluene-Field, corrected
Toluene-Field, non-corrected

B

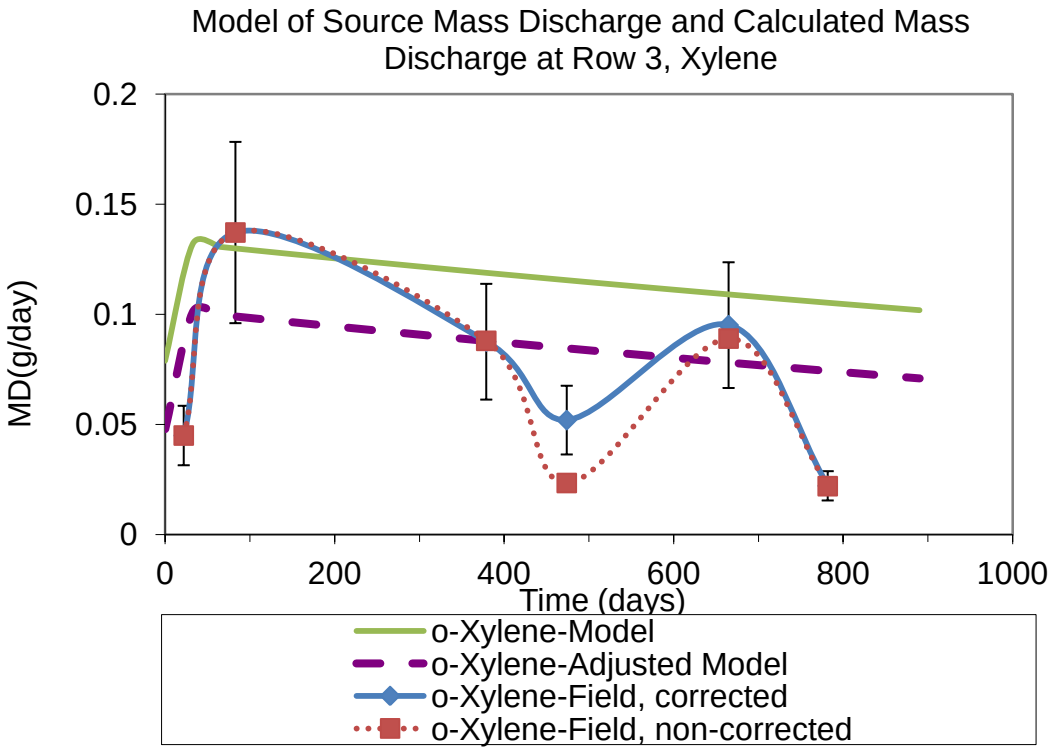

C

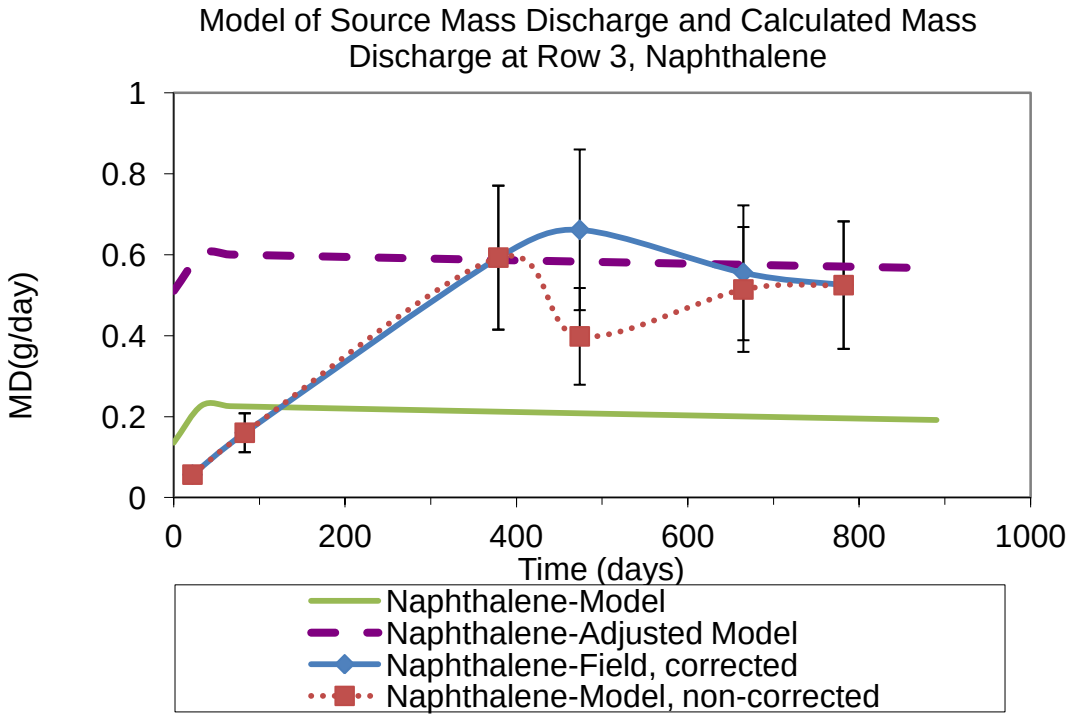

D

Figure 4.24: Raoult's Law model of mass discharge compared with field mass discharge results. A) benzene, B) toluene, C) xylene and D) naphthalene.

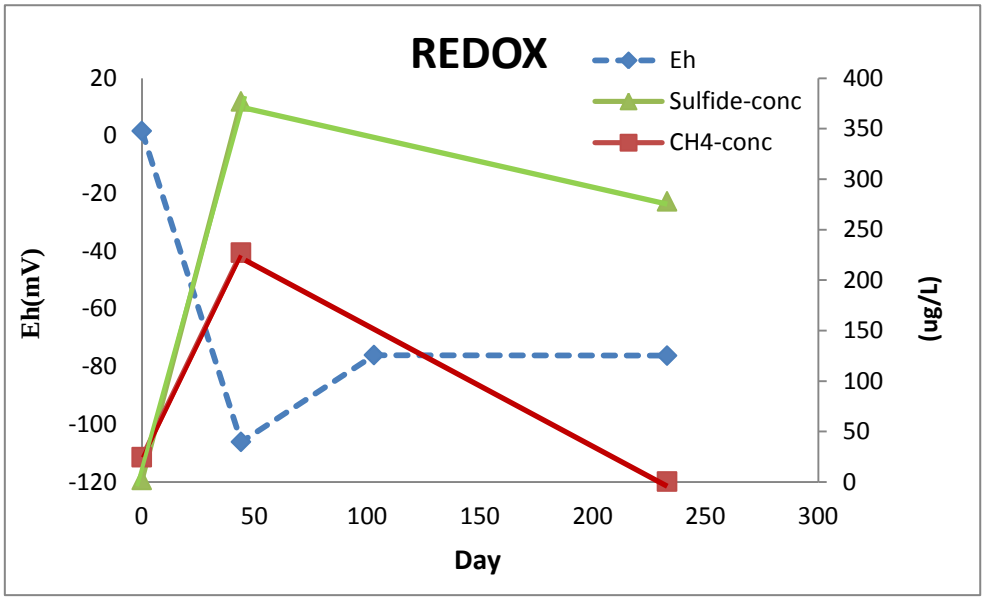
REDOX
Eh
Sulfide-conc
CH4-conc
Eh(mV)
(ug/L)
Day
20
0
-20
-40
-60
-80
-100
-120
400
350
300
250
200
150
100
50
0
0
50
100
150
200
250
300

A

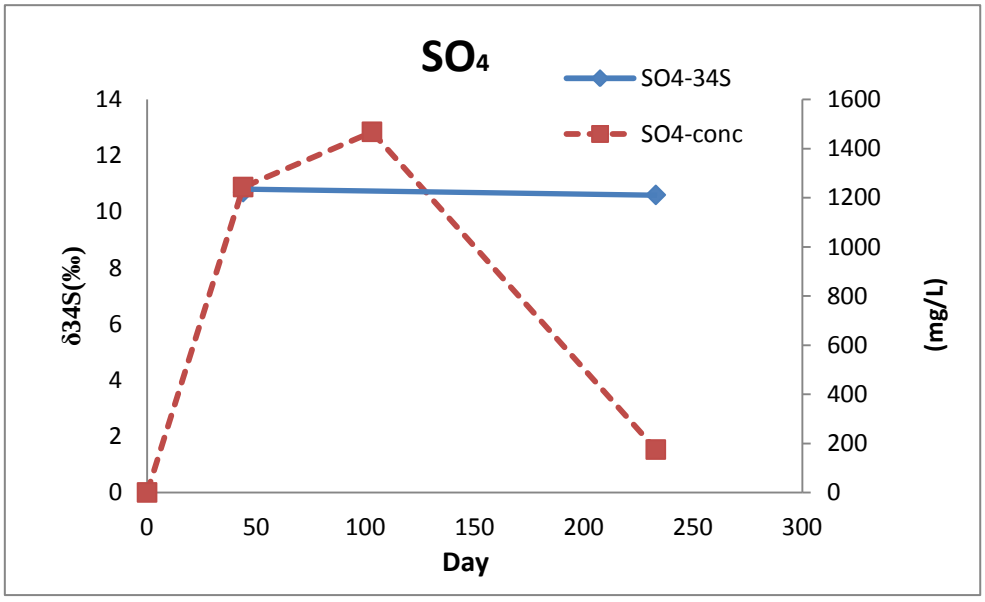
SO4
SO4-34S
SO4-conc
δ34S(‰)
(mg/L)
Day
14
12
10
8
6
4
2
0
1600
1400
1200
1000
800
600
400
200
0
0
50
100
150
200
250
300

B

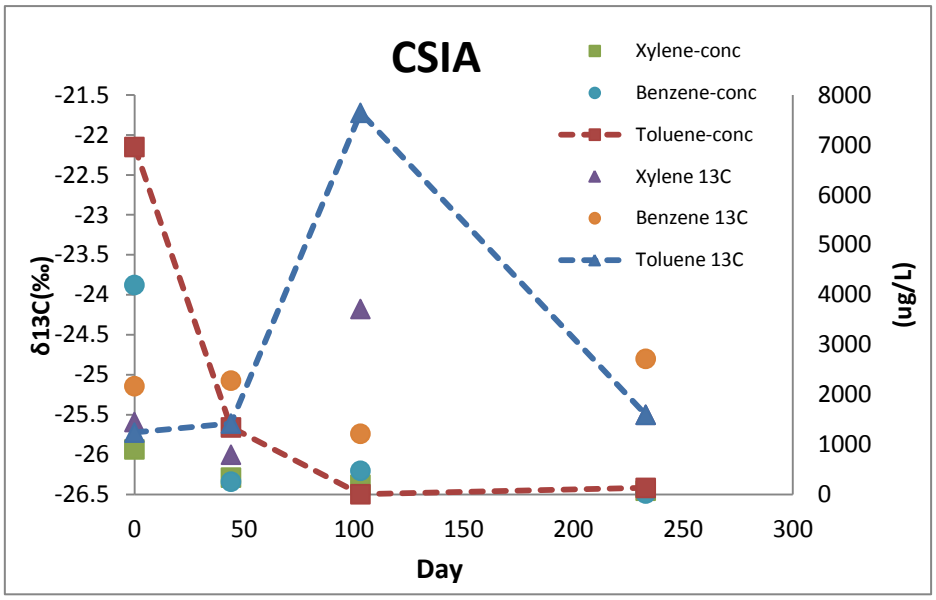

C

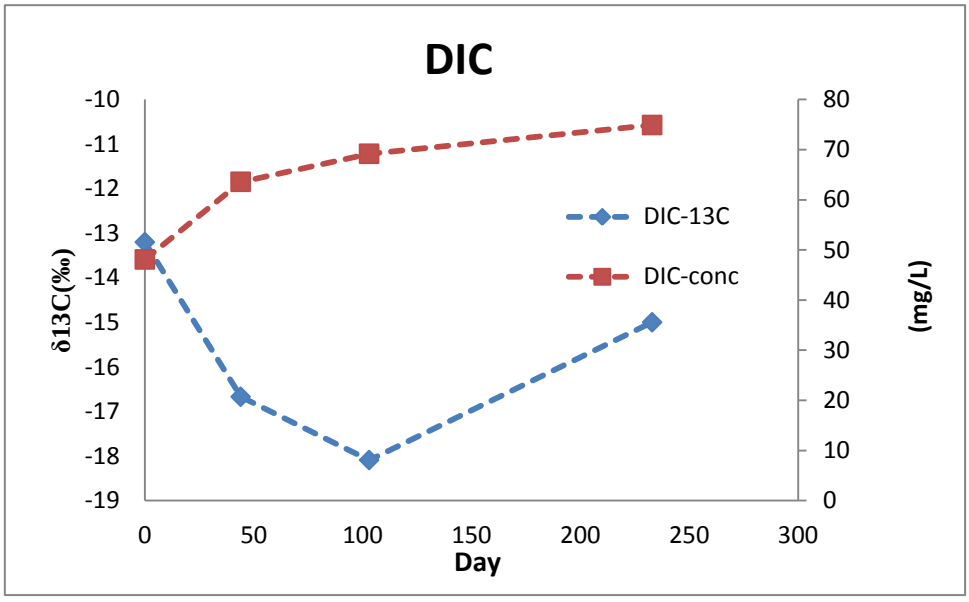

D

Figure 4.25: Progress results for S5-D3.

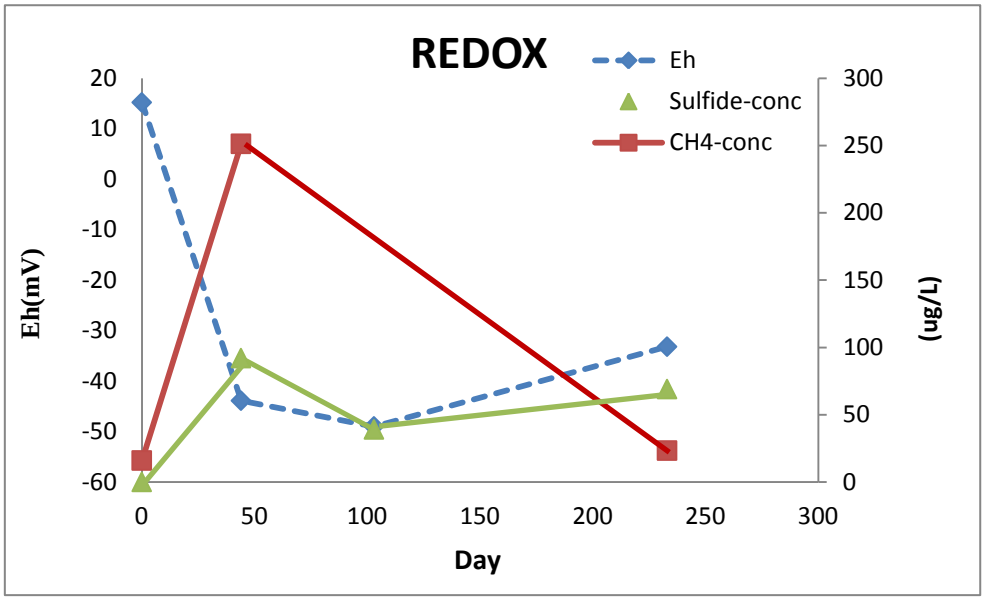
REDOX
Eh
Sulfide-conc
CH4-conc
Eh(mV)
(ug/L)
Day
20
10
0
-10
-20
-30
-40
-50
-60
300
250
200
150
100
50
0
0
50
100
150
200
250
300

A

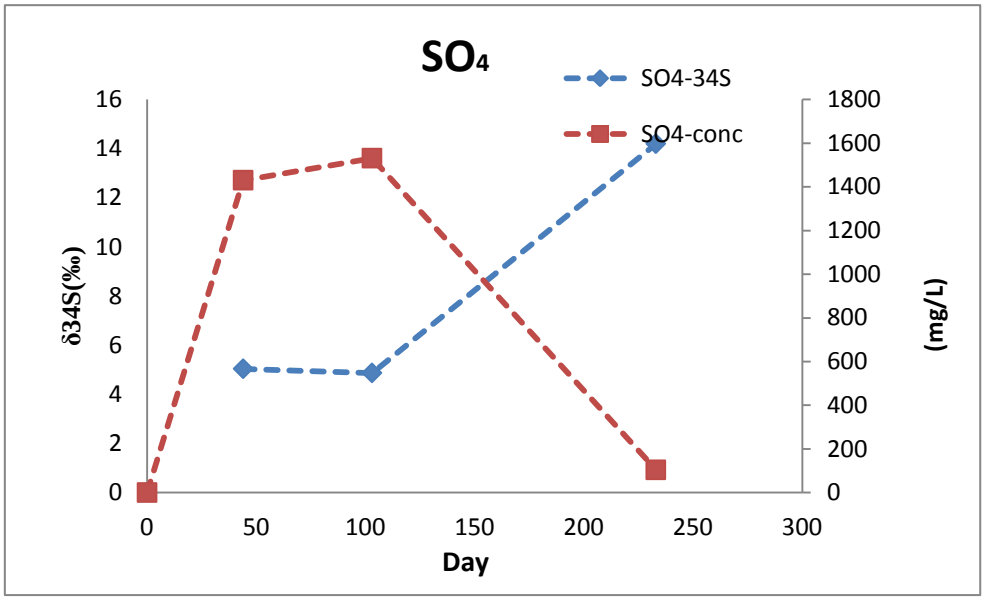
SO4
SO4-34S
SO4-conc
δ34S(‰)
(mg/L)
Day
16
14
12
10
8
6
4
2
0
1800
1600
1400
1200
1000
800
600
400
200
0
0
50
100
150
200
250
300

B

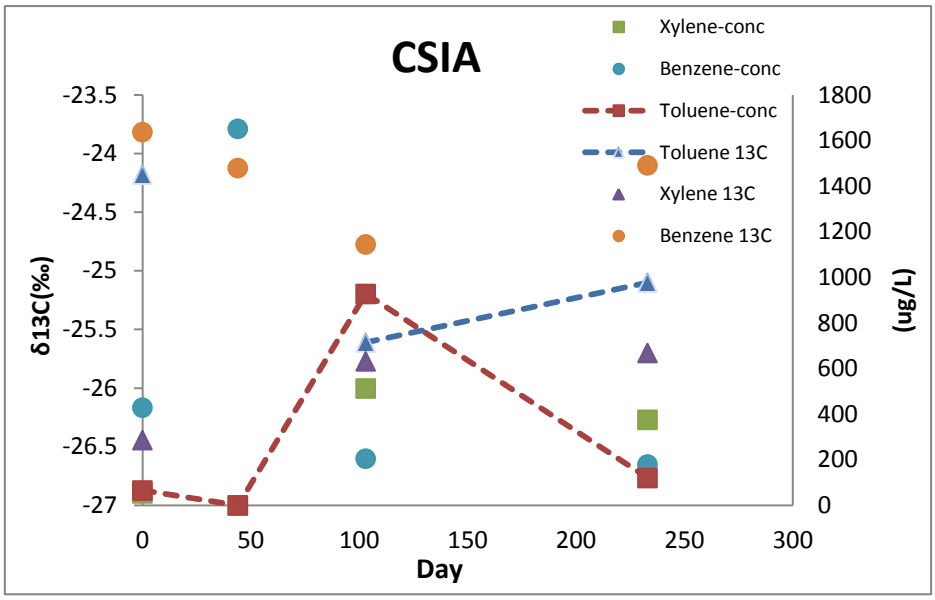

C

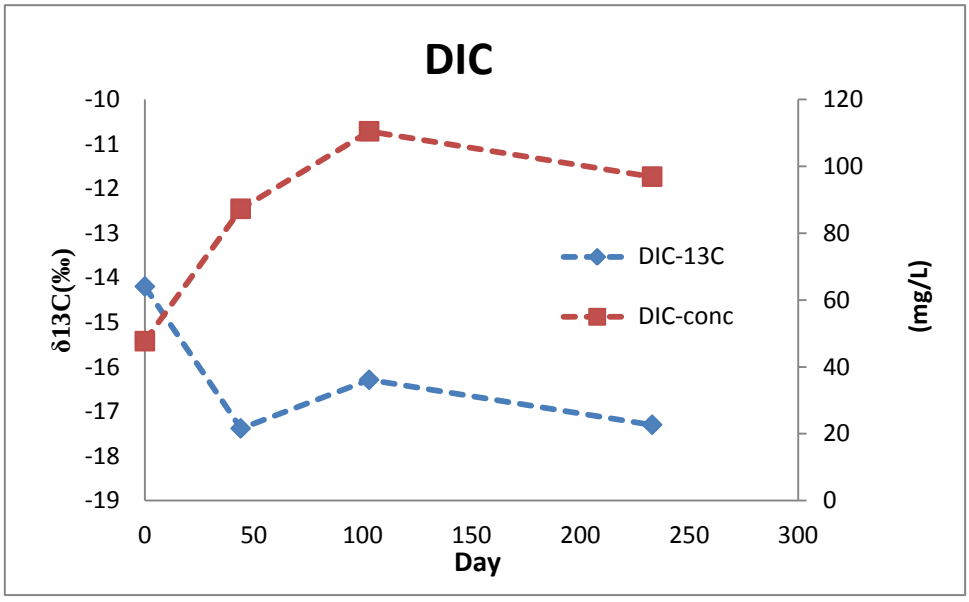

D

Figure 4.26: Progress results for R3-M4-D1.

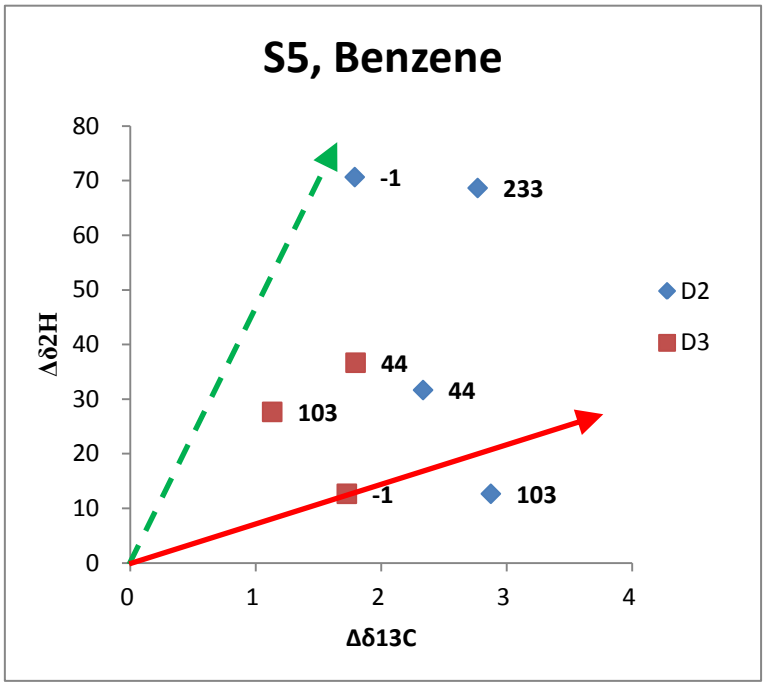
S5, Benzene
80
70
60
50
40
30
20
10
0
Δδ2H
0
1
2
3
4
Δδ13C
-1
233
44
44
103
-1
103
D2
D3

A

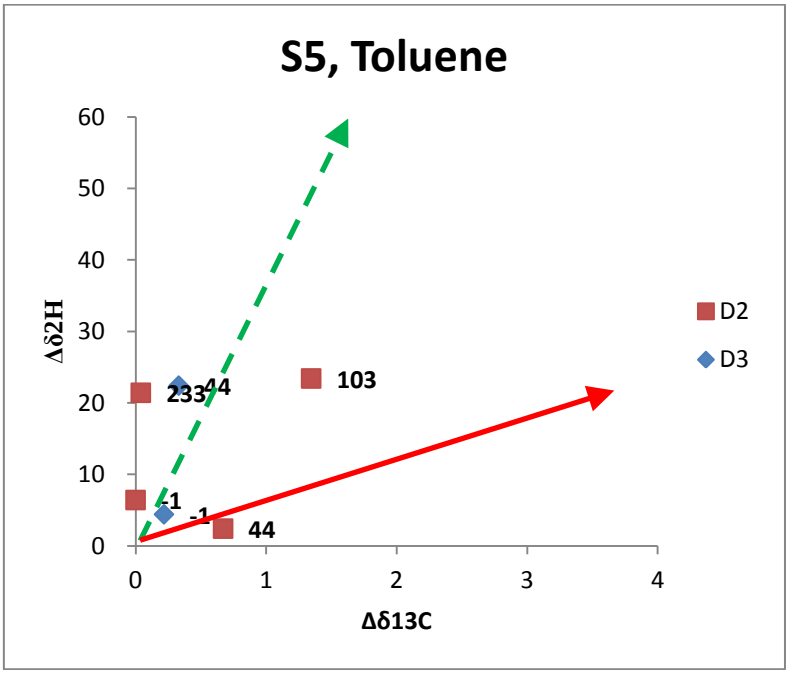
S5, Toluene
60
50
40
30
20
10
0
Δδ2H
0
1
2
3
4
Δδ13C
233
44
103
-1
-1
44
D2
D3

B

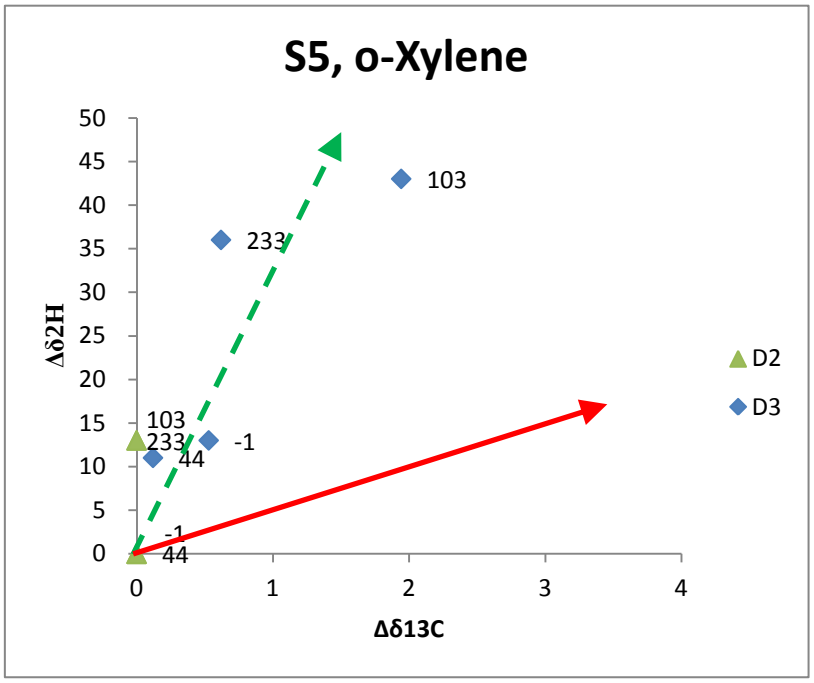

C

Figure 4.27: Dual isotope for A) benzene, B) toluene and C) o-xylene at S5. The red arrow is the anticipated evolution of compounds undergoing aerobic biodegradation, while the green arrow is the evolution anticipated under anaerobic conditions. The Day of the sampling is also indicated beside each point.

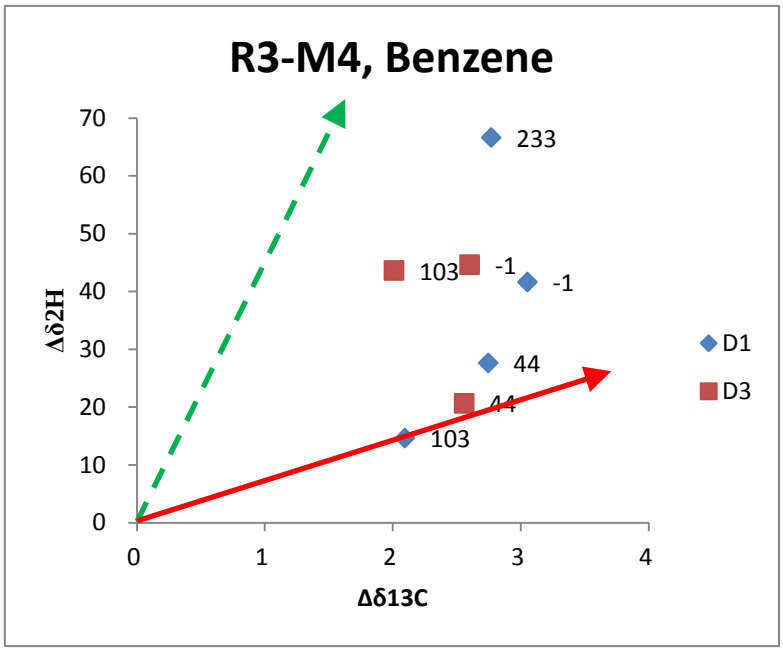
R3-M4, Benzene
70
60
50
40
30
20
10
0
Δδ2H
0
1
2
3
4
Δδ13C
233
103
-1
-1
44
44
103
D1
D3

A

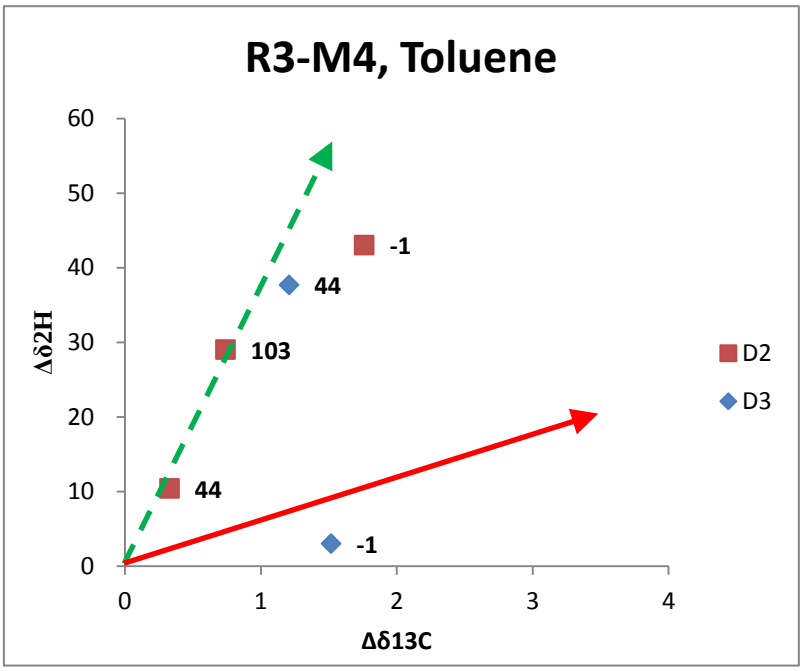
R3-M4, Toluene
60
50
40
30
20
10
0
Δδ2H
0
1
2
3
4
Δδ13C
-1
44
103
44
-1
D2
D3

B

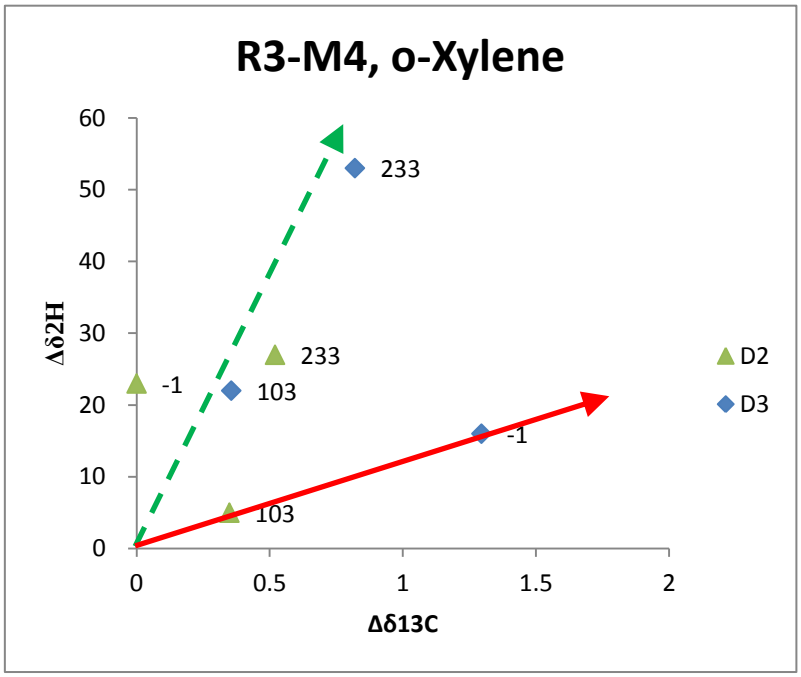

C

Figure 4.28: Dual isotope for A) benzene, B) toluene and C) o-xylene at R3-M4. The red arrow is the anticipated evolution of compounds undergoing aerobic biodegradation, while the green arrow is the evolution anticipated under anaerobic conditions. The Day of the sampling is also indicated beside each point.

Table 4.1: Schedule of field events.

Date	Day	Event
2012/8/15	-388	Source emplacement
2012/9/6	-366	1st mass discharge sampling
2012/11/6	-305	2nd mass discharge sampling
2013/8/27	-9	1st Flux baseline sampling
2013/9/5	-2	Baseline sampling
2013/9/6	-1	1st Process sampling (Row 3)
2013/9/7	0	1st Sulfate application
2013/9/17	10	EC mapping
2013/9/30	23	EC mapping
2013/10/14	37	EC mapping
2013/10/21	44	2nd Process sampling (Row 3)
2013/10/27	50	2nd Process sampling (Row 4)
2013/11/4	58	EC mapping
2013/11/5	59	2nd Sulfate application
2013/11/14	68	EC mapping
2013/12/2	86	EC mapping
2013/12/2	86	2nd Flux sampling
2013/12/19	103	3rd Process sampling (Row 3)
2013/12/19	103	EC mapping
2014/5/13	233	4th Process sampling (Row 3 and Row 4)
2014/6/11	262	3rd Sulfate application
2014/6/26	277	3rd Flux sampling
2014/10/6	394	4th Flux Sampling

Table 4.2: Summary of applications

Application	I	II	III
Date	Sep-7 2013	Nov-5 2013	Jun-11 2014
Volume (m3)	5	5	5
Concentration (g sodium sulfate/L)	5	20	15
Time Required for Infiltration Completed (hour)	18	14	24
Key Observations	Sulfate water more prefer to flow at M1-M3 side than M4-M6 side. It arrived at Row 3 less than 20 days.	Sulfate water infiltrated fastest among all three applications. Density-dependent flow is strong for 20 g sodium sulfate / L solution.	Sulfate arrived at EC1-0.5 mbgs in 30 minutes and at EC1-1 mbgs in 12 hours. Infiltration rate was much slower than the first two applications due to high water table

Table 4.3: EC in source area on Day 10

Sampling Point	Depth (mbgs)	EC (µS/cm)
EC1-D2	1.5	301.7
EC1-D3	2.5	310.7
EC2-D2	1.5	2480
EC2-D3	2.5	412.9
EC2-D4	3.5	312.3
EC3-D2	1.5	866
EC3-D3	2.5	343.7
EC4-D2	1.5	415
EC4-D3	2.5	332.1
S1-D2	1	306
S1-D3	1.5	298.1
S1-D4	2	303.1
S2-D2	1	5080
S2-D3	1.5	1340
S2-D4	2	324.5
S3-D2	1	2903
S3-D3	1.5	361
S3-D4	2	309.6
S4-D2	1	402.8
S4-D3	1.5	312
S5-D2	1	896
S5-D3	1.5	428
S5-D4	2	304.1

Table 4.4: EC in source area on Day 23

Sampling Point	Depth (mbgs)	EC (µS/cm)
EC1-D2	1.5	362
EC1-D3	2.5	392
EC2-D2	1.5	4840
EC2-D3	2.5	556
EC2-D4	3.5	358
EC3-D2	1.5	2850
EC3-D3	2.5	389
EC4-D2	1.5	676
EC4-D3	2.5	360
EC5-D2	1.5	1426
EC6-D2	1.5	393
EC7-D2	1.5	418
EC8-D2	1.5	427
S1-D2	1	348
S1-D3	1.5	340
S1-D4	2	368
S2-D2	1	347
S2-D3	1.5	2730
S2-D4	2	417
S3-D2	1	3210
S3-D3	1.5	2090
S3-D4	2	384
S4-D2	1	377
S4-D3	1.5	380
S5-D2	1	3150
S5-D3	1.5	474
S5-D4	2	347

Table 4.5: EC in source area on Day 37

Sampling Point	Depth (mbgs)	EC (µS/cm)
S2-D2	1	319
S2-D3	1.5	638
S2-D4	2	353
S3-D2	1	551
S3-D3	1.5	906
S3-D4	2	344
S4-D2	1	395
S4-D3	1.5	359
S5-D2	1	1271
S5-D3	1.5	1765
S5-D4	2	436
S5-D5	2.5	375

Table 4.6: EC in source area on Day 68

Sampling Point	Depth (mbgs)	EC (µS/cm)
S1-D1	0.5	350
S1-D2	1	230
S2-D1	0.5	2130
S2-D2	1	11190
S2-D3	1.5	8570
S2-D4	2	2490
S2-D5	2.5	280
S3-D2	1	8120
S3-D3	1.5	5770
S3-D4	2	2400
S3-D5	2.5	1670
S3-D6	3	250
S4-D1	0.5	3610
S4-D2	1	3480
S4-D3	1.5	5810
S4-D4	2	350
S5-D1	0.5	1830
S5-D2	1	4760
S5-D3	1.5	2160
S5-D4	2	290
R2-M2-D1	1.5	10600
R2-M2-D2	1.695	10530
R2-M2-D3	1.89	6510
R2-M2-D4	2.085	4220
R2-M2-D5	2.28	5510
R2-M2-D7	2.67	8540
R2-M2-D8	2.865	310
R3-M4-D1	1.5	1041
R3-M4-D2	1.695	1745
R3-M4-D3	1.89	2140
R3-M4-D4	2.085	2010
R3-M4-D5	2.28	1790
R3-M4-D6	2.67	1480
R3-M4-D7	2.865	980
R3-M4-D8	3.06	440
R3-M4-D9	3.255	250
R3-M4-D10	3.45	230

Table 4.7: EC at source area on Day 86

Sampling Point	Depth (mbgs)	EC (µS/cm)
S1-D1	0.5	350
S1-D2	1	230
S2-D1	0.5	2210
S2-D2	1	660
S2-D3	1.5	2680
S2-D4	2	1770
S2-D5	2.5	250
S2-D6	3	940
S2-D7	3.5	220
S3-D1	0.5	1220
S3-D2	1	1450
S3-D3	1.5	3850
S3-D4	2	560
S3-D5	2.5	220
S4-D1	0.5	1260
S4-D2	1	1220
S4-D3	1.5	810
S4-D4	2	270
S5-D1	0.5	1790
S5-D2	1	2660
S5-D3	1.5	2060
S5-D4	2	1170
S5-D5	2.5	520
S5-D6	3	250
R2-M2-D1	1.5	240
R2-M2-D2	1.695	3990
R2-M2-D3	1.89	1780
R2-M2-D4	2.085	210
R2-M2-D5	2.28	210

Table 4.8: EC at well EC2 on Day 103

Sampling Point	Depth (mbgs)	EC (µS/cm)
EC2-D1	0.5	4290
EC2-D2	1.5	1660
EC2-D3	2.5	3720
EC2-D4	3.5	2390
EC2-D5	4.5	N/A
EC2-D6	5.5	570

Table 4.9: EC at s5, Row 3 and Row 4 on Day 197

Sampling Point	Depth (mbgs)	EC (µS/cm)
S5-D1	0.5	2230
S5-D3	1.5	256
S5-D4	2	231
S5-D5	2.5	221
S5-D6	3	243
R3-M3-D1	1.5	202
R3-M3-D3	1.89	197
R3-M3-D5	2.28	276
R3-M3-D8	2.865	449
R3-M3-D10	3.255	389
R3-M3-D12	3.645	617
R3-M4-D1	1.5	650
R3-M4-D3	1.89	320
R3-M4-D5	2.28	446
R3-M4-D7	2.67	273
R3-M4-D9	3.06	371
R3-M4-D11	3.45	388
R4-M2-D10	3.255	1141
R4-M2-D12	3.645	1251
R4-M2-D13	3.84	1332
R4-M2-D14	5	1588
R4-M3-D1	1.5	525
R4-M3-D2	1.695	611
R4-M3-D5	2.28	985
R4-M3-D7	2.67	698
R4-M3-D9	3.06	745
R4-M3-D11	3.45	1118
R4-M3-D13	3.84	926
R4-M3-D14	5	923
R4-M4-D4	2.085	451
R4-M4-D6	2.475	568
R4-M4-D9	3.06	994
R4-M4-D13	3.84	1496

Table 4.10: Water table fluctuation at MW4 during the first sulfate application.

Elapsed Time (hh/mm/ss)	Water Table (mbgs)
0:00:00	0.28
0:40:00	0.22
1:20:00	0.23
1:45:00	0.22
3:30:00	0.23
5:00:00	0.22

Table 4.11: Water table fluctuations during the second sulfate application.

	Water Table (mbgs)			
Elapsed Time (hh/mm/ss)	MW1	MW2	MW3	MW4
0:00:00	0.34	0.36	0.38	0.48
0:05:00	0.32	0.33	0.36	0.45
0:08:00	0.31	0.315	0.335	0.44
0:20:00	0.265	0.26	0.29	0.38
0:30:00	0.26	0.245	0.28	0.38
0:50:00	0.255	0.24	0.275	0.375
1:15:00	0.255	0.245	0.275	0.375
1:30:00	0.255	0.245	0.275	0.375
2:00:00	0.255	0.245	0.275	0.375
3:00:00	0.255	0.24	0.27	0.37
4:30:00	0.255	0.24	0.27	0.37
5:30:00	0.255	0.24	0.265	0.365
7:30:00	0.25	0.24	0.27	0.365
9:00:00	0.25	0.24	0.27	0.365
24:00:00	0.32	0.35	0.36	0.445

Table 4.12: Water table fluctuations during the third sulfate application.

	Water Table (mbgs)			
Elapsed Time (hh/mm/ss)	MW1	MW2	MW3	MW4
0:00:00	0.18	0.21	0.21	0.3
0:10:00	0.16	0.19	0.18	0.27
1:00:00	0.15	0.18	0.17	0.26
2:10:00	0.16	0.18	0.17	0.25
3:30:00	0.16	0.18	0.17	0.26
7:50:00	0.16	0.18	0.17	0.26

Table 4.13: Baseline sulfide concentration on Day -9.

Sampling point	Depth (mbgs)	Sulfide (ug/L)
R3-L2-D1	0.5	41
R3-L2-D2	0.75	49
R3-L2-D3	1	51
R3-L2-D4	1.25	39
R3-M3-D1	1.5	33
R3-M3-D3	1.89	90
R3-M3-D6	2.475	82
R3-L3-D2	0.75	37
R3-L3-D4	1.25	39
R3-L4-D2	0.75	30
R3-L4-D3	1	39
R3-L4-D4	1.25	32
R3-M5-D1	1.5	10
R3-M5-D3	1.89	16
R4-M1-D1	1.5	36
R4-M2-D2	1.695	5
R4-M2-D4	2.085	ND
R4-M3-D1	1.5	ND
R4-M3-D2	1.695	ND
R4-M3-D4	2.085	11
R4-M3-D5	2.28	3
R4-M4-D2	1.695	27
R4-M4-D4	2.085	3
R4-M4-D5	2.28	9
R4-M5-D1	1.5	25
R4-M5-D3	1.89	55
R4-M5-D5	2.28	20
R4-M6-D4	2.085	24

Table 4.14: Sulfide concentration on Day 197.

Sampling point	Depth (mbgs)	Sulfide (ug/L)
R3-M3-D1	1.5	363
R3-M3-D3	1.89	161
R3-M3-D5	2.28	263
R3-M3-D8	2.865	69
R3-M3-D10	3.255	220
R3-M3-D12	3.645	427
R3-M4-D1	1.5	511
R3-M4-D3	1.89	538
R3-M4-D5	2.28	508
R3-M4-D7	2.67	174
R3-M4-D9	3.06	156
R3-M4-D11	3.45	190
S5-D1	0.5	149
S5-D3	1.5	278
S5-D5	2.5	79
S5-D7	3.5	69
S5-D8	4	87
R4-M3-D11	3.255	79
R4-M4-D4	2.085	82
R3-M4-D13	3.645	57

Table 4.15: Summary of BTXN mass discharge for PHC flux sampling (g/day).

		Row 3			
Day		Benzene	Toluene	Xylene	Naphthalene
-366		2.75	0.39	0.05	0.00
-305		6.52	1.00	0.13	0.16
-9		0.72	0.56	0.09	0.59
86	Corrected	0.23	0.18	0.05	0.49
	Non-corrected	0.18	0.07	0.02	0.39
277	Corrected	0.03	0.27	0.10	0.56
	Non-corrected	0.03	0.26	0.09	0.51
394	Corrected	0.02	0.06	0.02	0.52
	Non-corrected	0.02	0.06	0.02	0.52
		Row 4			
Day		Benzene	Toluene	Xylene	Naphthalene
-9		2.21	0.67	0.15	0.37
277		0.10	0.01	0.02	0.39
394		0.02	0.00	0.00	0.40

Table 4.16: Summary of emplaced NAPL properties and theoretical SO_4^{2-} consumption per unit PHC degradation (mol SO_4^{2-}/ mol PHC).

Compound	Formula	Molar mass (g/mol)	Density (g/mL)	Sulfate stoichiometric requirement (mol SO_4^{2-}/ mol PHC)
2,2,4-TMP	C_8H_{18}	114.23	0.692	6.25
Isopentane	C_5H_{12}	72.15	0.616	4.00
Cyclopentane	C_5H_{10}	70.10	0.751	3.75
Octane	C_8H_{18}	114.23	0.703	6.25
Benzene	C_6H_6	78.11	0.877	3.75
Toluene	C_7H_8	92.14	0.870	4.50
Naphthalene	$C_{10}H_8$	128.17	1.14	6.00
o-Xylene	C_8H_{10}	106.17	0.878	5.25
1-2-4- TMB	C_9H_{12}	120.19	0.876	6,00
MTBE	$C_5H_{12}O$	88.15	0.740	3.75
Hexane	C_6H_{14}	86.18	0.655	4.75
Pentane	C_5H_{12}	72.15	0.626	4.00

5. Summary and Conclusion

The resistivity data collection system was successfully implemented in the Borden sulfate land application experiment. It recorded the change of EC that accurately depicted the pattern of sulfate migration between the source zone and Row 3. The data logger results demonstrate that resistivity probes are useful to adjust sulfate applications. However, as described in section 2.4.3, the data logger provided a logarithmic relationship between the recorded reading X and actual EC, so that the accuracy of X is reduced with increasing EC. The X ranged from 0.2 to 0.83 when EC changes ranged from 300 μS/cm to 8000 μS/cm, while the resolution of X was sharply reduced when EC larger than 8000 μS/cm. The resolution at the EC range of interest (300 – 5000 μS/cm) can be as good as 0.1 μS/cm. Changing the resistor in the data logger can increase the resolution at one EC range, but at a cost in the resolution in other EC range.

According to the sulfate flux monitoring results, the distribution of SO_4^{2-} corresponded well to the EC distribution, confirmed the practicability of using EC as a sulfate indicator. In sulfate applications at other sites, the EC-data logger system should be very useful in quickly defining the pathway of the applied sulfate solution, thus allowing optimization quickly.

The sulfate application was designed using a modeling tool. While it anticipated much of the actual performance seen during the field experiment, it underestimated the advection and overestimated the dispersion. The actual pathway of sulfate migration from each sulfate application was captured through EC and sulfate measurements and was essentially as predicted in the model. The longevity of sulfate in the source was often less than the designed sulfate residence time (40 days). The longevity was good in the shallow source zone, but it was not good at depths greater than 1.5 mbgs.

The SALTFLOW model precisely predicted sulfate flow in the first and third applications, while it underestimated the vertical flow component in the second application. The model is a good tool to simulate density-dependent salt flow when the stratigraphy condition is known. The optimum concentration (density), water mounding, and application location and rate for sulfate solution can be estimated with the modeling tool. According to the EC monitoring

results, 5 g sodium sulfate/L did not provide sufficient depth penetration, while 15-20 g sodium sulfate/L created excessively deep flow downgradient. Therefore, about 10 g/L Na_2SO_4 could be an ideal concentration for this application approach.

The height between pond level and the water table can also be controlled in this application method. This height also affects the sulfate water penetration at the source zone. For the Borden case, infiltration of a 10 g/L Na_2SO_4 solution with an infiltration pond height about 10 cm above the initial water table would provide the best coverage of the source zone and the dissolved PHC plume.

Strongly anaerobic conditions and sulfate reduction and methanogenesis were promoted by the sulfate application. Biomarkers and CSIA indicate both aerobic and anaerobic biodegradation occurred. Both sulfate reduction and methanogenesis might be involved in the PHC mass removal. Toluene and o-xylene mass discharges, corrected for dilution by the applied water, were lower than predicted by a Raoult's Law source depletion model, suggesting TX mass loss was promoted by sulfate application. No such enhanced mass loss was evident for benzene and naphthalene after sulfate application. Results suggested biodegradation under sulfate reducing conditions account for much of the attenuation of toluene and o-xylene. No enhanced benzene mass discharge decline due to sulfate application was demonstrated. Source depletion and ongoing biodegradation was likely the dominant processes. CSIA and biomarker analyses confirmed some benzene aerobic/anaerobic biodegradation occurred.

Overall, the sulfate land application appears to be a viable method to enhance PHC mass removal from source zones and associated plumes. The delivery requires careful hydrogeological design and some real-time monitoring of EC or sulfate to confirm sulfate is delivered as required. $^{13}C_{DIC}$ and $^{34}S_{SO4}$were effective for monitoring the occurrence of sulfate reduction. Periodic monitoring of both ^{13}C and ^{2}H isotopic composition of dissolved hydrocarbons, especially BTXN, appears to provide a useful tool to confirm the biodegradation processes accounting for mass loss. Consideration of the fate of the high concentrations of Na^+ and $SO_4^=$ being applied is also required to confirm water quality goals are not compromised by the sulfate application. Additional field applications are underway to further assess this technology and the tools to efficiently document its performance.

Reference

Acton, D.W., and J.F. Barker. 1992. In Situ Biodegradation Potential of Aromatic Hydrocarbons in Anaerobic Groundwaters. Journal of Contaminant Hydrology, 9: 325-352.

Aelion, C.M., P. Iochener, D. Hunkeler, R. Aravena, 2009. Environmental Isotopes in Biodegradation and Bioremediation. Taylor & Francis Group, LLC. Boca Raton, FL, USA.

Anderson, T.R., and D.R. Lovley. 2000. Anaerobic Bioremediation of Benzene under Sulfate-Reducing Conditions in a Petroleum-Contaminated Aquifer. Environmental Science & Technology. Vol. 34, No, 11, 2261-2266

Appelo, C.A.J., and D. Postma. 2005. Geochemistry, Groundwater and Pollution 2nd edition. Ben Akkerman collection Stedelijk Museum, Amsterdam, Netherland.

Aravena, R., and D. Hunkeler, 2009. Investigating the origin and fate of organic contaminants in groundwater using stable isotope analysis, Ch. 8 in: Environmental Isotopes in Biodegradation and Bioremediation, editors: Aelion, M.C., Höhener, P., Hunkeler, D., Aravena, R. CRC Press, 464 pp.

Atlas, R.M. 1981. Microbial Degradation of Petroleum Hydrocarbons: An Environmental Perspective. Micro-biological Reviews 45, no. 1: 180-209.

Bear, J., 1972. Dynamics of Fluids in Porous Media. American Elsevier Publishing Company, Inc. New York, USA.

Beland-Pelletier, C., M. Fraser, J. Barker, and T. Ptak. 2011. Estimating Contaminant Mass Discharge: A Field Comparison of the Multilevel Point Measurement and the Integral Pumping Investigation Approaches and Their Uncertainties. Journal of Contaminant Hydrology, 122 (2011) 63-75.

Bouchard, D. and D. Hunkeler, 2014. Solvent-based Dissolution Method to Sample Gas-phase Volatile Organic Compounds for Compound-specific Isotope Analysis. Journal of Chromatography A, 1325 (2014) 16-22.

Chapelle, F.H. 1999. Bioremediation of Petroleum Hydrocarbon-contaminated Ground Water: The Perspectives of History and Hydrology. Ground Water 37. No. 1: 122-132.

Chen, Y.D., L. Gui, J.F. Barker, and Y. Jiang. 2008. Biodegradability of Trimethylbenzene Isomers under the Strictly Anaerobic Conditions in Groundwater Contaminated by Gasoline. Environmental Geology, 56 (6): 1123-1128.

Chen, Y.D., J.F. Barker, and L. Gui. 2007. A Strategy for Aromatic Hydrocarbon Bioremediation under Anaerobic Conditions and the Impact of Ethanol: A Microcosm Study. Journal of Contaminant Hydrology 96 17-31.

Cherry, J.A., and P.E. Johnson, A multi-Level Device for Monitoring in Fractured Rock, Ground-Water Monitoring Review, 2(3), 41-44, 1982.

Clark, I.D. and P. Fritz. 1997. Environmental Isotopes in Hydrogeology. CRC Press LLC, Boca Raton, Florida, USA.

Corseuil, H.X., C. Hunt, R. dos Santos Ferreira, and P.J.J. Alvarez. 1998. The Influence of the Gasoline Oxygenate Ethanol on Aerobic and Anaerobic BTX Biodegradation. Water Research 32 (7), 2065-2072.

Cunningham, J.A., H. Rahme, G.G. Hopkins, C. Lebron, and M. Reinhard. 2001. Enhanced

In-Situ Biodegradation of BTEX-Contaminated Groundwater by Combined Injection of Nitrate and Sulfate. Environmental Science and Technology 35:1663-1670.

Deutsch, W.J. 1997. Groundwater Geochemistry: Fundamentals and Applications to Contamination. New York: Lewis Publishers.

Einarson, M. 2006. Multilevel Ground-Water Monitoring. Practical Handbook of Environmental Site Characterization and Ground-Water Monitoring, Second Edition. 807-848.

Fraser, M.J., 2007. Long-Term Fate of an Emplaced Coal Tar Creosote Source. MSc. Thesis, Department of Earth Sciences, University of Waterloo. Waterloo, Ontario, Canada.

Freitas, J.G. and J.F. Barker. 2008. Sampling VOCs with Porous Suction Samplers in the Presence of Ethanol: How Much Are We Losing? Ground Water Monitoring & Remediation 28, no. 3 83-92.

Frind, E.O., 1982 Simulation of Long-Term Transient Density-Dependent Transport in Groundwater, Adv. Water Resour., 5(2) 73-88, 1982a.

Habicht, K.S., L. Salling, B. Thamdrup, and D.E. Canfield. 2005. "Effect of Low Sulfate Concentrations on Lactate Oxidation and Isotope Fractionation During Sulfate Reduction by *Archaeoglobus fulgidus* Strain Z. Applied Environmental Microbiology 71, no. 7: 3770-3777

Hach Company. 2004. DR/2400 Spectrophotometer Procedure Manual, Method 8131. 747-750.

Hunkeler, D., N. Andersen, R. Aravena, S.M. Bernasconi, and B.J. Butler, 2001. Hydrogen and carbon isotopic fractionation during aerobic biodegradation of benzene. *Environ. Sci. Technol.* 35: 3462–3467.

ITRC, 2010. Use and Measurement of Mass Flux and Mass Discharge. ITRC Integrated DNAPL Site Strategy Team. Washington, DC.

Khan, F.I., T. Husain, and R. Hejazi. 2004. An Overview and Analysis of Site Remediation Technologies. Journal of Environmental Management, 71, 95-122.

King, M.W.G., and J.F. Barker. 1999. Migration and Natural Fate of a Coal Tar Creosote Plume: 1. Overview and Plume Development. Journal of Contaminant Hydrology 39, no. 3–4: 249–279.

Kovacik, G.R. 2013. Field Implementation of CO_2 Supersaturated Water Injection. MSc. Project report, Department of Earth Sciences, University of Waterloo. Waterloo, Ontario, Canada.

Leahy, J.G., and R.R. Colwell. 1990. Microbial Degradation of Hydrocarbons in the Environment. Microbiological Reviews 52, no. 3: 305-315.

Linderfelt, W.R., 1994. Field Study of Capture Zones in a Shallow Sand Aquifer. Ph.D. Thesis, New Mexico Institute of Mining and Technology, Socorro, New Mexico.

Lunardini, Jr., R.C, and R.L. Dickey, III. 2003. Enhanced Anaerobic Bioremediation of Petroleum Hydrocarbons in Groundwater Using Sulfate. In In-Situ and On-Site Bioremediation – 2003. Processings of the Seventh International In Situ and On-Site Bioremediation Symposium. Ed. V.S. Magar and M.E. Kelley. Columbus, Ohio: Battelle Press.

Mackay, D.M., D.L. Freyberg, and P.V. Roberts. 1986. A Natural Gradient Experiment on Solute Transport in a Sand Aquifer: 1. Approach and Overview of Plume Movement.

Water Resources Research 22, 2017-2029.

Mancini, S.A., A.C. Ulrich, G. Lacrampe-Couloume, B. Sleep, E.A. Edwards, and B. Sherwood Lollar. 2003. Carbon and hydrogen isotopic fractionation during anaerobic biodegradation of benzene,*Appl. Environ. Microbiol.* 69: 191–198.

Meckenstock, R.U., B. Morasch, C. Gribler, and H.H. Richnow, 2004. Stable isotope fractionation analysis as a tool to monitor biodegradation in contaminated aquifers. J. Contam. Hydrol. 75: 215-255.

Mocanu, M.T., 2006. Behavior of Oxygenates and Aromatic Hydrocarbons in Groundwater from Gasoline Residuals. MSc. Thesis, Department of Earth Science, University of Waterloo. Waterloo, Ontario, Canada.

Mohsen, M.S., and V.P. Singh. 1990. A Note on Saltwater Intrusion in Costal Aquifers. Water Resource Management 4: 123-134, Kluwer Academic Publishers.

Molson, J.W., and E.O. Frind. 2013. SALTFLOW Version 3.0 User Guide, Density-Dependent Flow and Mass Transport Model in Three Dimensions. Department of Earth Science, University of Waterloo. Waterloo, Ontario, Canada.

Patrick, G.C. and J.F. Barker, 1985. A Natural-Gradient Tracer Study of Dissolved Benzene, Toluene and Xylene in Ground Water. Proc. of the Second Canadian/American Conference on Hydrogeology: ”Hazardous Wastes in Ground Water, A Soluble Dilemma,” Banff, Alberta, Canada, June 25-29, 1985, National Water Well Assoc., Dublin, OH, USA, pp. 141-147.

Roychoudhury, A.N., and D.W. McCormick. 2006. Kinetics of Sulfate Reduction in a Coastal Aquifer Contaminated with Petroleum Hydrocarbons. Biogeochemistry 81:17-31.

Stevenson, D.R., 2013. Developing a Probe for Real-Time Monitoring of Reagent Injections. MASc. Thesis, Department of Civil Engineering, University of Waterloo. Waterloo, Ontario, Canada.

Strebel, O., Boettcher, J. and Fritz, P., 1990. Use of isotope fractionation of sulfate-sulfur and sulfate-oxygen to assess bacterial desulfurication in a sandy aquifer. J. Hydrol., 121: 155-172.

Sudicky, E.A., and W.A. Illman. 2011. Lessons Learned from a Suite of CFB Borden Experiments. Ground Water. Vol. 49, No. 5. 630-648

Sudicky, E.A., 1986. A Natural Gradient Experiment on Solute Transport in a Sand Aquifer: Spatial Variability of Hydraulic Conductivity and Its Role in the Dispersion Process. Water Resources Research 22, 2069-2082.

Sudicky, E.A, J.A. Cherry, and E.O. Frind., 1983. Migration of Contaminants in Groundwater at a Landfill: a Case Study: 4. A Natural Gradient Dispersion Test. Journal of Hydrology 63, 81-108.

Suthersan, S., J. Horst, D. Nelson, and M. Schnobrich. 2011. Insights from years of performance that are shaping injection-based remediation systems. Remediation, Spring 2011, pp.9-25.

Suthersan, S., K. Houston, M. Schnobrich, and J. Horst. 2011. Engineered Anaerobic Bio-Oxidation Systems for Petroleum Hydrocarbon Residual Source Zones with Soluble Sulfate Application. Ground Water Monitoring & Remediation 31, no. 3/ Summer 2011

Wiedemeier, T.H., H.S. Rifai, C.J. Newell, and J.T. Wilson. 1999. Natural Attenuation of

Fuels and Chlorinated Solvents in the Subsurface. New York: John Wiley and Sons, Inc.

Appendix A

List of selected monitoring points for EC measurements in Figure 3.1 - 3.6, EC measurement for Day -9, 23, 37, 58, 86 and 103.

Sampling Day	Row 3				Row 4			
-9	M1-D1	M1-D4	M1-D8		M1-D1	M1-D4	M1-D8	
	M2-D1	M2-D2	M2-D4	M2-D6	M2-D2	M2-D4	M2-D6	M2-D8
	M2-D8	M2-D10	M2-D12		M2-D10	M2-D12		
	M3-D1	M3-D2	M3-D3	M3-D4	M3-D1	M3-D2	M3-D4	M3-D5
	M3-D5	M3-D6	M3-D7	M3-D9	M3-D7	M3-D9	M3-D11	M3-D13
	M3-D11	M3-D13			M4-D2	M4-D3	M4-D4	M4-D5
	M4-D2	M4-D3	M4-D4	M4-D5	M4-D7	M4-D9	M4-D11	M4-D13
	M4-D6	M4-D7	M4-D9	M4-D11	M5-D1	M5-D3	M5-D5	M5-D11
	M4-D13				M6-D4	M6-D10		
	M5-D1	M5-D3	M5-D5	M5-D8	L1-D2			
	M5-D11				L2-D2	L2-D3	L2-D4	
	M6-D4	M6-D10			L3-D2	L3-D3	L3-D4	
	L2-D1	L2-D2	L2-D3	L2-D4	L4-D2	L4-D3	L4-D4	
	L3-D2	L3-D4			L5-D4			
	L4-D2	L4-D3	L4-D4					

Sampling Day	Row 3							
23	M1-D1	M1-D2	M1-D3	M1-D4				
	M2-D1	M2-D2	M2-D3	M2-D4	M2-D5			
	M3-D1	M3-D2	M3-D3	M3-D4				
	M4-D1	M4-D2	M4-D3					
	M5-D1	M5-D2	M5-D3					
	L1-D2	L1-D3	L1-D4					
	L2-D2	L2-D3	L2-D4					
	L3-D2	L3-D3	L3-D4					
	L4-D2	L4-D3	L4-D4					
	L5-D2	L5-D3	L5-D4					
37	M1-D1	M1-D2	M1-D3	M1-D4	M1-D5	M1-D6		
	M2-D1	M2-D2	M2-D3	M2-D4	M2-D5	M2-D6	M2-D7	M2-D8
	M2-D10							
	M3-D1	M3-D2	M3-D3	M3-D4	M3-D5			
	M4-D1	M4-D2	M4-D3	M4-D4	M4-D5	M4-D6	M4-D7	M4-D8
	M5-D1	M5-D2	M5-D3	M5-D4	M5-D5	M5-D6		
	M6-D1	M6-D2	M6-D3	M6-D4				
	L1-D2	L1-D3	L1-D4					
	L2-D2	L2-D3	L2-D4					
	L3-D2	L3-D3	L3-D4					
	L4-D2	L4-D3	L4-D4					
	L5-D2	L5-D3	L5-D4					

Sampling Day	Row 3							
58	M1-D1	M1-D2	M1-D3	M1-D4	M1-D5	M1-D6	M1-D7	M1-D8
	M1-D9							
	M2-D1	M2-D2	M2-D3	M2-D4	M2-D5	M2-D6	M2-D9	M2-D10
	M2-D13							
	M3-D1	M3-D2	M3-D3	M3-D5	M3-D6	M3-D8	M3-D9	M3-D10
	M4-D1	M4-D2	M4-D3	M4-D4	M4-D5	M4-D6	M4-D7	M4-D8
	M4-D9	M4-D10	M4-D11	M4-D12				
	M5-D1	M5-D2	M5-D3	M5-D5	M5-D6	M5-D7	M5-D8	
	M6-D1	M6-D3	M6-D4	M6-D7				
	L1-D1	L1-D2	L1-D3	L1-D4				
	L2-D1	L2-D2	L2-D3	L2-D4				
	L3-D2	L3-D3						
	L4-D1	L4-D2	L4-D3	L4-D4				
	L5-D1	L5-D2	L5-D3	L5-D4				
86	M1-D1	M1-D8						
	M2-D1	M2-D2	M2-D3	M2-D4	M2-D5	M2-D6	M2-D9	M2-D10
	M2-D13	M2-D14						
	M3-D1	M3-D2	M3-D3	M3-D5	M3-D6	M3-D9	M3-D11	M3-D13
	M4-D1	M4-D2	M4-D3	M4-D4	M4-D5	M4-D6	M4-D7	M4-D8
	M4-D9	M4-D10	M4-D11	M4-D12	M4-D13	M4-D14		
	M5-D1	M5-D2	M5-D3	M5-D5	M5-D8	M5-D9	M5-D10	M5-D13
	L1-D1	L1-D3						
103	M2-D1	M2-D2	M2-D3	M2-D4	M2-D5	M2-D6	M2-D9	M2-D10
	M2-D13	M2-D14						
	M3-D1	M3-D2	M3-D3	M3-D5	M3-D6	M3-D8	M3-D9	M3-D10
	M3-D11	M3-D12	M3-D14					
	M4-D1	M4-D2	M4-D3	M4-D4	M4-D5	M4-D6	M4-D7	M4-D8
	M4-D9	M4-D10	M4-D11	M4-D12	M4-D13	M4-D14		
	M5-D1	M5-D3	M5-D5	M5-D6	M5-D7	M5-D9	M5-D10	M5-D12
	M5-D13	M5-D14						

Appendix B

Resistivity Data Logger System Development

B1: Field Performance, First Period (Sep 7th 2013 – Nov 3rd 2013)

Readings from the datalogger in this period ranged between 0.9995 – 1.0000 (Figure B1, enlarged part) for points where 0.0 - 3 g/L Na_2SO_4 was expected. The range of readings was too small to interpret. The arrival of sulfate could perhaps be detected, but the dilution could not be estimated.

Several tests were then carried out in the lab to confirm the operation of the probes, which had been constructed in house (Section 2.4.2). Solutions having ECs of 400, 2000, 4000, and 6000 μS/cm were used in the tests. Results showed that the higher the EC, the larger the response, which means the probes detected various EC values. However, the response value still ranged only from 0.99 – 1.00; too small for our purpose.

B2: Field Performance, Second Period (Nov 5th 2013 – Dec 20th 2013)

Clearly modification to the data logger and/or to the programming code was required in order to enlarge the range of response. A resistor with a specific resistance was added to the datalogger circuit board to control the reading range, and the CRBasic code was also modified accordingly. After that, however, the field response was still poor having a consistently decreasing trend instead of an increasing trend when the manually measured EC was increasing. The probe readings ranged only from 0.95 to 0.92, which is still too narrow a range (Figure 3.7, after vertical line). Another puzzling phenomenon was that all the probes had the same response at the same time. Therefore, it appears that the data taken from that period was not mainly responding to actual EC, or at least some other parameter overwhelmed the effect of sample EC. Perhaps the system was responding mainly to changes in temperature, because the downward trend of data correspond to the decreasing temperature during that period of time when the season was turning into winter, and temperature impacted all probes.

B3: Lab Efforts (Feb 6th 2014 – Feb 20th 2014)

Since the measurement object of the probe was still not being met, another attempt was made to confirm the validity of code and wire connection.

At the beginning of the lab tests, identical code and connections were firstly used to test the response of a single probe in tap water and DI water that have dramatically different EC. This test suggested that the probe measured some parameter, but clearly not EC. A multiplexer was also added in later tests to double-check the multiple-probe operation, but the results still led to the same confusion.

Then, a new wire connection between multiplexer and data logger, and a different code with lower delay time were used in another lab test. Three probes were tested in 3 different Na_2SO_4 solutions (EC = 300, 4000 8000 μS/cm). The probes worked properly under the new settings, but the measurement range (from 0.7 to 0.9) was still not sufficiently sensitive.

As discussed in section 2.4.3, the datalogger measurement, X, is related to the resistance of the solution (R_s) and the data logger system (R_f) as shown in equation 2.3. Since R_s is a

constant, changing the resistor connected to the datalogger affects R_f, and thus changing the ranges of measured values, X. Therefore, different resistors were tried and a resistance between 500 and 600 ohm provided the best range of X. A 557 ohm resistor was selected as it gave an X ranging from 0.2 to 0.83 for solutions having EC from 300 to 8000 µS/cm.

Figure B2 shows the curve between EC and data logger reading X for the lab test. The comparison indicates the datalogger system works properly and the measurements are representative of solution EC.

Figure B1: Datalogger readings from Sep 7th 2013 to Dec 20th 2013. The flat part shows the first period of field measurement and the decreasing trend shows the second period.

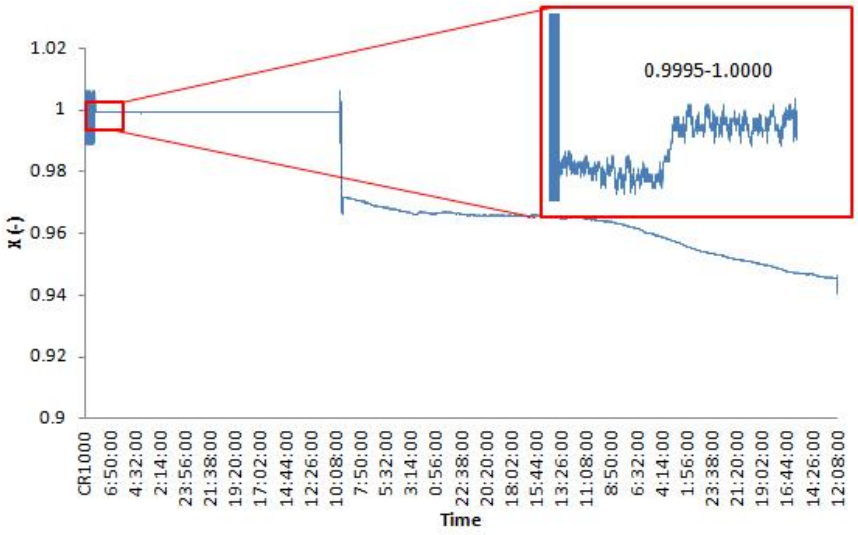

Figure B2: Relationship between EC and datalogger reading for a successful lab test.

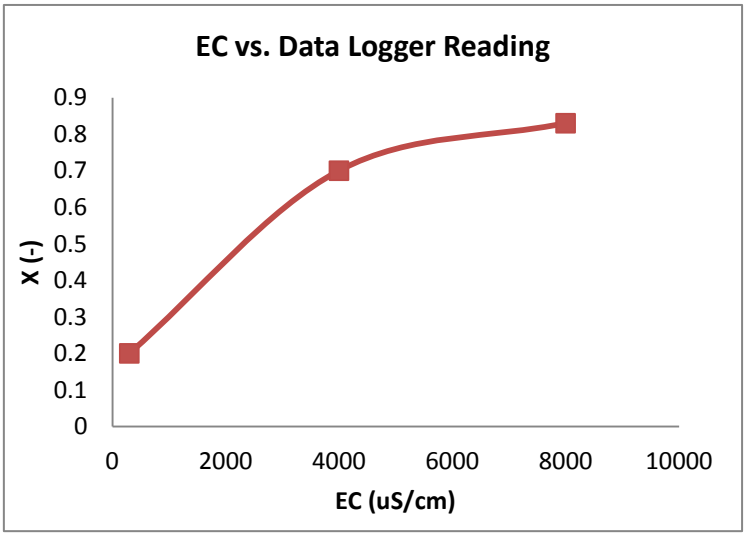

Appendix C

UVOST Logs for NAPL Characterization (Kovacik, 2013).

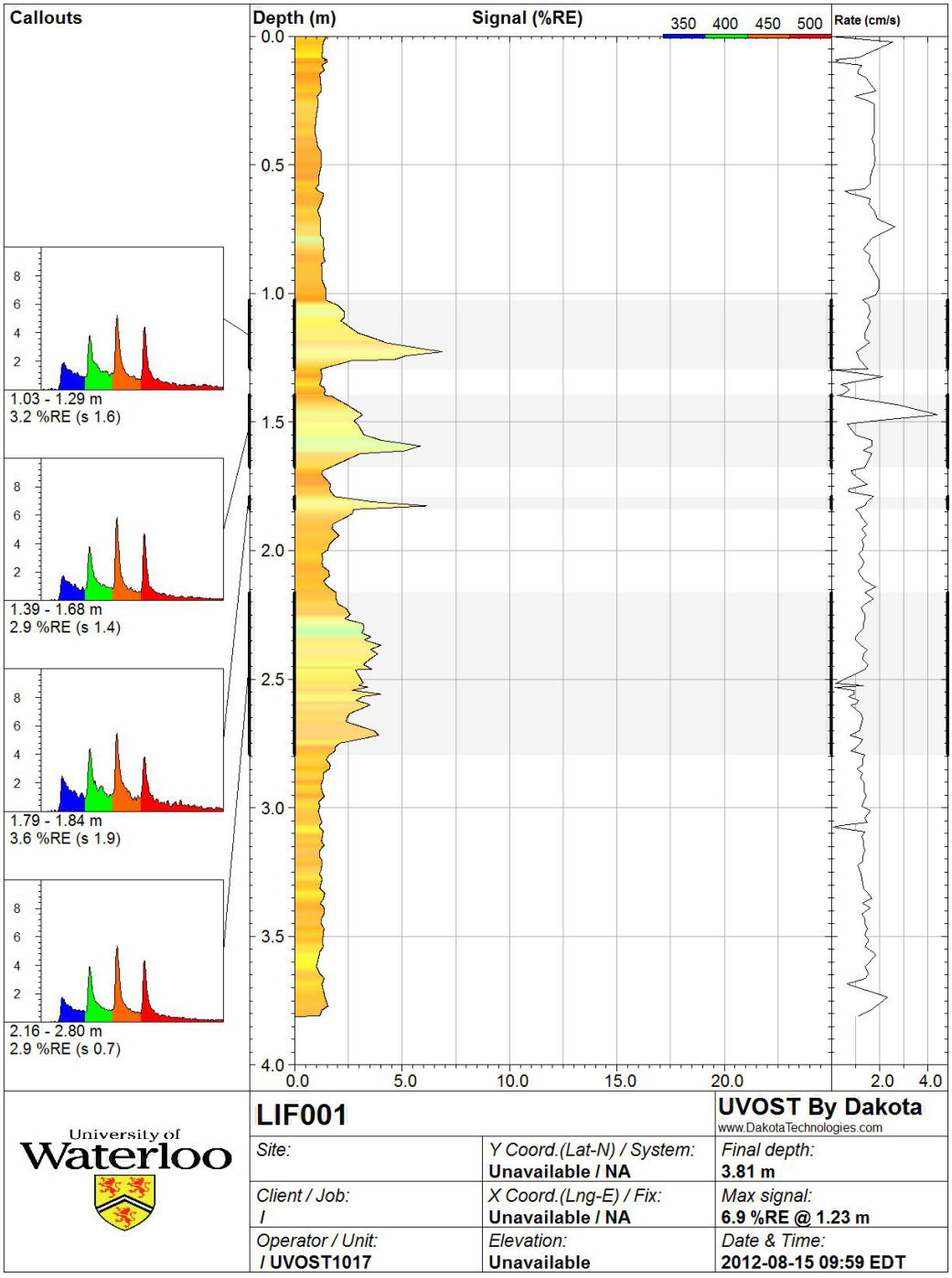

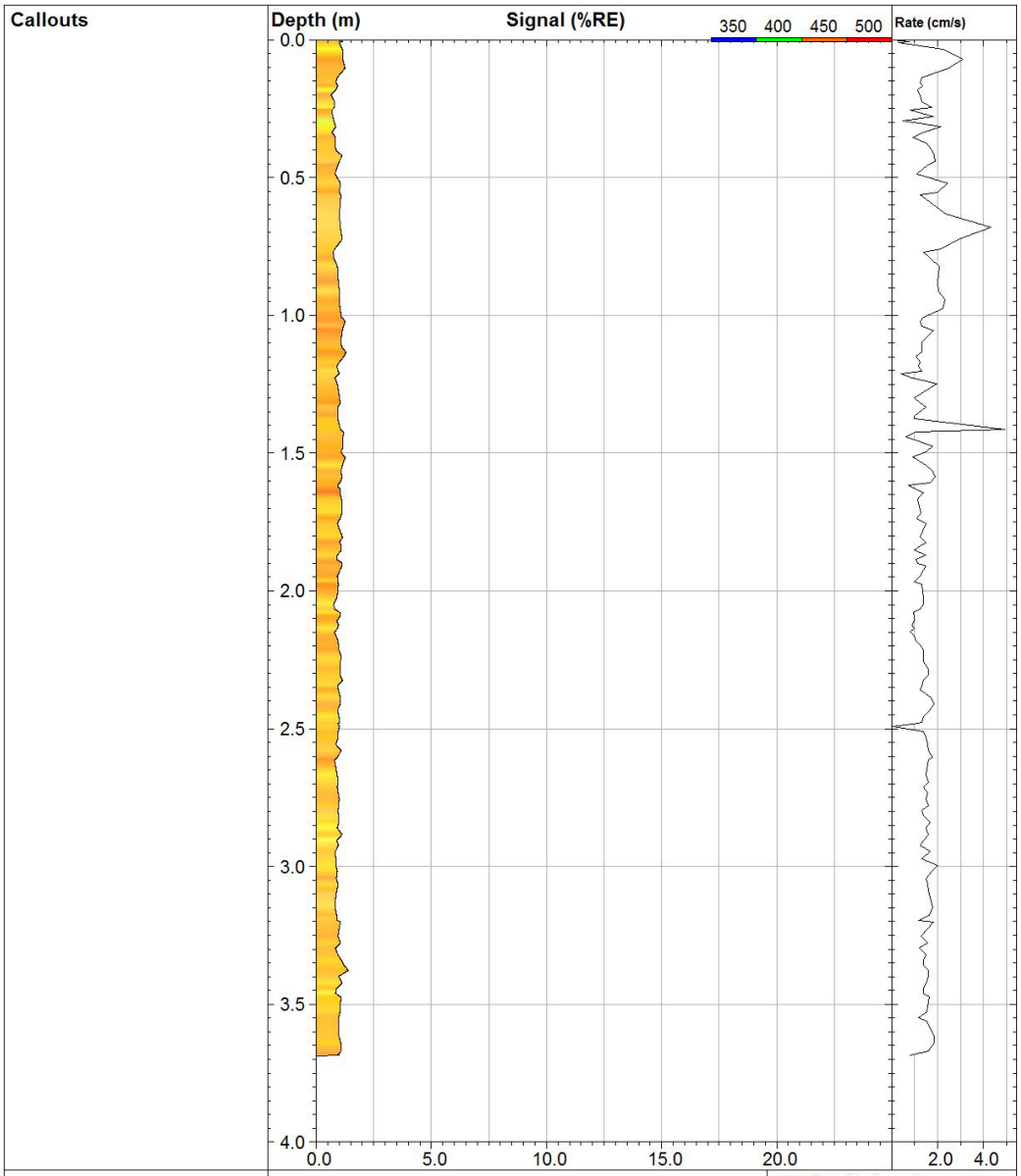

University of Waterloo

LIF002

UVOST By Dakota
www.DakotaTechnologies.com

Site: **CFB Borden**	*Y Coord.(Lat-N) / System:* **Unavailable / NA**	*Final depth:* **3.69 m**
Client / Job: **University of Waterloo / V**	*X Coord.(Lng-E) / Fix:* **Unavailable / NA**	*Max signal:* **1.4 %RE @ 3.38 m**
Operator / Unit: **K. Reed / UVOST1017**	*Elevation:* **Unavailable**	*Date & Time:* **2012-08-15 10:26 EDT**

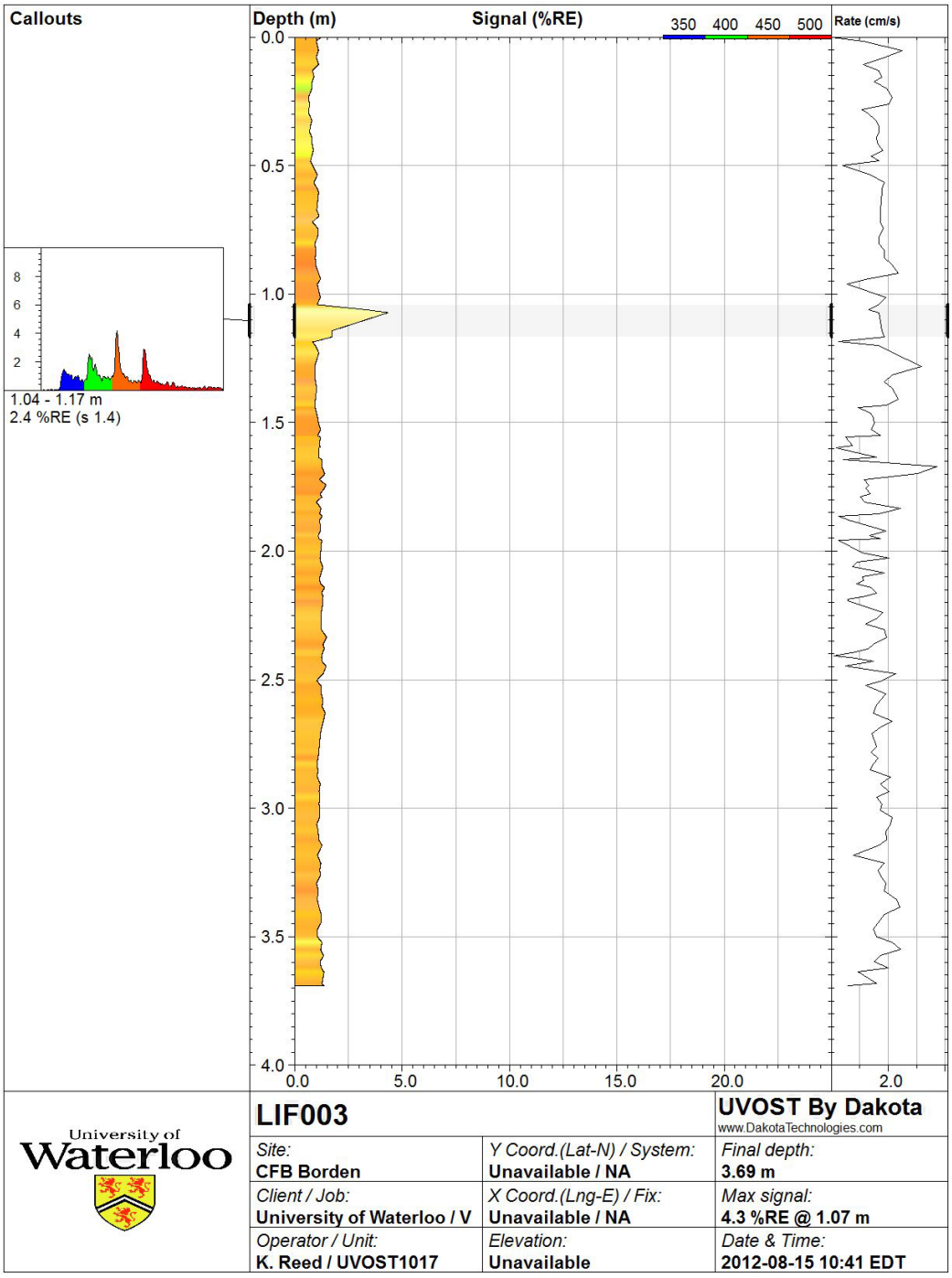
Callouts
Depth (m)
Signal (%RE)
350 400 450 500
Rate (cm/s)
0.0
0.5
1.0
1.5
2.0
2.5
3.0
3.5
4.0
0.0
5.0
10.0
15.0
20.0
2.0
8
6
4
2
1.04 - 1.17 m
2.4 %RE (s 1.4)
University of Waterloo
LIF003
UVOST By Dakota
www.DakotaTechnologies.com
Site:
CFB Borden
Y Coord.(Lat-N) / System:
Unavailable / NA
Final depth:
3.69 m
Client / Job:
University of Waterloo / V
X Coord.(Lng-E) / Fix:
Unavailable / NA
Max signal:
4.3 %RE @ 1.07 m
Operator / Unit:
K. Reed / UVOST1017
Elevation:
Unavailable
Date & Time:
2012-08-15 10:41 EDT

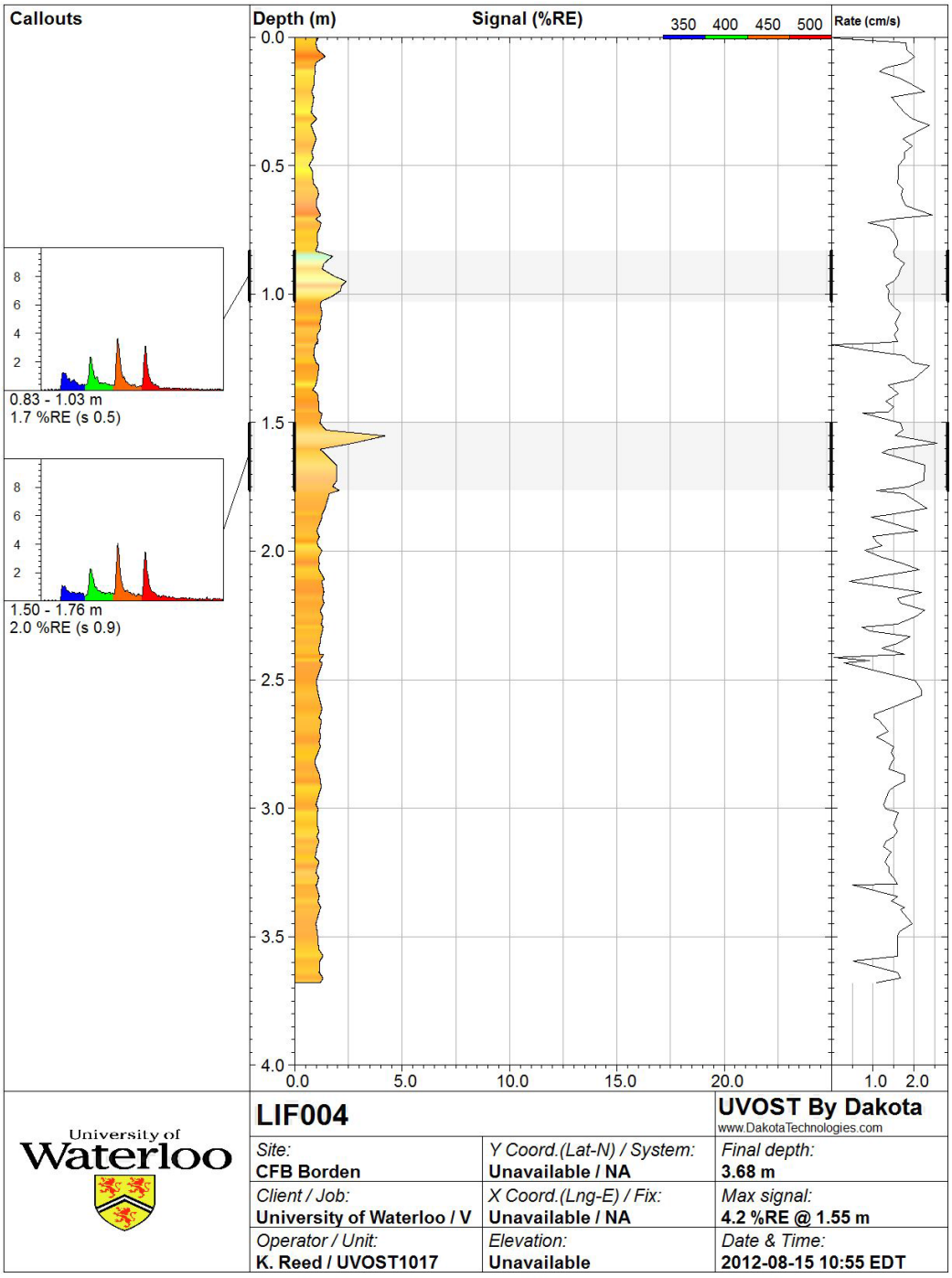

University of Waterloo

LIF004		UVOST By Dakota www.DakotaTechnologies.com
Site: **CFB Borden**	*Y Coord.(Lat-N) / System:* **Unavailable / NA**	*Final depth:* **3.68 m**
Client / Job: **University of Waterloo / V**	*X Coord.(Lng-E) / Fix:* **Unavailable / NA**	*Max signal:* **4.2 %RE @ 1.55 m**
Operator / Unit: **K. Reed / UVOST1017**	*Elevation:* **Unavailable**	*Date & Time:* **2012-08-15 10:55 EDT**

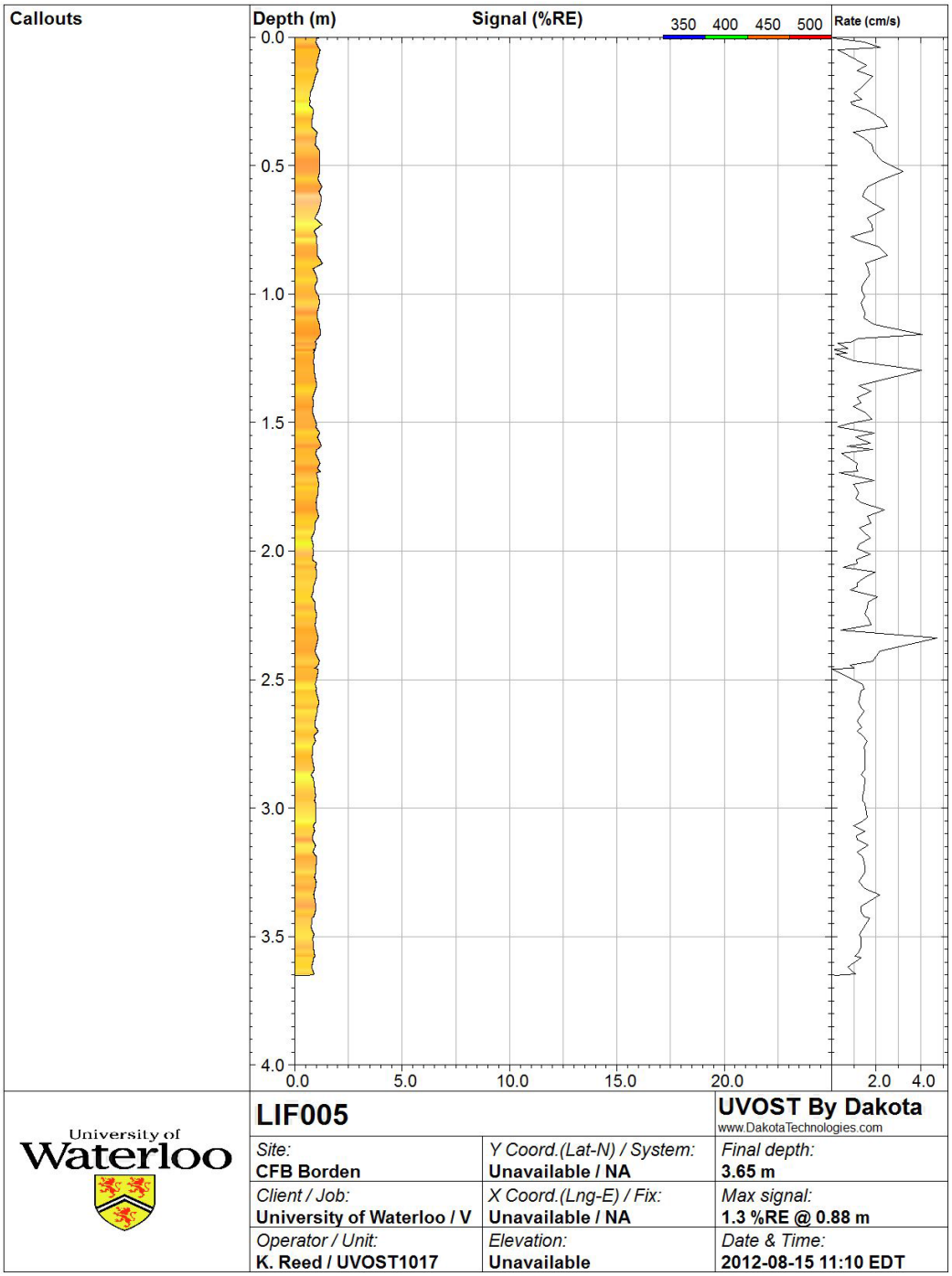

University of Waterloo

LIF005

UVOST By Dakota
www.DakotaTechnologies.com

Site: **CFB Borden**	*Y Coord.(Lat-N) / System:* **Unavailable / NA**	*Final depth:* **3.65 m**
Client / Job: **University of Waterloo / V**	*X Coord.(Lng-E) / Fix:* **Unavailable / NA**	*Max signal:* **1.3 %RE @ 0.88 m**
Operator / Unit: **K. Reed / UVOST1017**	*Elevation:* **Unavailable**	*Date & Time:* **2012-08-15 11:10 EDT**

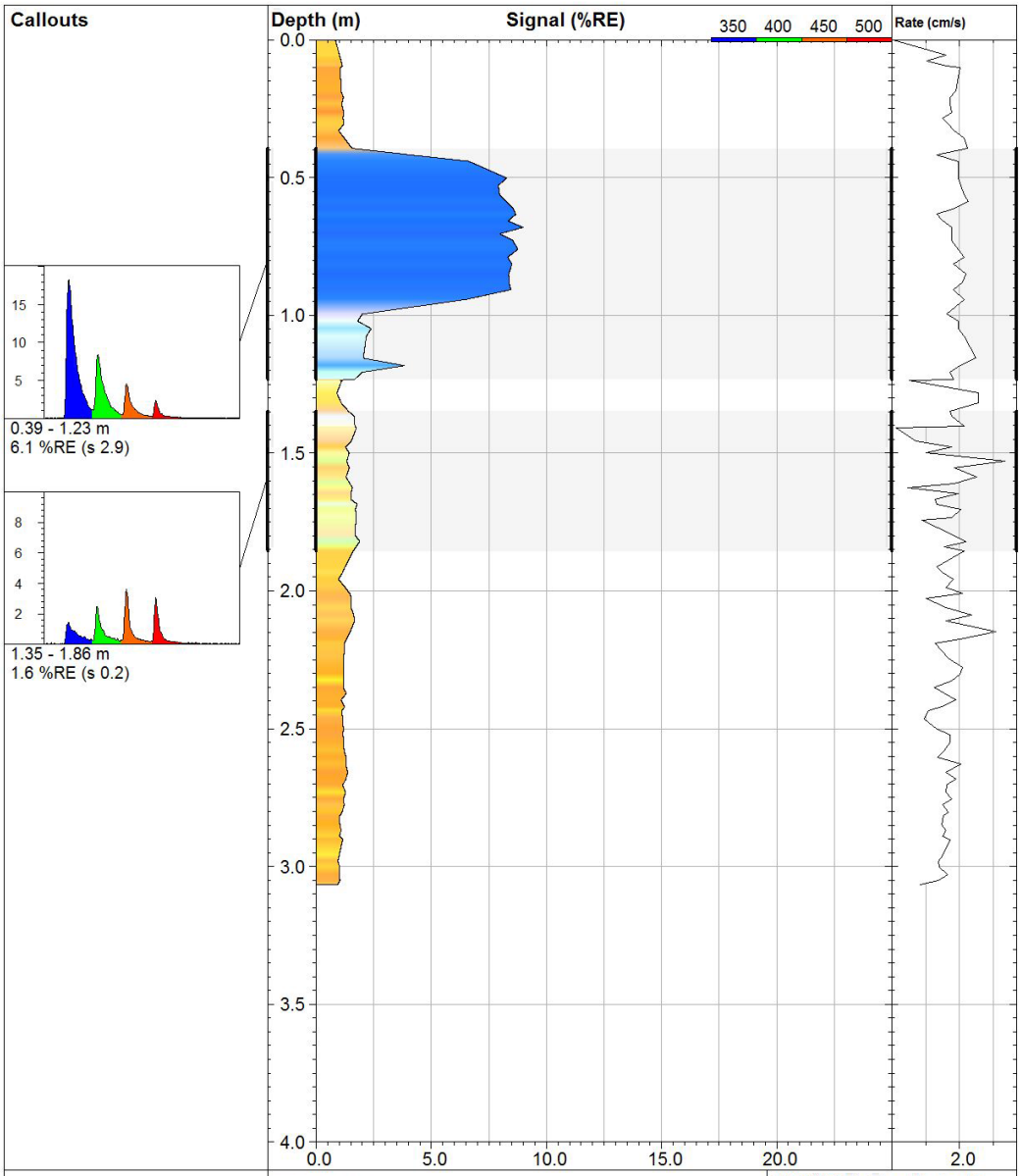
Callouts
Depth (m)
Signal (%RE)
350 400 450 500
Rate (cm/s)
0.0
0.5
1.0
1.5
2.0
2.5
3.0
3.5
4.0
0.0 5.0 10.0 15.0 20.0
2.0
15
10
5
0.39 - 1.23 m
6.1 %RE (s 2.9)
8
6
4
2
1.35 - 1.86 m
1.6 %RE (s 0.2)
University of Waterloo
LIF006
UVOST By Dakota
www.DakotaTechnologies.com
Site:
CFB Borden
Y Coord.(Lat-N) / System:
Unavailable / NA
Final depth:
3.07 m
Client / Job:
University of Waterloo / V
X Coord.(Lng-E) / Fix:
Unavailable / NA
Max signal:
9.0 %RE @ 0.68 m
Operator / Unit:
K. Reed / UVOST1017
Elevation:
Unavailable
Date & Time:
2012-08-15 11:27 EDT

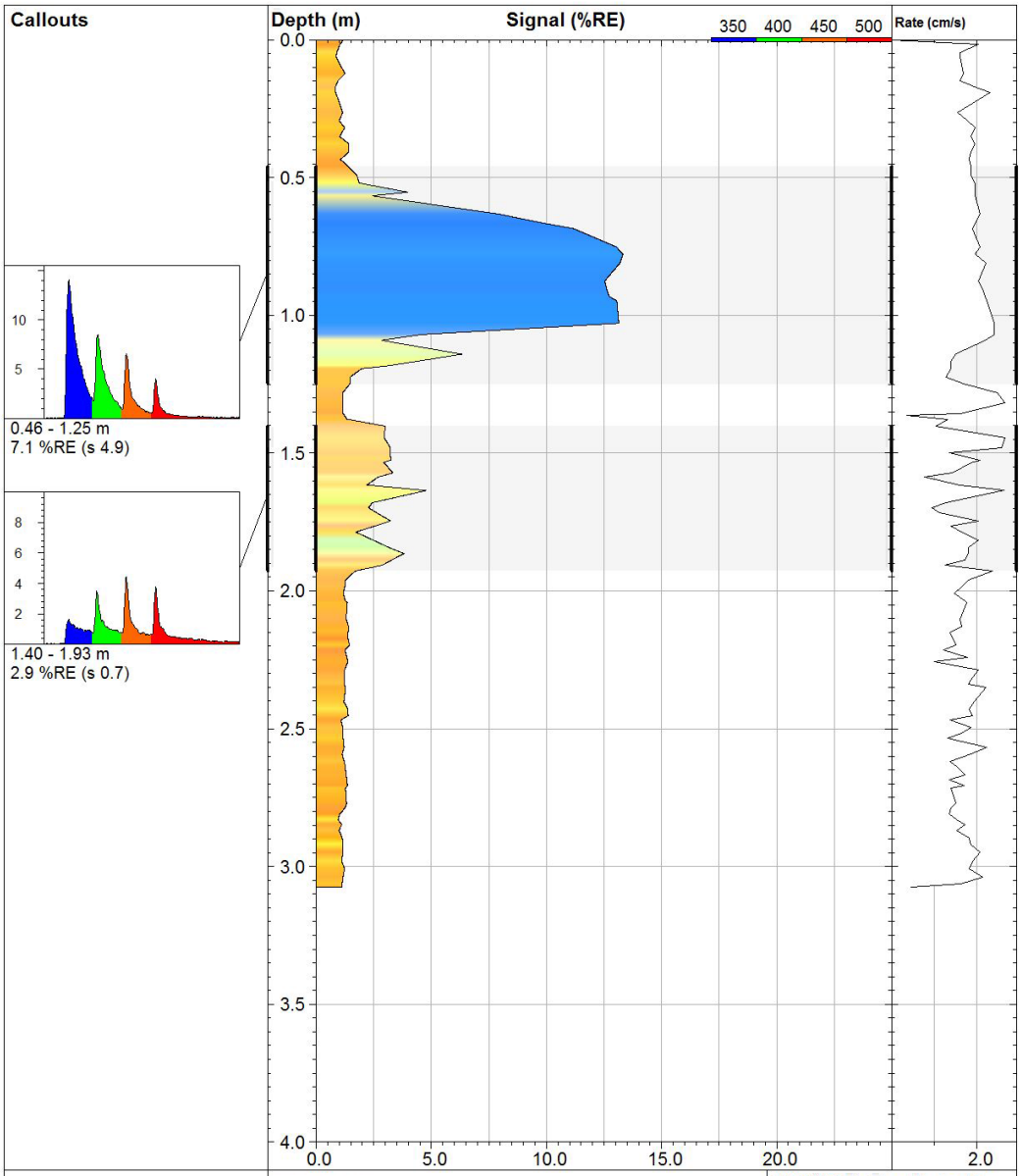
Callouts
Depth (m)
Signal (%RE)
350 400 450 500
Rate (cm/s)
0.0
0.5
1.0
1.5
2.0
2.5
3.0
3.5
4.0
0.0
5.0
10.0
15.0
20.0
2.0
10
5
0.46 - 1.25 m
7.1 %RE (s 4.9)
8
6
4
2
1.40 - 1.93 m
2.9 %RE (s 0.7)
University of Waterloo
LIF007
UVOST By Dakota
www.DakotaTechnologies.com
Site:
CFB Borden
Y Coord.(Lat-N) / System:
Unavailable / NA
Final depth:
3.08 m
Client / Job:
University of Waterloo / V
X Coord.(Lng-E) / Fix:
Unavailable / NA
Max signal:
13.3 %RE @ 0.78 m
Operator / Unit:
K. Reed / UVOST1017
Elevation:
Unavailable
Date & Time:
2012-08-15 11:44 EDT

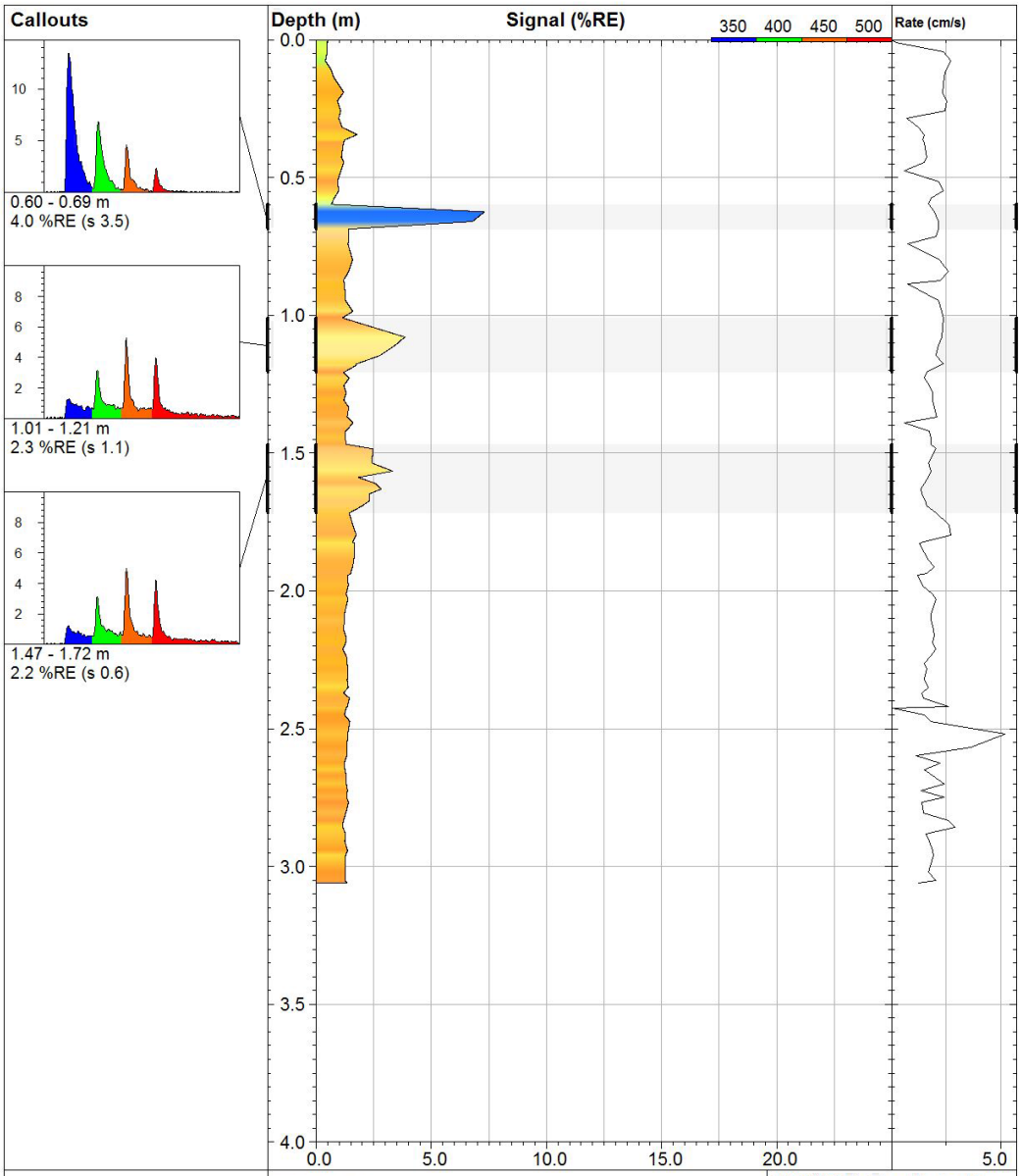
Callouts
0.60 - 0.69 m
4.0 %RE (s 3.5)
1.01 - 1.21 m
2.3 %RE (s 1.1)
1.47 - 1.72 m
2.2 %RE (s 0.6)
Depth (m)
Signal (%RE)
350 400 450 500
Rate (cm/s)
0.0 0.5 1.0 1.5 2.0 2.5 3.0 3.5 4.0
0.0 5.0 10.0 15.0 20.0
5.0
University of Waterloo
LIF008
UVOST By Dakota
www.DakotaTechnologies.com
Site:
CFB Borden
Y Coord.(Lat-N) / System:
Unavailable / NA
Final depth:
3.06 m
Client / Job:
University of Waterloo / V
X Coord.(Lng-E) / Fix:
Unavailable / NA
Max signal:
7.3 %RE @ 0.62 m
Operator / Unit:
K. Reed / UVOST1017
Elevation:
Unavailable
Date & Time:
2012-08-15 12:20 EDT

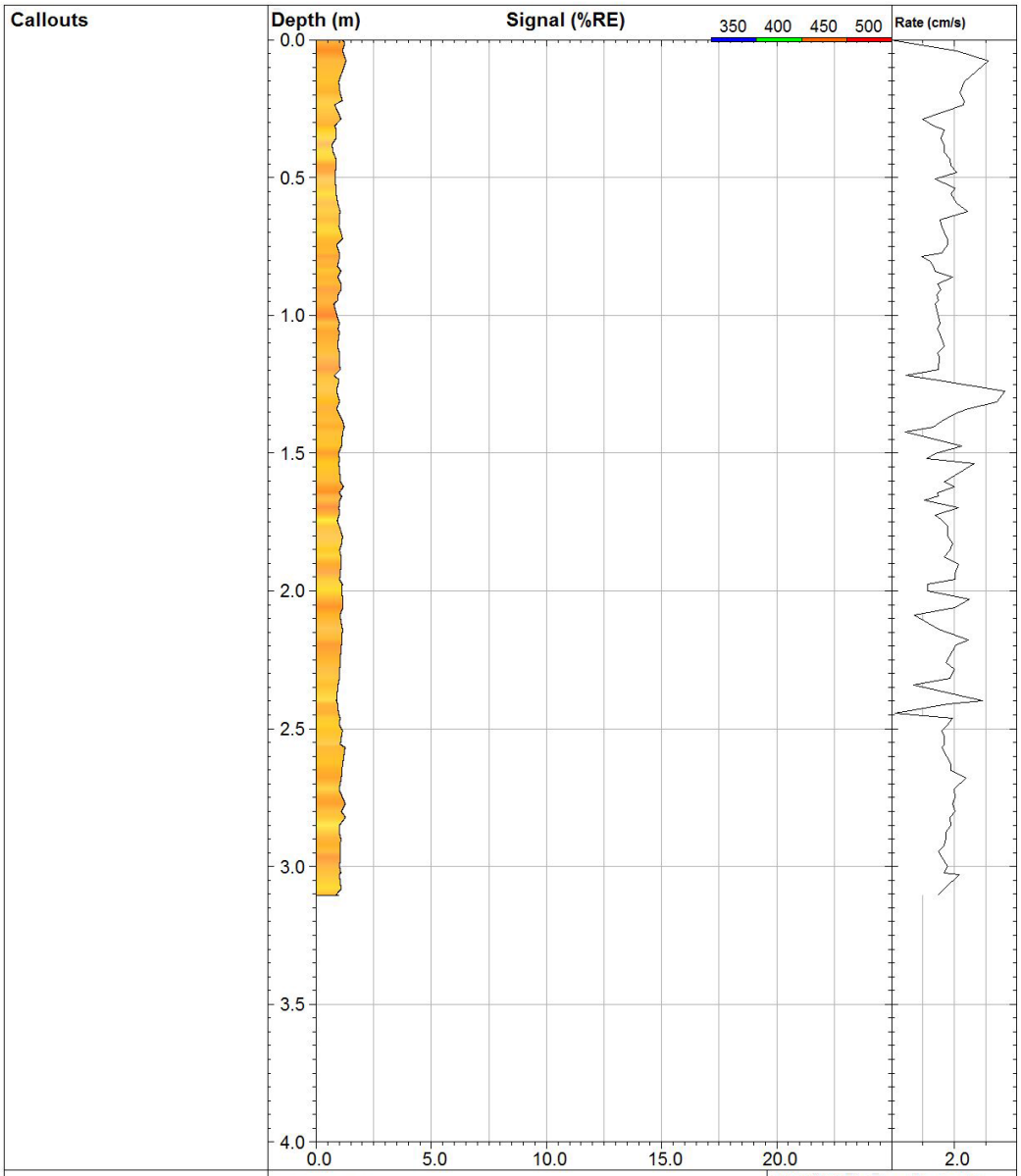

University of Waterloo

LIF009

UVOST By Dakota
www.DakotaTechnologies.com

Site: **CFB Borden**	*Y Coord.(Lat-N) / System:* **Unavailable / NA**	*Final depth:* **3.10 m**
Client / Job: **University of Waterloo / V**	*X Coord.(Lng-E) / Fix:* **Unavailable / NA**	*Max signal:* **1.3 %RE @ 0.08 m**
Operator / Unit: **K. Reed / UVOST1017**	*Elevation:* **Unavailable**	*Date & Time:* **2012-08-15 12:38 EDT**

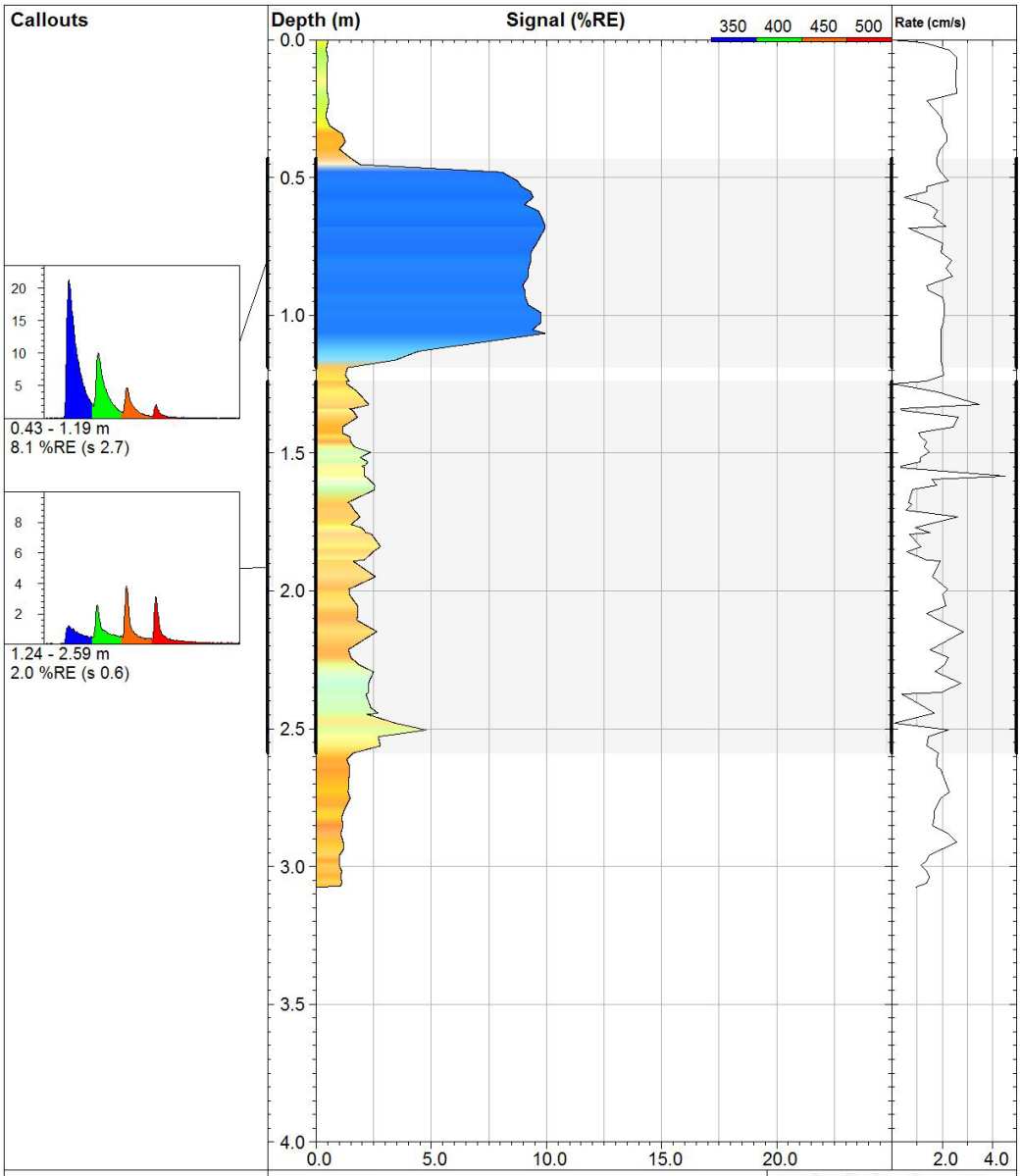

University of Waterloo

LIF010

UVOST By Dakota
www.DakotaTechnologies.com

Site: **CFB Borden**	*Y Coord.(Lat-N) / System:* **Unavailable / NA**	*Final depth:* **3.07 m**
Client / Job: **University of Waterloo / V**	*X Coord.(Lng-E) / Fix:* **Unavailable / NA**	*Max signal:* **9.9 %RE @ 0.68 m**
Operator / Unit: **K. Reed / UVOST1017**	*Elevation:* **Unavailable**	*Date & Time:* **2012-08-15 13:11 EDT**

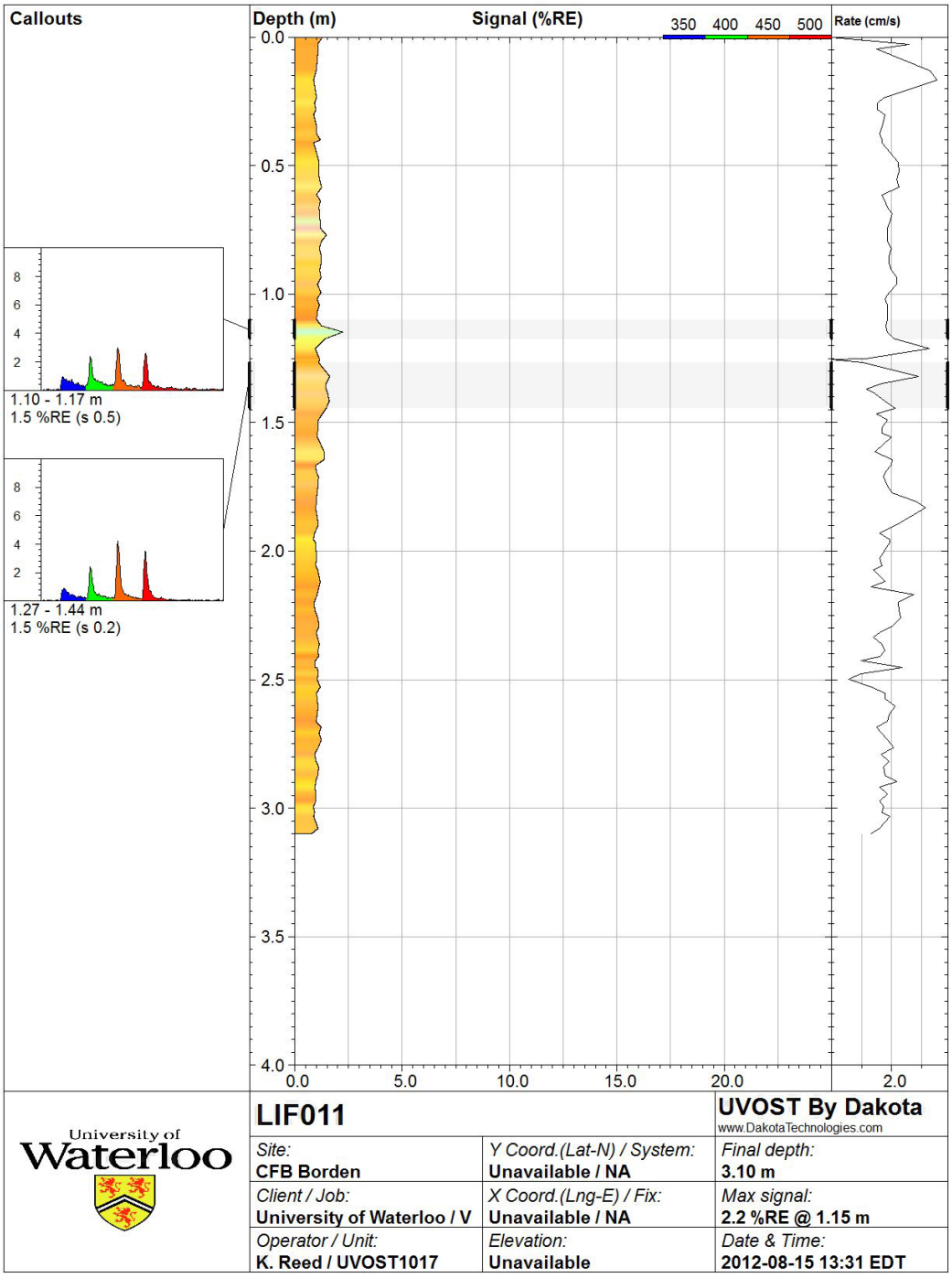

University of Waterloo

LIF011

UVOST By Dakota
www.DakotaTechnologies.com

Site: **CFB Borden**	*Y Coord.(Lat-N) / System:* **Unavailable / NA**	*Final depth:* **3.10 m**
Client / Job: **University of Waterloo / V**	*X Coord.(Lng-E) / Fix:* **Unavailable / NA**	*Max signal:* **2.2 %RE @ 1.15 m**
Operator / Unit: **K. Reed / UVOST1017**	*Elevation:* **Unavailable**	*Date & Time:* **2012-08-15 13:31 EDT**

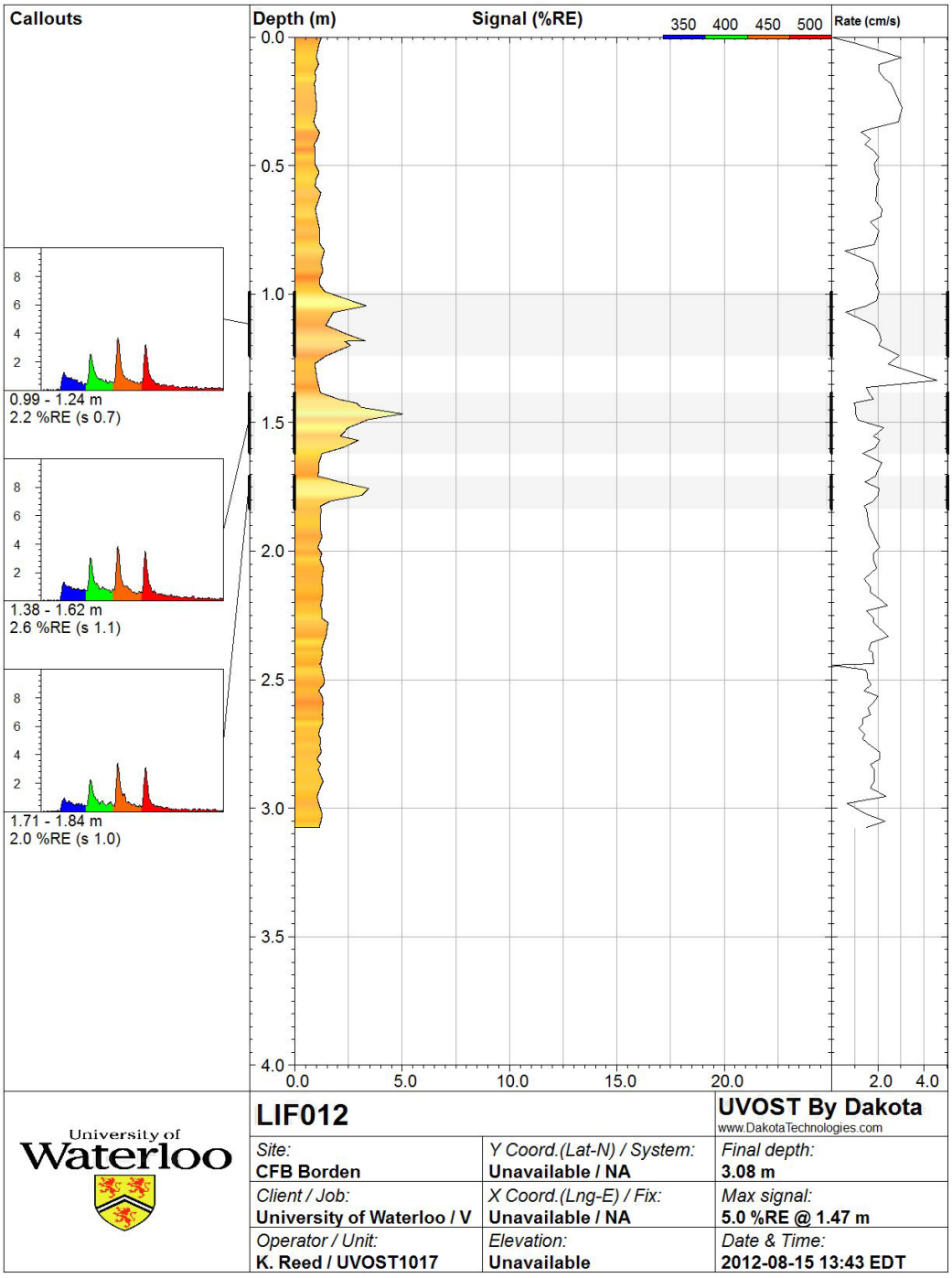
Callouts
Depth (m)
Signal (%RE)
350 400 450 500
Rate (cm/s)
0.0
0.5
1.0
1.5
2.0
2.5
3.0
3.5
4.0
0.0 5.0 10.0 15.0 20.0
2.0 4.0
8 6 4 2
0.99 - 1.24 m
2.2 %RE (s 0.7)
1.38 - 1.62 m
2.6 %RE (s 1.1)
1.71 - 1.84 m
2.0 %RE (s 1.0)
University of Waterloo
LIF012
UVOST By Dakota
www.DakotaTechnologies.com
Site:
CFB Borden
Y Coord.(Lat-N) / System:
Unavailable / NA
Final depth:
3.08 m
Client / Job:
University of Waterloo / V
X Coord.(Lng-E) / Fix:
Unavailable / NA
Max signal:
5.0 %RE @ 1.47 m
Operator / Unit:
K. Reed / UVOST1017
Elevation:
Unavailable
Date & Time:
2012-08-15 13:43 EDT

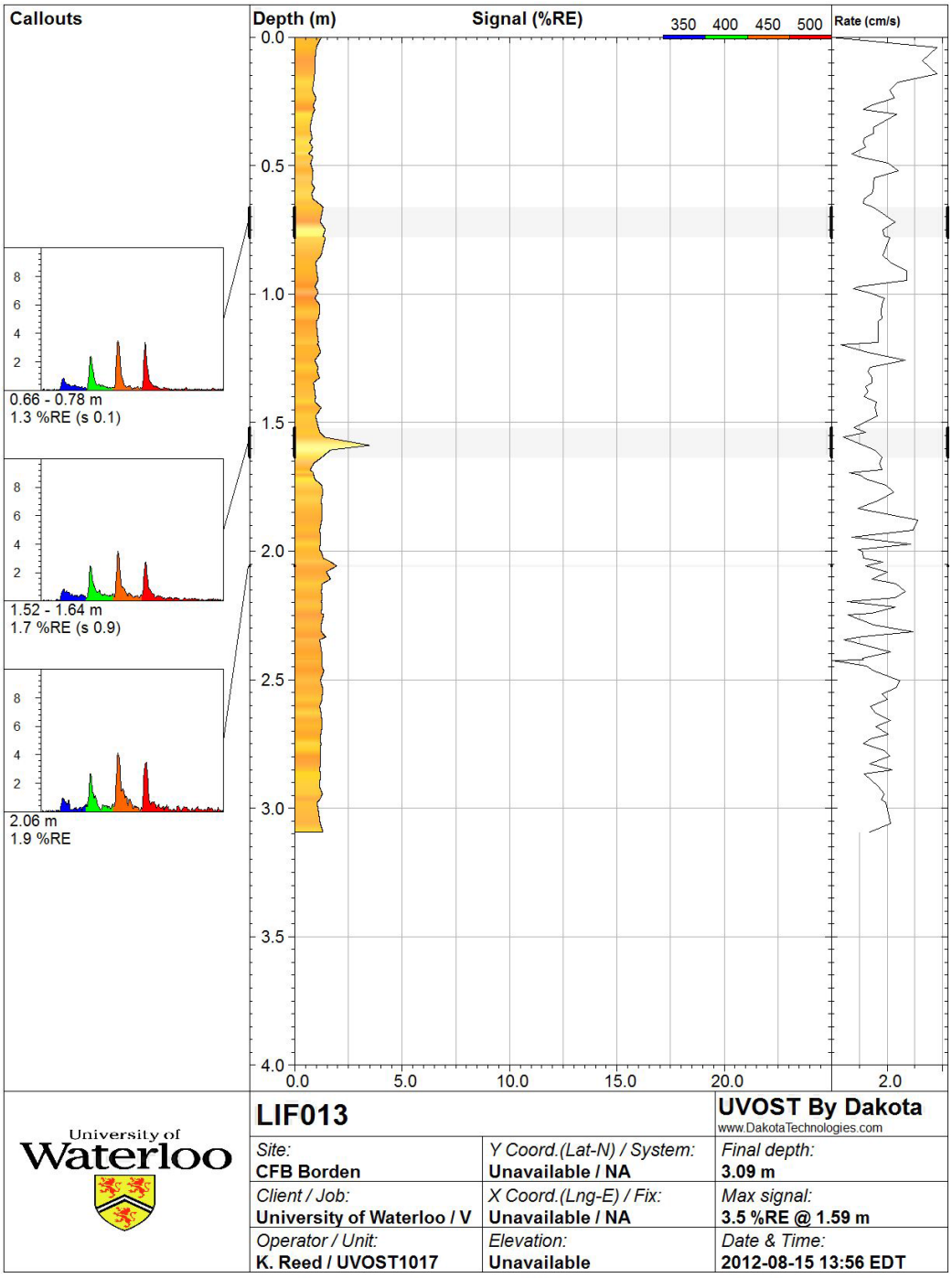
Callouts
Depth (m)
Signal (%RE)
350 400 450 500
Rate (cm/s)
0.66 - 0.78 m
1.3 %RE (s 0.1)
1.52 - 1.64 m
1.7 %RE (s 0.9)
2.06 m
1.9 %RE
0.0
0.5
1.0
1.5
2.0
2.5
3.0
3.5
4.0
0.0
5.0
10.0
15.0
20.0
2.0
University of Waterloo
LIF013
UVOST By Dakota
www.DakotaTechnologies.com
Site:
CFB Borden
Y Coord.(Lat-N) / System:
Unavailable / NA
Final depth:
3.09 m
Client / Job:
University of Waterloo / V
X Coord.(Lng-E) / Fix:
Unavailable / NA
Max signal:
3.5 %RE @ 1.59 m
Operator / Unit:
K. Reed / UVOST1017
Elevation:
Unavailable
Date & Time:
2012-08-15 13:56 EDT

Appendix D

PHC concentrations at Row 3 (Kovacik, 2013).

Sample Identification (AQUEOUS SAMPLES)	Date Sampled	Benzene ug/L	toluene ug/L	o-xylene ug/L	Naphthalene ug/L
R3-M2-D1	6-Sep-12	461.3	56.5	16.0	0.0
R3-M2-D4	6-Sep-12	20.8	0.0	0.0	0.0
R3-M3-D1	6-Sep-12	38076.2	4561.5	404.8	0.0
R3-M3-D4	6-Sep-12	648.1	121.1	18.5	0.0
R3-M3-D7	6-Sep-12	451.4	86.0	27.5	932.2
R3-M4-D1	6-Sep-12	38543.2	6317.1	792.7	1061.5
R3-M4-D4	6-Sep-12	1190.9	310.0	51.3	0.0
R3-M4-D7	6-Sep-12	362.0	108.9	26.7	0.0
R3-M5-D1	11-Sep-12	54.2	0.0	0.0	0.0
R3-M5-D4	11-Sep-12	146.6	0.0	0.0	0.0
R3-M2-D1	6-Nov-12	157.9	22.5	15.4	ND
R3-M2-D4	6-Nov-12	319.3	29.1	0.0	ND
R3-M3-D1	6-Nov-12	58166.5	9475.6	1354.5	1313.4
R3-M3-D4	6-Nov-12	51372.4	7442.8	979.4	647.0
R3-M4-D1	6-Nov-12	48316.8	6787.7	658.6	1627.4
R3-M4-D4	6-Nov-12	50568.7	8914.8	1217.4	980.3
R3-M4-D7	6-Nov-12	20747.6	3255.5	314.4	ND
R3-M5-D1	6-Nov-12	4192.3	399.7	79.1	827.3
R3-M5-D4	6-Nov-12	2128.4	6.1	0.0	ND

Appendix E

Mass Discharge: Raoult's Law Prediction Versus Measured Mass Discharge (Row 3)

This section provides a comparison between field mass discharge at Row 3 and Raoult's Law model mass discharge prediction (Fraser, 2007). Also, an adjusted prediction adjusted assuming additional mass discharge decline due to natural biodegradation. is provided as per section 3.x. Benzene, toluene, xylene and naphthalene plots are given in Figure 3.21

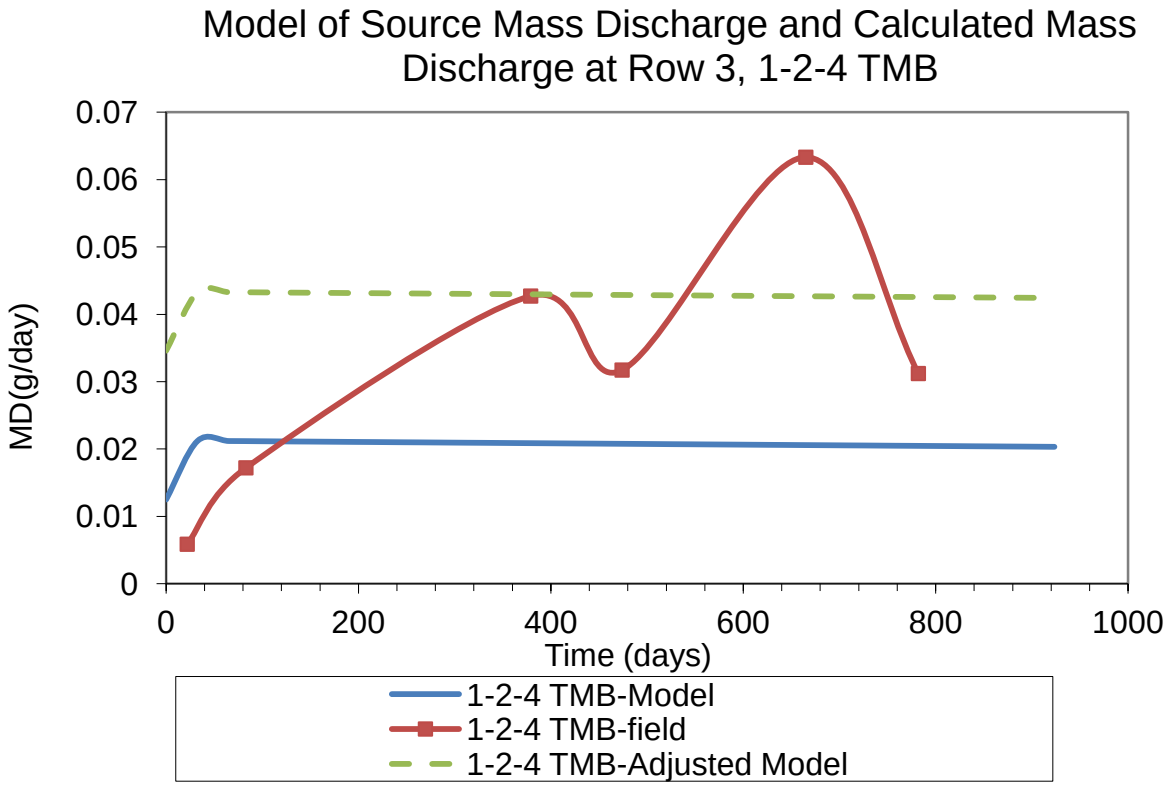

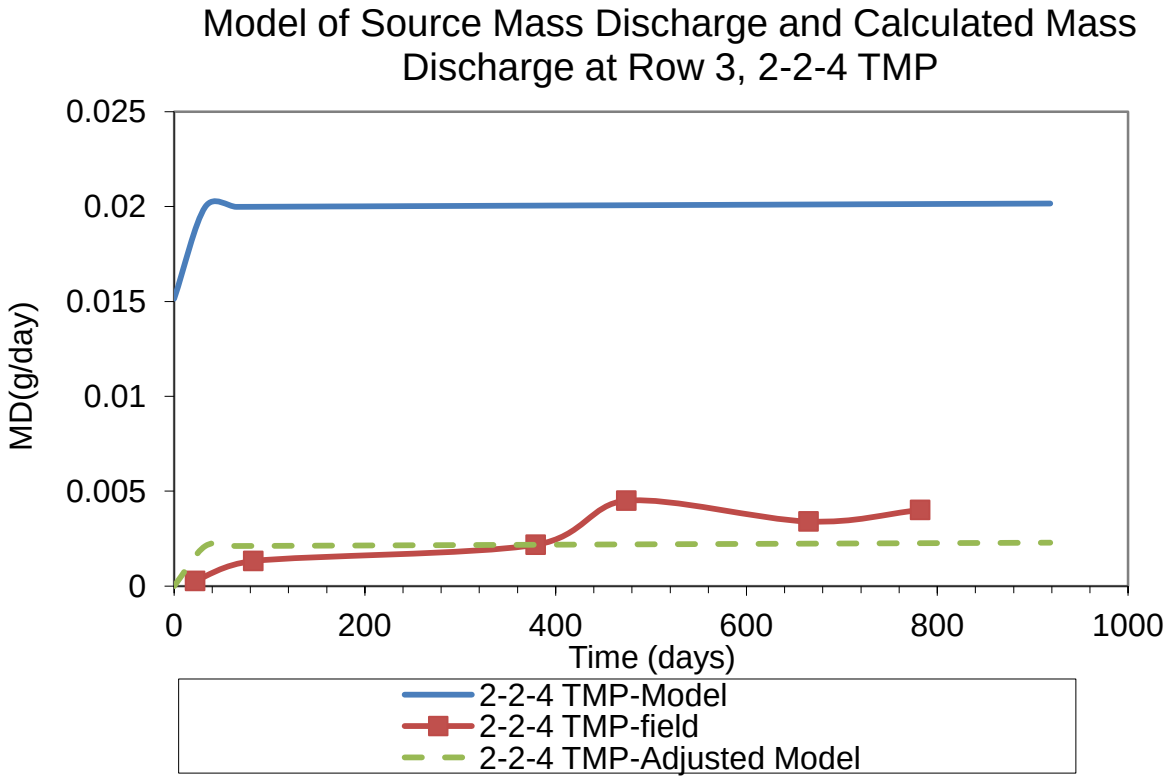
Model of Source Mass Discharge and Calculated Mass Discharge at Row 3, 2-2-4 TMP
MD(g/day)
0.025
0.02
0.015
0.01
0.005
0
0
200
400
600
800
1000
Time (days)
2-2-4 TMP-Model
2-2-4 TMP-field
2-2-4 TMP-Adjusted Model

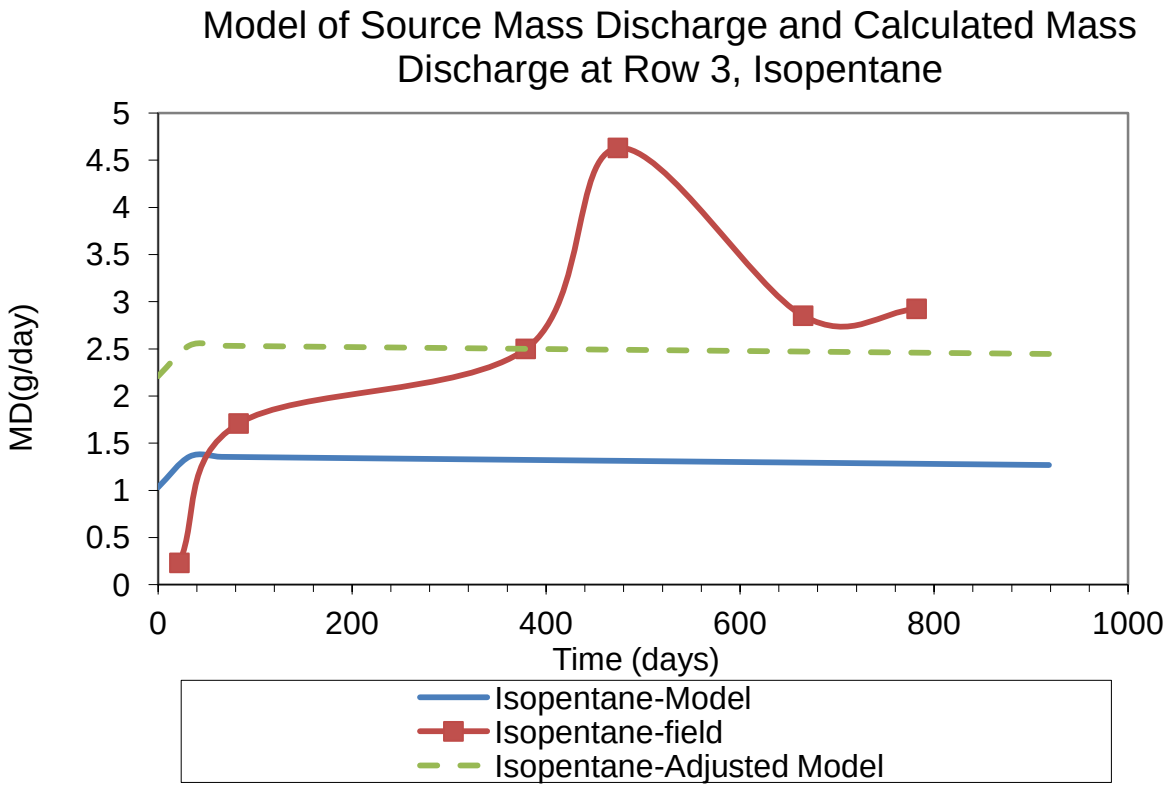
Model of Source Mass Discharge and Calculated Mass Discharge at Row 3, Isopentane
MD(g/day)
5
4.5
4
3.5
3
2.5
2
1.5
1
0.5
0
0
200
400
600
800
1000
Time (days)
Isopentane-Model
Isopentane-field
Isopentane-Adjusted Model

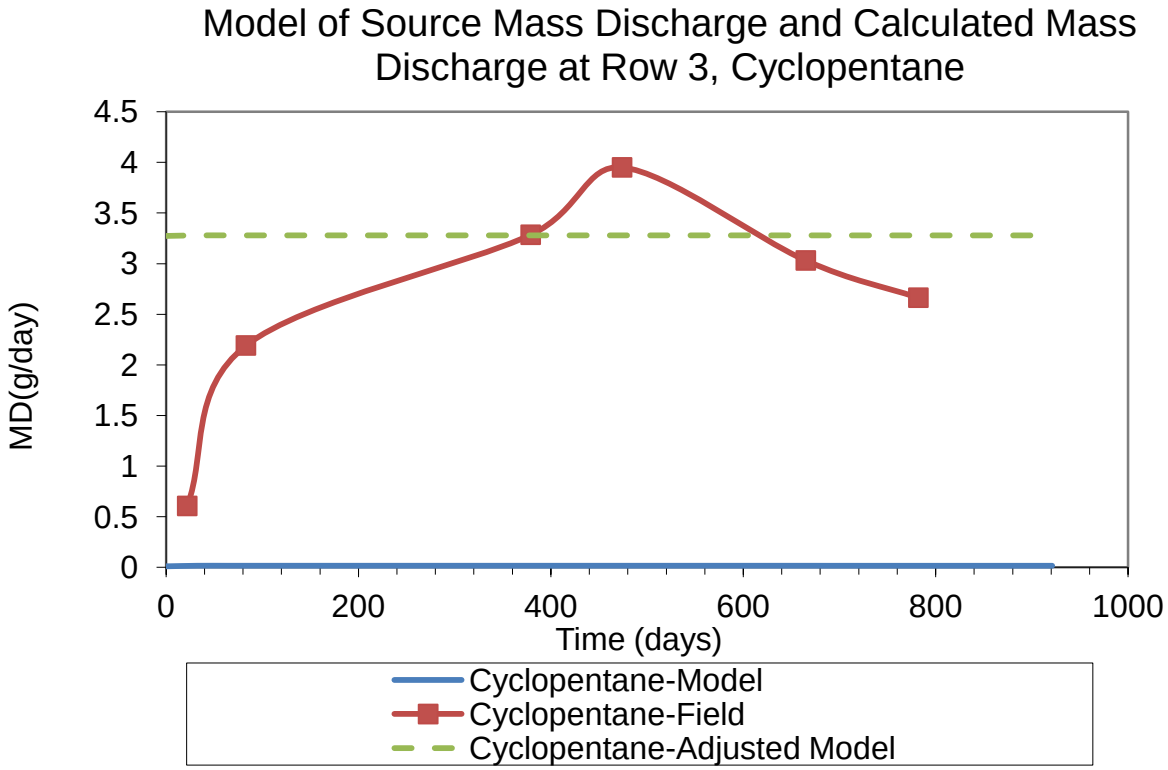
Model of Source Mass Discharge and Calculated Mass Discharge at Row 3, Cyclopentane
MD(g/day)
4.5
4
3.5
3
2.5
2
1.5
1
0.5
0
0
200
400
600
800
1000
Time (days)
Cyclopentane-Model
Cyclopentane-Field
Cyclopentane-Adjusted Model

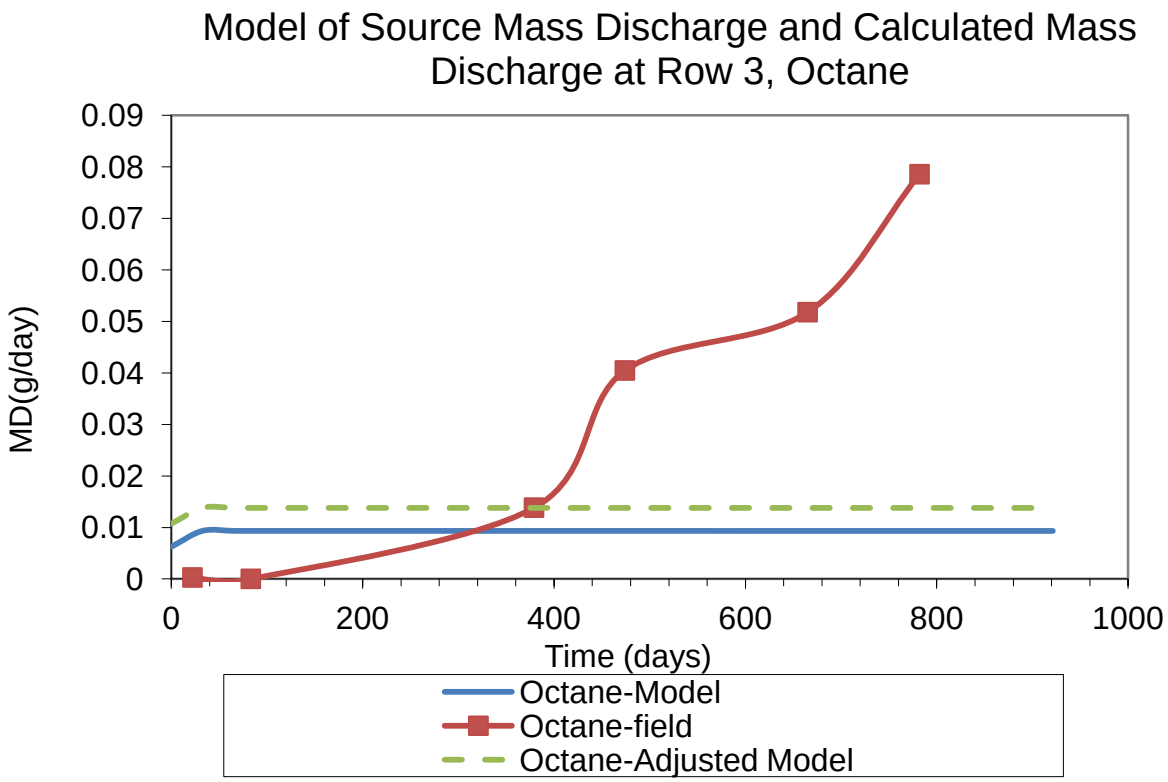
Model of Source Mass Discharge and Calculated Mass Discharge at Row 3, Octane
MD(g/day)
0.09
0.08
0.07
0.06
0.05
0.04
0.03
0.02
0.01
0
0
200
400
600
800
1000
Time (days)
Octane-Model
Octane-field
Octane-Adjusted Model

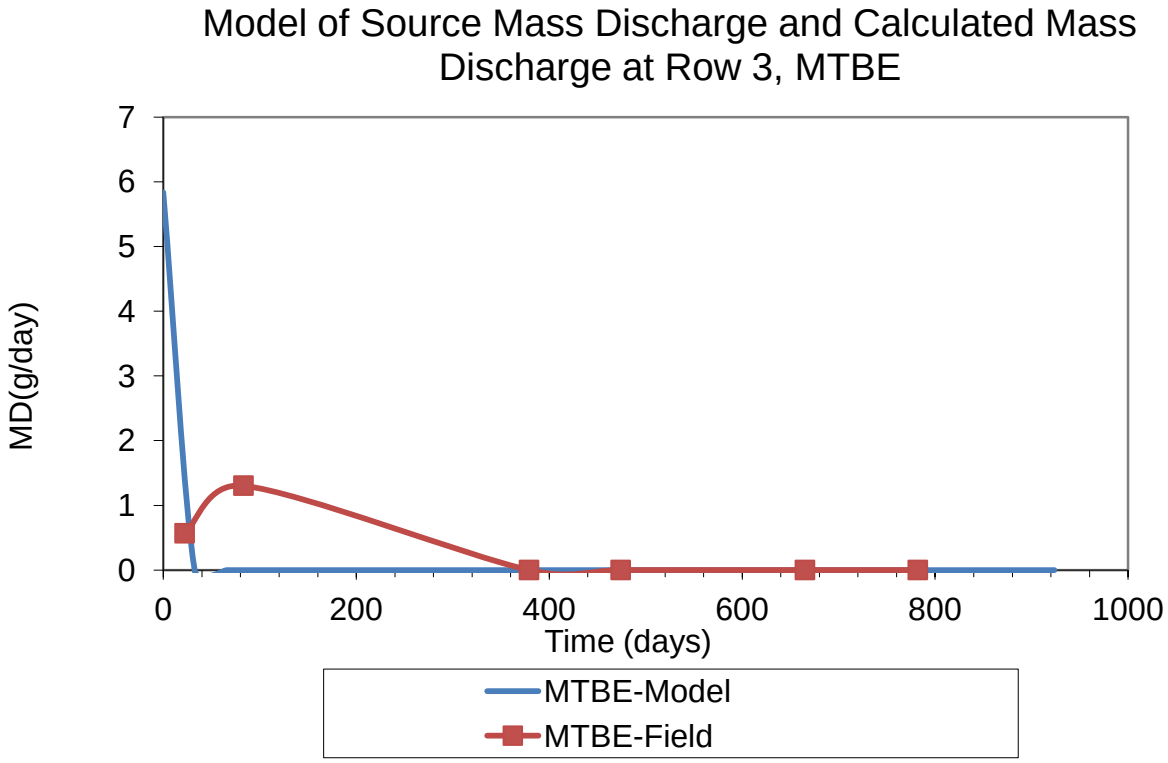
Model of Source Mass Discharge and Calculated Mass Discharge at Row 3, MTBE
MD(g/day)
7
6
5
4
3
2
1
0
0
200
400
600
800
1000
Time (days)
MTBE-Model
MTBE-Field

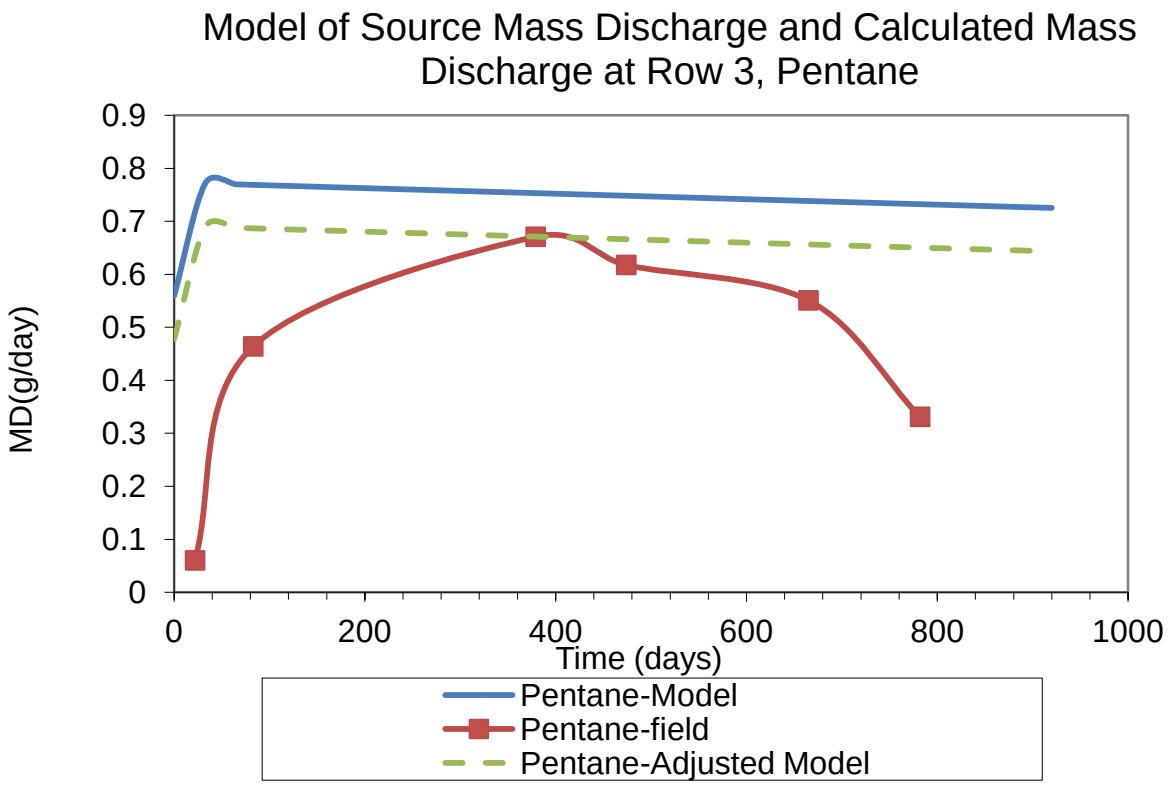
Model of Source Mass Discharge and Calculated Mass Discharge at Row 3, Pentane
MD(g/day)
0.9
0.8
0.7
0.6
0.5
0.4
0.3
0.2
0.1
0
0
200
400
600
800
1000
Time (days)
Pentane-Model
Pentane-field
Pentane-Adjusted Model

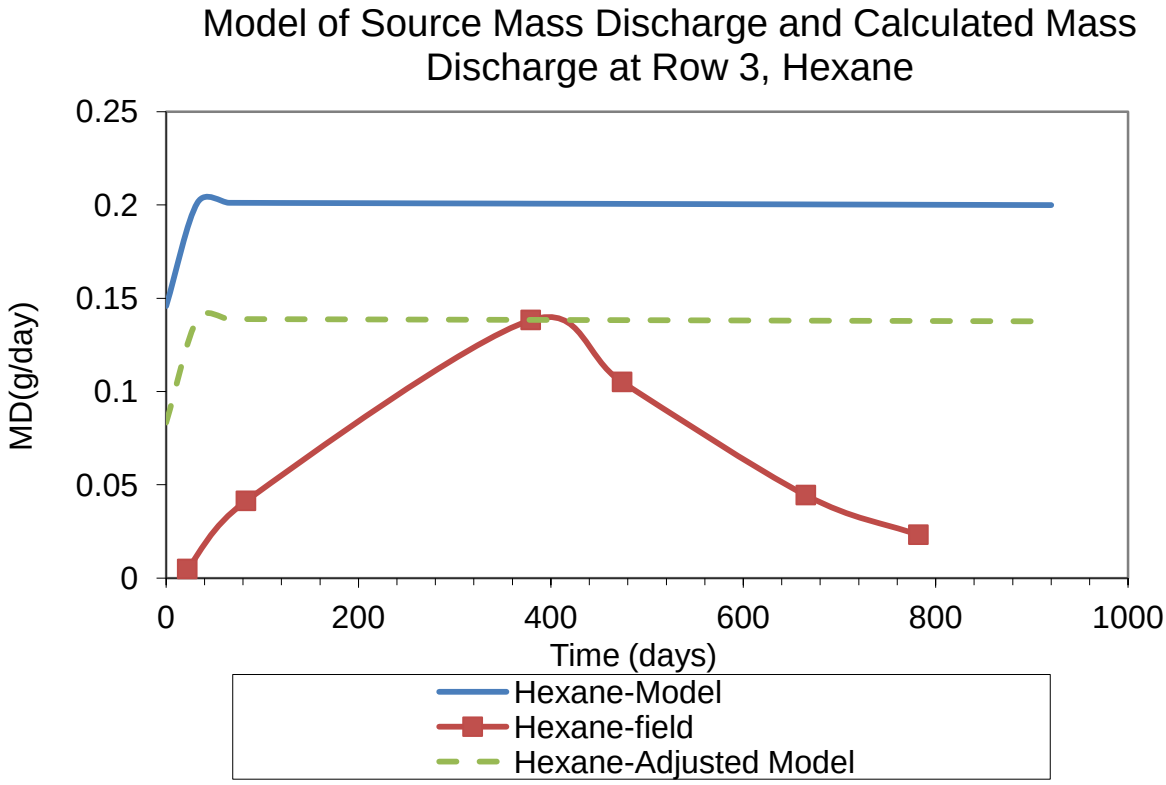
Model of Source Mass Discharge and Calculated Mass Discharge at Row 3, Hexane
MD(g/day)
0.25
0.2
0.15
0.1
0.05
0
0
200
400
600
800
1000
Time (days)
Hexane-Model
Hexane-field
Hexane-Adjusted Model

Appendix F

Tables for Hydrocarbon Concentration in Progress Monitoring

ND: non-detected

Sample Identification	Day	iso-Pentane	Pentane	Cyclo pentane	3Methyl Pentane	Hexane	iso-Hexane	Benzene	iso-Octane	toluene	octane	o-xylene	124 TMB	Naphthalene
		ug/L	ug/L	ug/L	ug/L	ug/L	ug/L	ug/L	ug/L	ug/L	ug/L	ug/L	ug/L	ug/L
R3-M3-D1	-1	10205.8	3118.8	5723.6	6.6	702.6	35.1	18.9	108.5	24.1	ND	ND	ND	765.7
R3-M3-D3	-1	10473.0	3281.0	6015.5	10.0	901.9	36.7	31.5	53.0	ND	ND	ND	ND	782.9
R3-M4-D1	-1	10407.2	2670.5	8650.3	4.7	389.1	34.4	428.4	133.3	65.2	8.8	52.7	86.1	1803.6
R3-M4-D3	-1	11994.7	3271.4	15424.7	4.2	583.9	35.7	733.5	20.3	760.7	ND	328.1	274.3	2800.7
S3-D2	-1	12317.7	4674.4	10637.4	12.3	2772.1	46.7	34.3	1481.9	1516.3	532.4	1431.9	875.5	3945.0
S3-D3	-1	9846.8	3083.3	11712.5	6.4	1220.7	35.3	346.8	447.6	2969.8	64.6	1538.1	613.7	3293.3
S5-D2	-1	10075.9	3191.8	11542.3	3.9	801.9	32.9	109.0	216.0	3045.3	31.3	1518.2	558.6	3791.0
S5-D3	-1	9969.7	2452.6	14867.9	ND	386.6	29.0	4197.6	59.3	6959.4	1.1	907.8	432.7	3081.9
S3-D2	-1	13590.7	5602.2	9802.6	16.3	3200.0	60.8	ND	719.6	382.3	141.8	724.8	797.0	2613.6
R3-M3-D1	44	15054.0	1317.7	15836.7	9.1	54.6	49.3	64.2	214.0	40.5	ND	55.4	175.1	2131.3
R3-M3-D3	44	10805.5	844.7	9596.2	9.4	107.8	35.1	50.5	109.5	14.8	ND	48.5	41.5	998.9
R3-M4-D1	44	14850.1	413.7	15430.0	6.9	56.7	45.6	1651.5	274.4	ND	ND	ND	356.2	2547.0
R3-M4-D3	44	17417.8	4038.4	15067.6	9.2	383.7	49.4	2349.9	53.2	7.4	ND	ND	24.4	1812.3
S3-D3	44	17724.1	6558.4	19007.0	11.1	2554.1	44.0	368.6	570.0	2008.7	103.8	1484.1	694.9	3386.4
S5-D2	44	18282.3	2857.2	17652.3	10.2	300.1	59.4	58.4	408.0	1274.8	4.7	1098.3	619.5	3516.3
S5-D3	44	17200.0	2392.0	18451.5	7.7	44.8	47.6	261.6	137.8	1409.3	ND	358.5	279.5	2713.2
R3-M4-D11	50	12158.2	4288.6	8345.4	9.7	1487.2	40.1	33.7	174.2	16.3	ND	ND	122.9	903.7
R4-M3-D1	50	9023.9	2577.9	15168.0	4.1	721.0	36.4	2031.8	134.2	1487.4	2.1	46.3	41.8	2526.2
R4-M3-D2	50	10752.9	2333.5	16883.2	5.2	140.2	41.5	5767.1	4.5	51.4	ND	ND	ND	3066.4
R4-M3-D5	50	14647.1	5914.4	12070.6	9.6	1353.3	50.0	177.4	9.0	ND	1.3	ND	ND	2214.8

Sample Identification	Day	iso-Pentane ug/L	Pentane ug/L	Cyclo pentane ug/L	3Methyl Pentane ug/L	Hexane ug/L	iso-Hexane ug/L	Benzene ug/L	iso-Octane ug/L	toluene ug/L	octane ug/L	o-xylene ug/L	124 TMB ug/L	Naphthalene ug/L
R4-M4-D3	50	13353.0	3316.5	18738.0	5.2	654.9	46.0	5606.8	10.3	1123.5	ND	70.1	ND	3068.1
R4-M4-D4	50	16847.0	5584.6	19257.8	7.8	1561.6	49.4	1023.7	75.3	43.3	1.2	ND	ND	3025.4
S5-D6	50	1022.1	431.2	382.9	ND	779.9	ND	ND	527.8	ND	0.8	ND	ND	ND
R3 M3 D1	103	13022.3	640.7	10080.1	10.9	50.7	44.5	46.6	275.0	62.1	ND	40.5	20.7	1977.0
R3 M3 D3	103	14934.6	372.7	12648.9	11.5	36.8	49.2	409.6	225.1	12.0	ND	42.3	31.1	1388.2
R3 M4 D1	103	6039.7	1825.3	7689.1	5.8	589.7	34.1	204.9	243.4	946.0	ND	523.0	346.6	2252.3
R3 M4 D3	103	15288.7	898.9	16245.0	9.5	34.4	50.2	1956.5	66.0	1550.7	ND	330.8	58.0	2281.4
R3 M4 D11	103	14071.9	3597.9	12597.8	12.9	854.2	30.7	813.5	152.6	512.1	ND	78.3	45.4	953.7
R3 M4 D11L	103	14318.1	3539.9	12509.9	10.6	838.7	30.5	830.3	148.8	516.8	ND	79.6	47.7	981.8
S3 D2	103	12524.8	5401.6	7780.4	18.6	3386.5	61.3	ND	1147.7	118.8	ND	385.2	596.6	1475.1
S3 D3	103	20777.3	7883.4	18054.5	14.2	2179.8	68.1	145.6	453.8	1021.7	28.9	1226.9	581.0	3044.1
S5 D2	103	6055.2	1128.8	13629.7	5.7	3.3	41.5	4428.8	253.0	5222.7	ND	1601.1	481.2	3467.3
S5 D3	103	21026.2	2846.4	18198.0	12.3	5.5	63.1	479.2	269.6	8.2	ND	165.5	349.7	2726.1
S5 D6	103	4260.9	1153.3	3009.5	7.8	384.4	11.6	21.2	623.4	16.7	4.0	77.8	ND	ND
S3 D2	233	7659.8	3069.1	2417.9	20.2	2809.3	41.2	0.0	643.3	29.9	68.1	118.2	412.8	613.6
S3 D3	233	18410.9	6795.2	16977.8	12.6	2237.1	61.6	65.6	365.2	551.3	37.5	1108.6	605.9	3069.2
S5 D2	233	18900.2	6727.6	17730.6	13.5	1083.0	65.4	114.2	455.8	3570.2	12.8	1653.7	662.7	3968.7
S5 D3	233	20710.7	1772.7	16667.9	12.8	20.4	67.8	24.8	249.8	136.7	0.0	80.5	407.3	2860.5
S5 D6	233	384.4	151.2	84.8	13.2	22.8	7.8	89.3	606.1	0.0	0.0	0.0	0.0	0.0
R3 M3 D1	233	2441.1	745.5	2389.7	0.0	119.9	11.1	0.0	69.6	0.0	0.0	11.1	161.6	1147.6
R3 M3 D3	233	11687.8	3186.1	8355.4	7.8	182.1	32.7	0.0	172.7	11.5	0.0	239.4	226.8	1885.4
R3 M4 D1	233	10345.1	1243.8	12448.0	5.3	33.5	32.8	179.3	183.7	120.0	0.0	375.3	434.2	2772.7
R3 M4 D3	233	11307.7	2598.2	6167.2	8.9	70.9	42.1	31.8	97.0	11.7	0.0	50.5	220.9	1889.5
R3 M4 D11	233	5670.9	1141.8	3609.6	2.9	24.1	15.6	0.0	104.6	0.0	0.0	23.8	0.0	741.1
R4 M2 D13	233	131.6	20.9	138.2	0.0	0.0	0.0	0.0	4.6	0.0	0.0	0.0	0.0	0.0

Sample Identification	Day	iso-Pentane ug/L	Pentane ug/L	Cyclo pentane ug/L	3Methyl Pentane ug/L	Hexane ug/L	iso-Hexane ug/L	Benzene ug/L	iso-Octane ug/L	toluene ug/L	octane ug/L	o-xylene ug/L	124 TMB ug/L	Naphthalene ug/L
R4 M3 D5	233	13453.8	235.5	17368.3	12.2	31.0	55.5	1586.5	66.4	0.0	0.0	0.0	0.0	2145.3
R4 M3 D13	233	10553.8	296.7	9358.9	13.0	37.4	36.1	235.5	21.8	6.0	0.0	0.0	0.0	1493.1
R4 M4 D1	233	16617.1	3998.0	16581.3	6.8	139.5	46.7	296.6	220.4	2405.4	0.0	660.5	146.3	1189.9
R4 M4 D2	233	9770.6	2148.4	11924.1	6.6	104.3	33.0	167.1	110.4	643.7	0.0	228.9	47.8	1414.2
R4 M4 D3	233	15983.4	101.5	14373.1	10.5	1.9	26.1	709.5	3.3	0.0	0.0	0.0	0.0	1269.2
R4 M4 D4	233	3263.3	78.5	1094.8	4.6	6.3	0.0	14.9	0.0	0.0	0.0	0.0	0.0	482.0
R4 M4 D14	233	9939.4	91.5	7326.3	6.4	22.6	11.9	266.2	2.0	0.0	0.0	0.0	0.0	721.7

Appendix G

Biomarker results, from Day -7 to Day 44

Toluene-*cis*-dihydrodiol (aerobic Toluene)

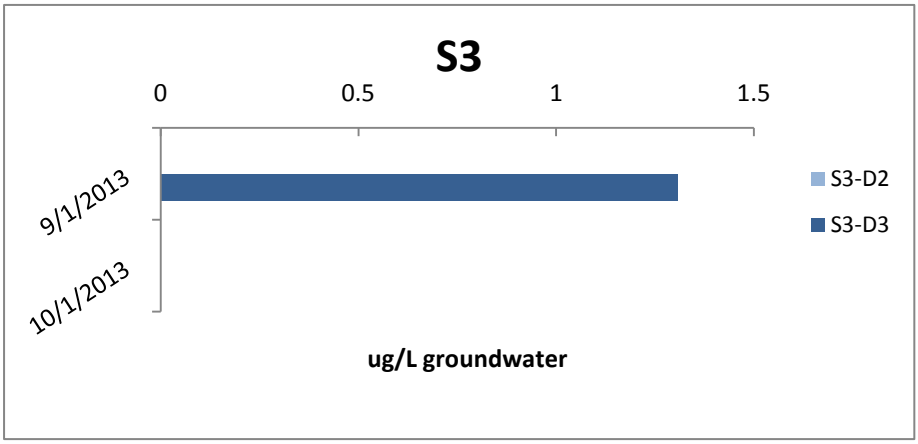

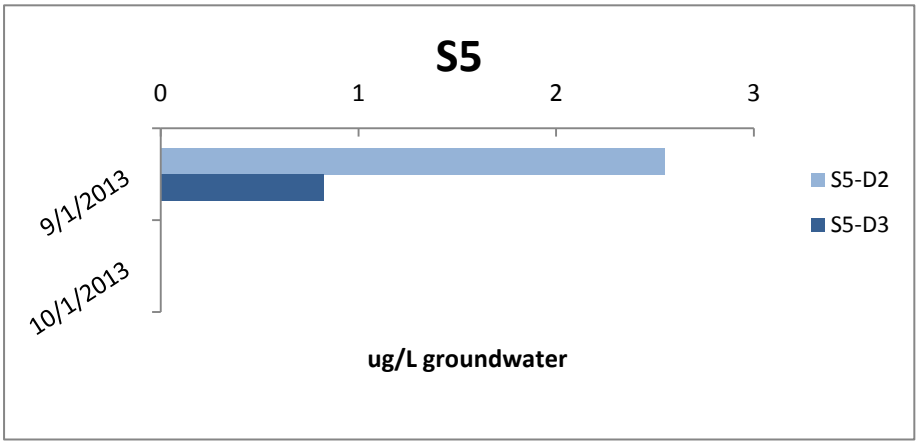

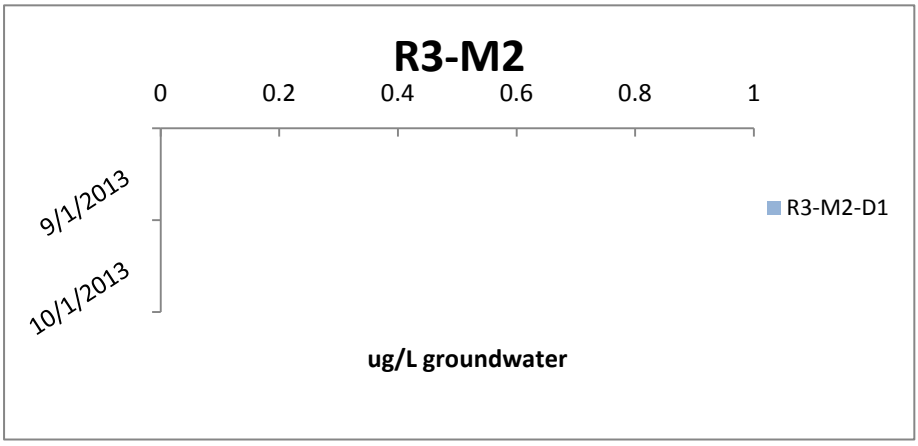

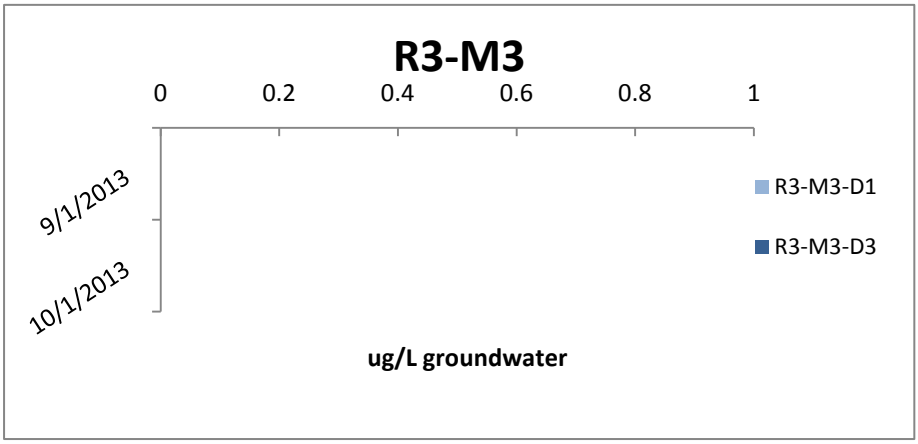
R3-M3
0
0.2
0.4
0.6
0.8
1
9/1/2013
10/1/2013
R3-M3-D1
R3-M3-D3
ug/L groundwater

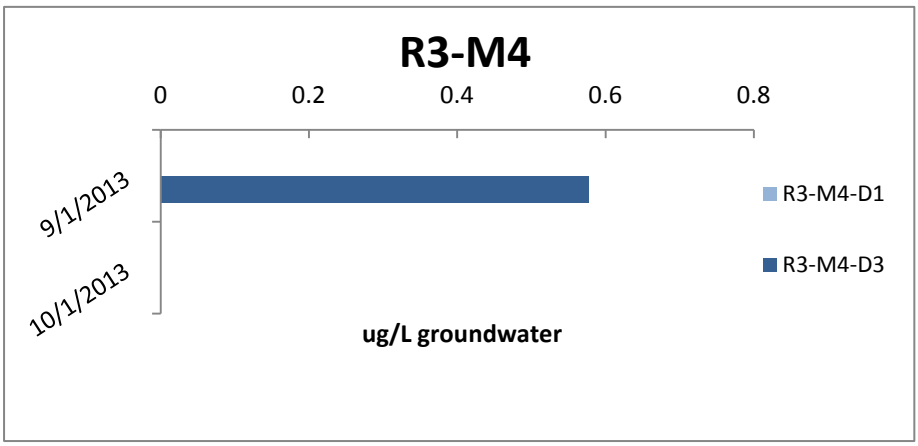
R3-M4
0
0.2
0.4
0.6
0.8
9/1/2013
10/1/2013
R3-M4-D1
R3-M4-D3
ug/L groundwater

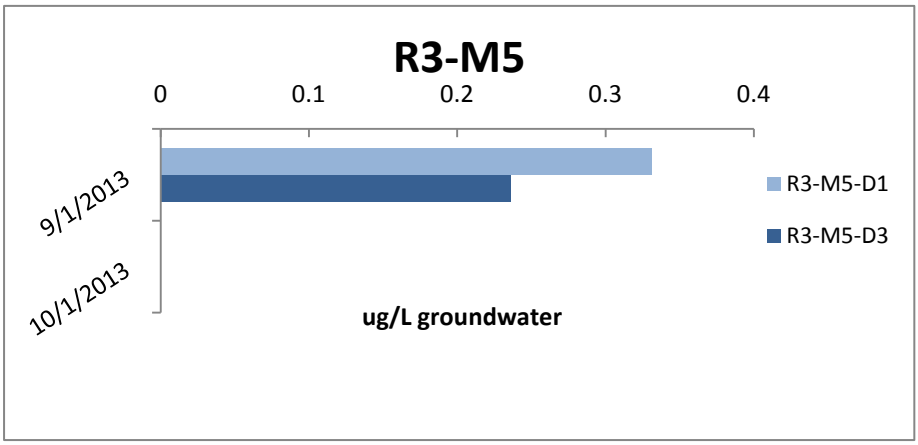
R3-M5
0
0.1
0.2
0.3
0.4
9/1/2013
10/1/2013
R3-M5-D1
R3-M5-D3
ug/L groundwater

todC $_{mRNA}$ (aerobic toluene)

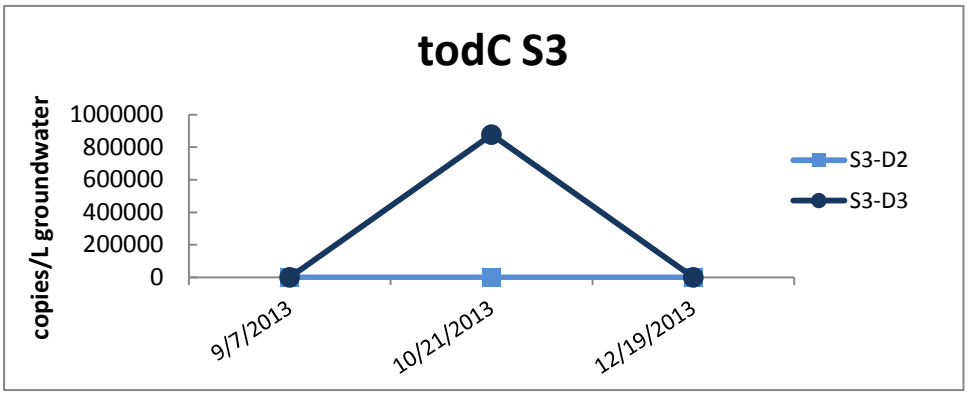

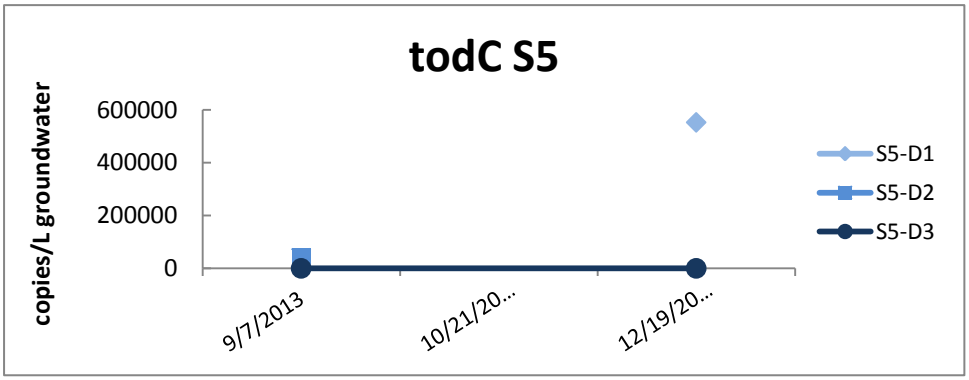

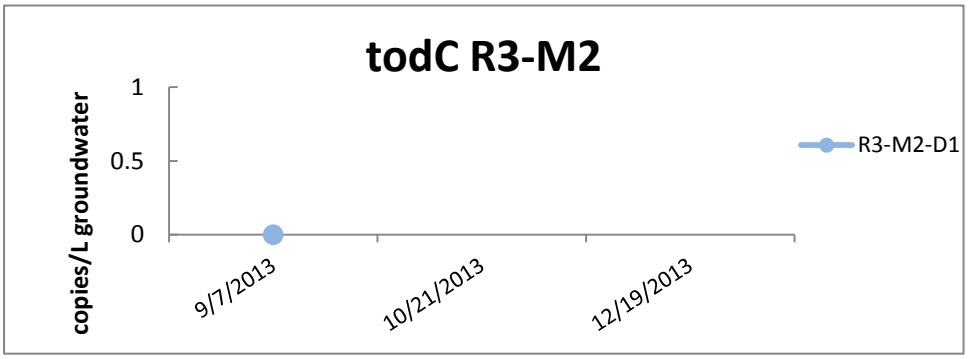

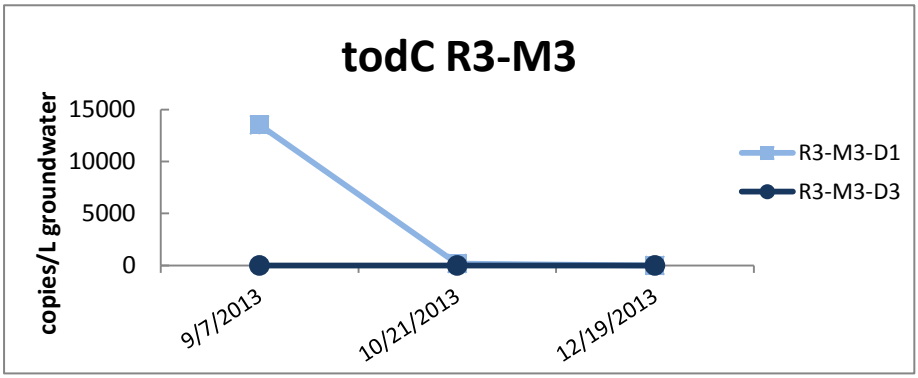
todC R3-M3
copies/L groundwater
15000
10000
5000
0
9/7/2013
10/21/2013
12/19/2013
R3-M3-D1
R3-M3-D3

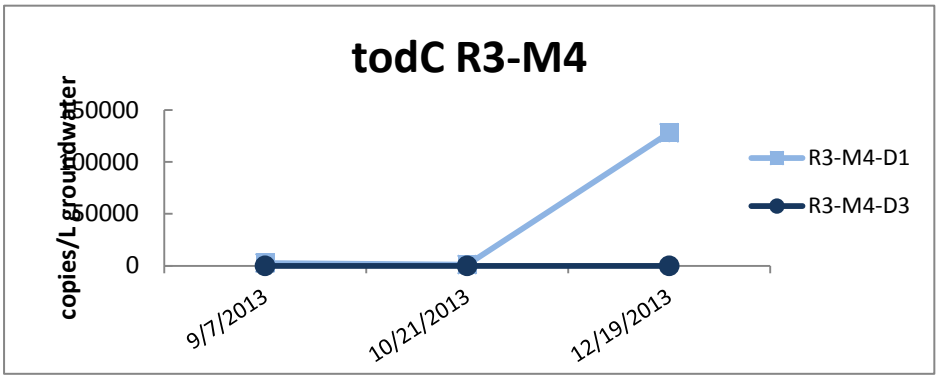
todC R3-M4
copies/L groundwater
0
9/7/2013
10/21/2013
12/19/2013
R3-M4-D1
R3-M4-D3

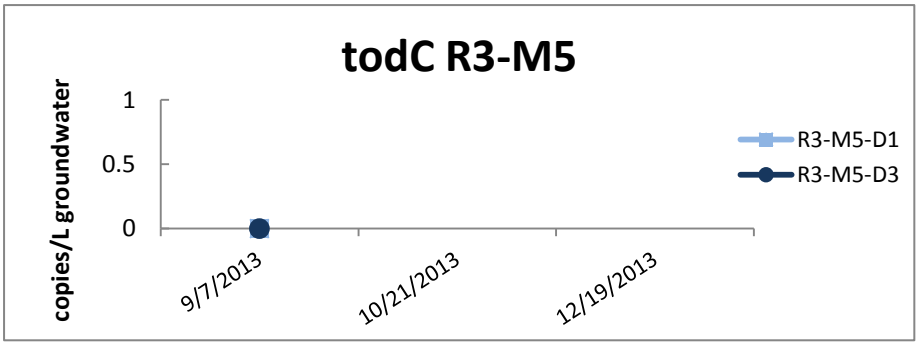
todC R3-M5
copies/L groundwater
1
0.5
0
9/7/2013
10/21/2013
12/19/2013
R3-M5-D1
R3-M5-D3

Benzylsuccinate (anaerobic Toluene)

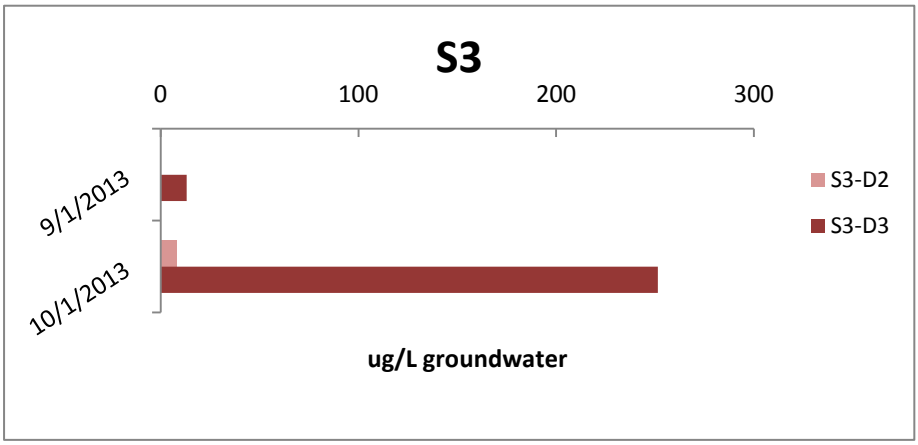

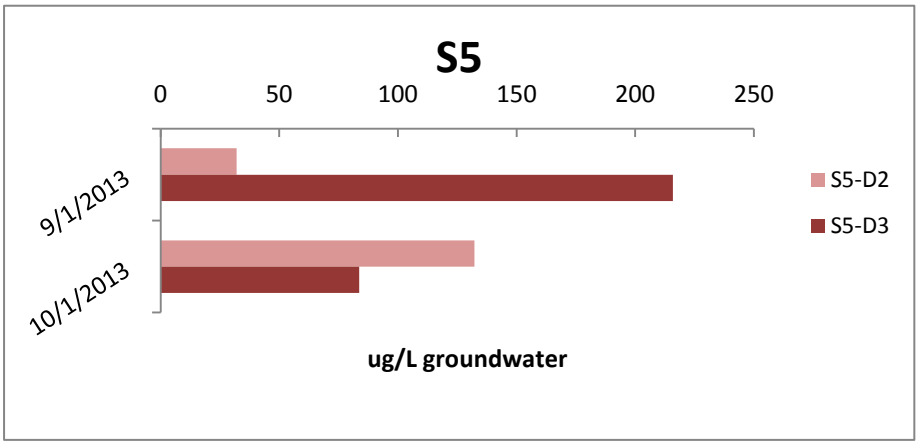

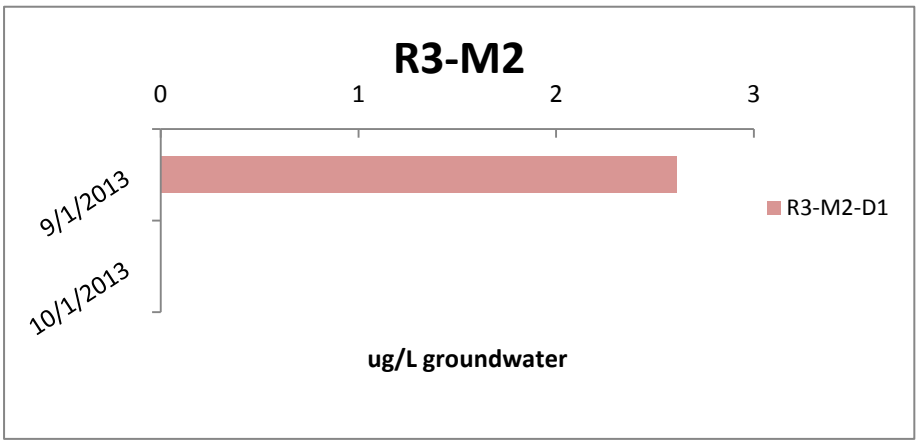

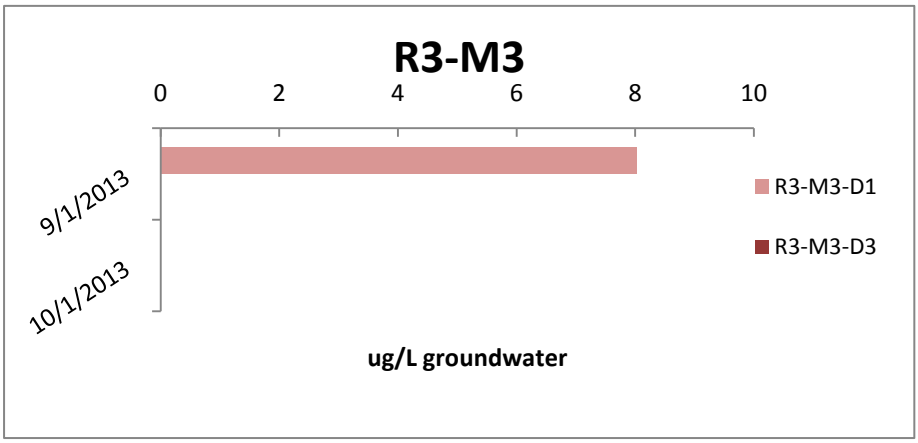
R3-M3
0
2
4
6
8
10
9/1/2013
10/1/2013
R3-M3-D1
R3-M3-D3
ug/L groundwater

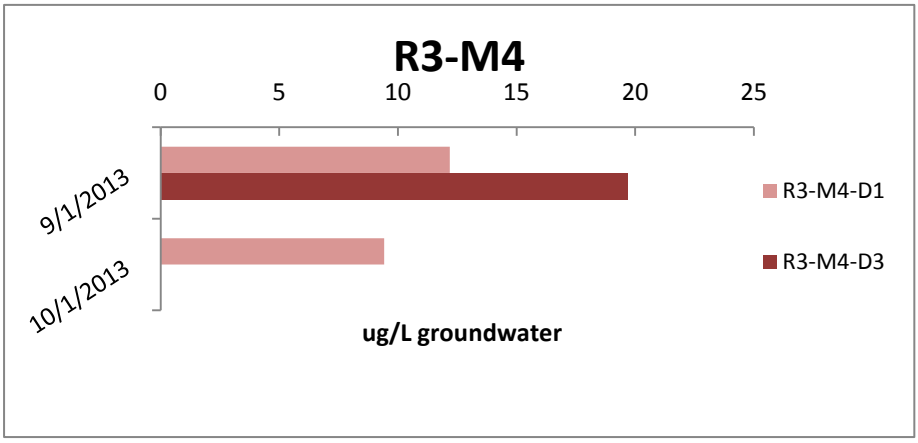
R3-M4
0
5
10
15
20
25
9/1/2013
10/1/2013
R3-M4-D1
R3-M4-D3
ug/L groundwater

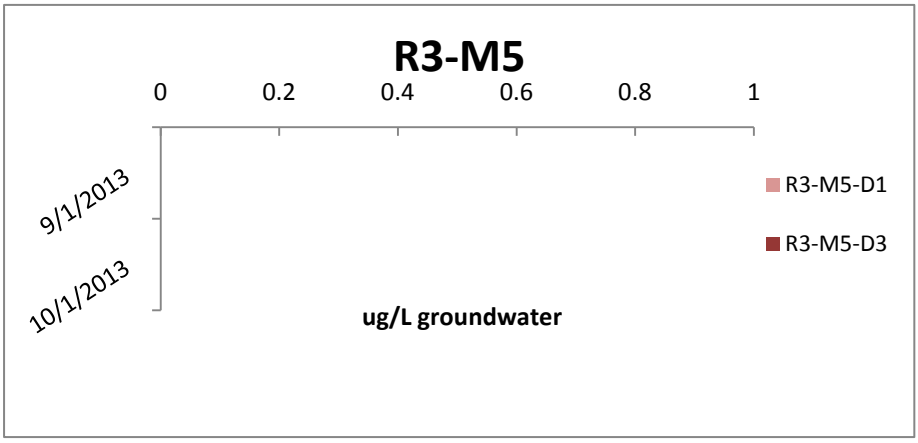
R3-M5
0
0.2
0.4
0.6
0.8
1
9/1/2013
10/1/2013
R3-M5-D1
R3-M5-D3
ug/L groundwater

bssA-SRB$_{mRNA}$ (anaerobic toluene)

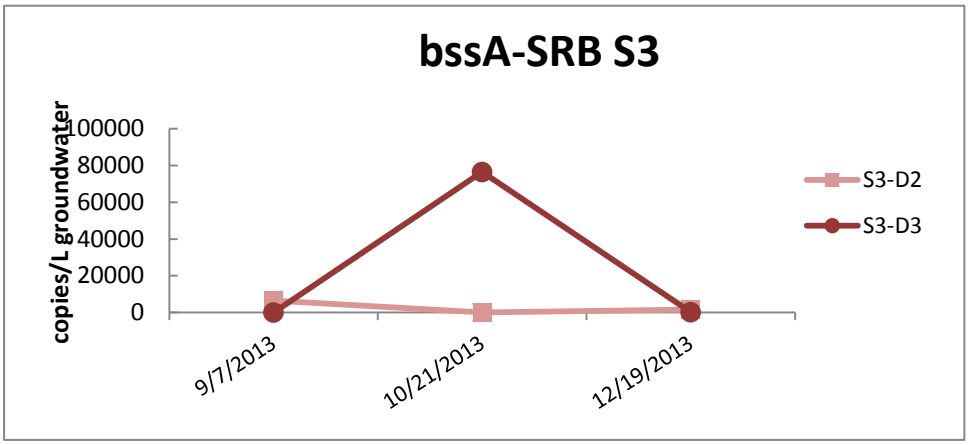

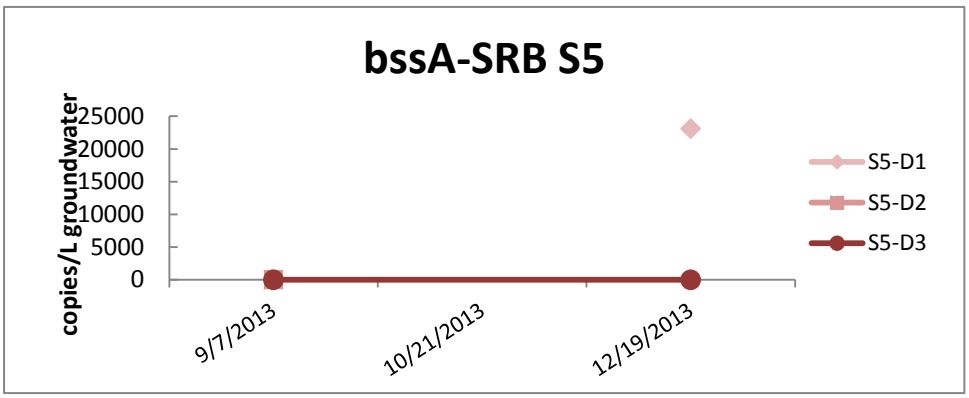

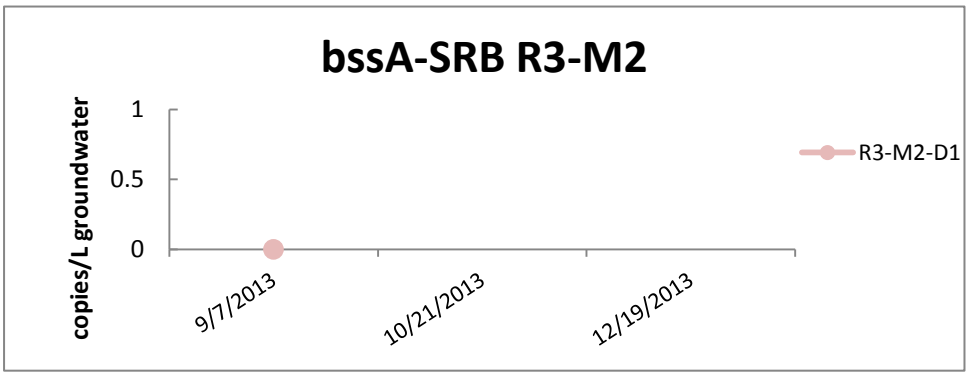

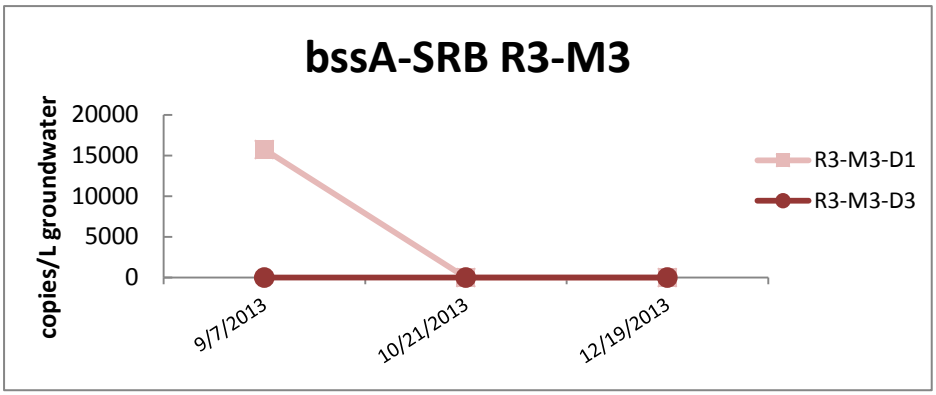
bssA-SRB R3-M3
copies/L groundwater
20000
15000
10000
5000
0
9/7/2013
10/21/2013
12/19/2013
R3-M3-D1
R3-M3-D3

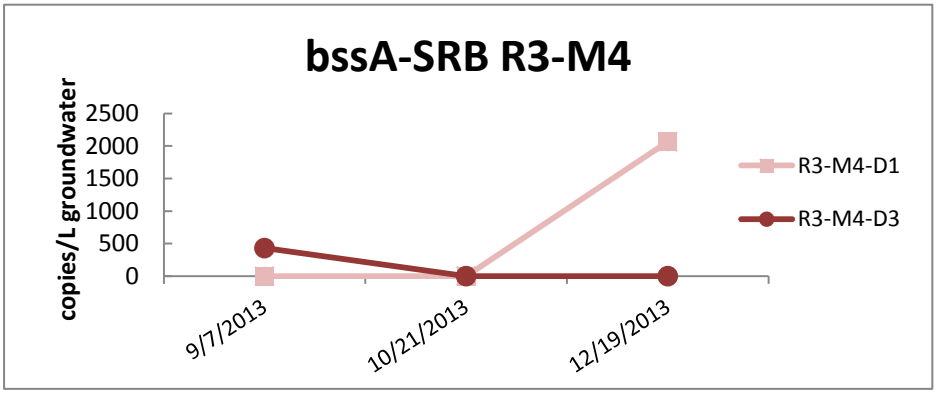
bssA-SRB R3-M4
copies/L groundwater
2500
2000
1500
1000
500
0
9/7/2013
10/21/2013
12/19/2013
R3-M4-D1
R3-M4-D3

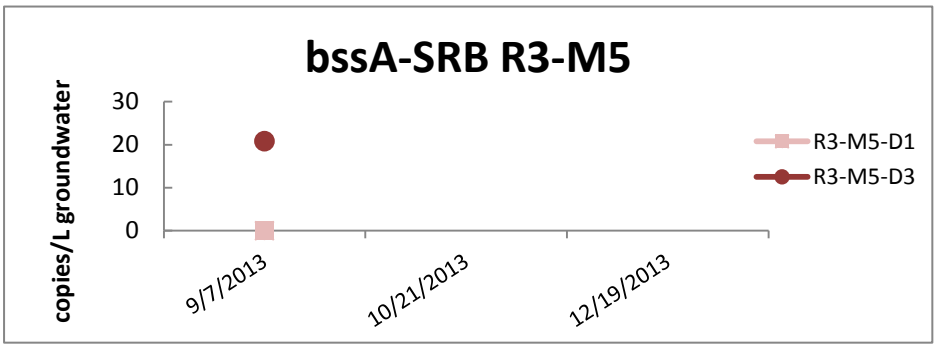
bssA-SRB R3-M5
copies/L groundwater
30
20
10
0
9/7/2013
10/21/2013
12/19/2013
R3-M5-D1
R3-M5-D3

abcA$_{mRNA}$ (anaerobic Benzene)

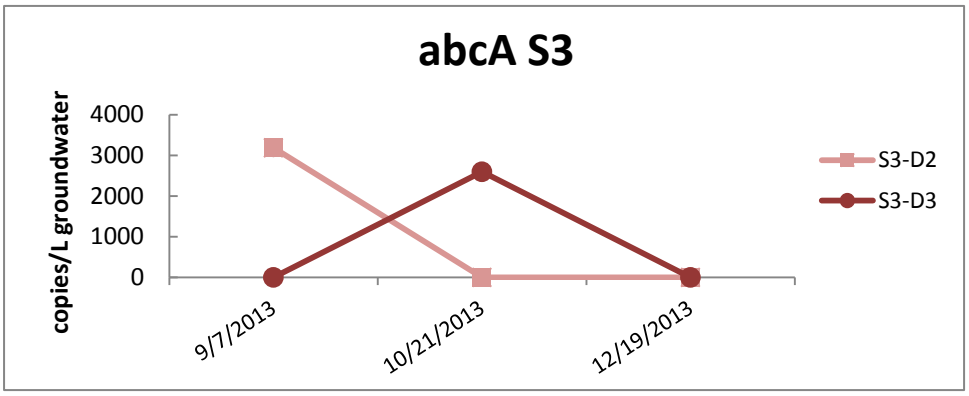

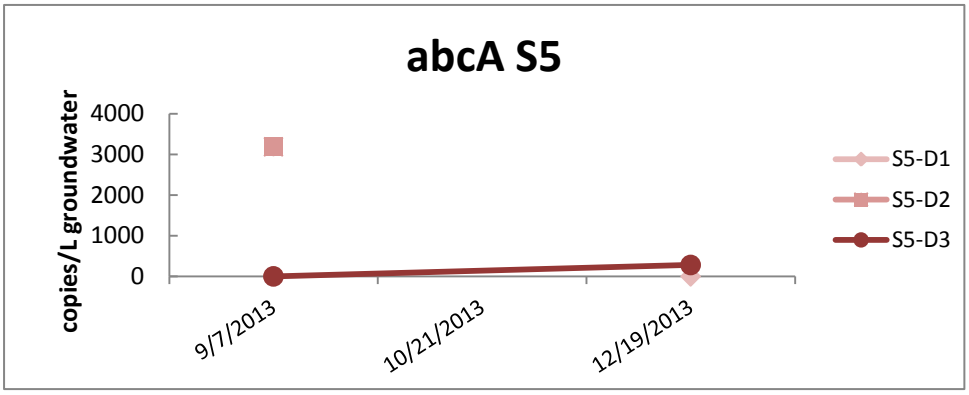

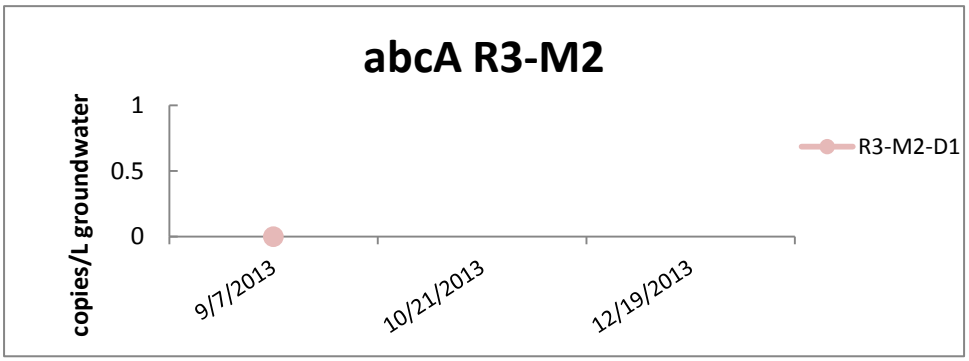

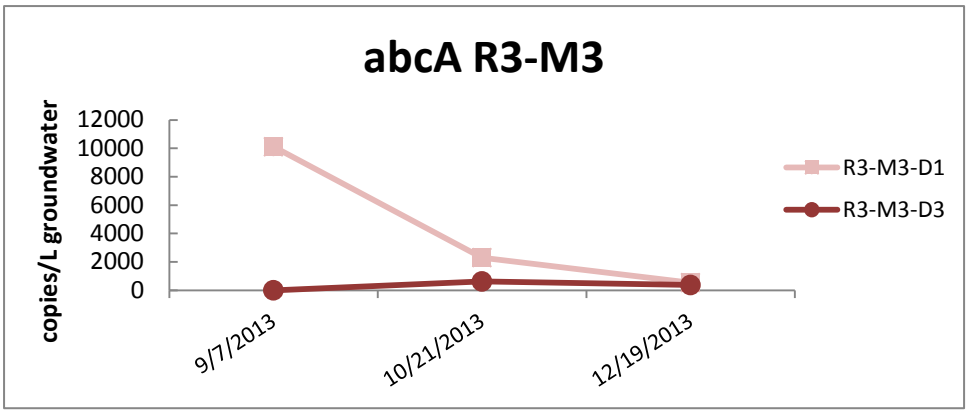
abcA R3-M3
copies/L groundwater
12000
10000
8000
6000
4000
2000
0
9/7/2013
10/21/2013
12/19/2013
R3-M3-D1
R3-M3-D3

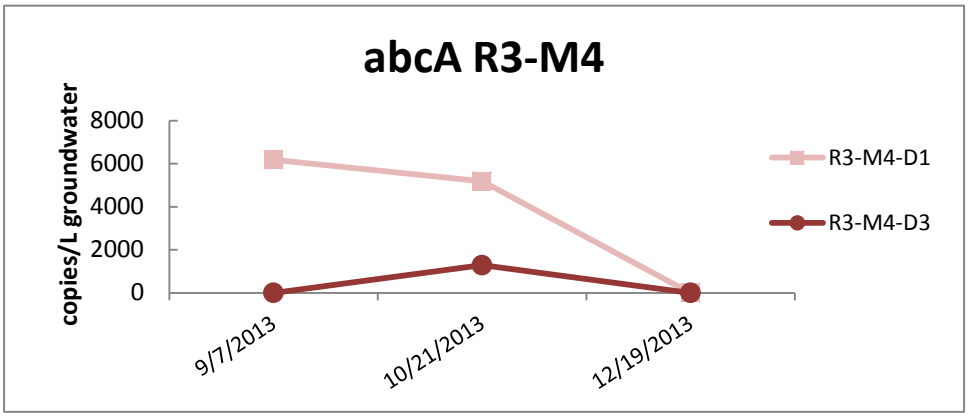
abcA R3-M4
copies/L groundwater
8000
6000
4000
2000
0
9/7/2013
10/21/2013
12/19/2013
R3-M4-D1
R3-M4-D3

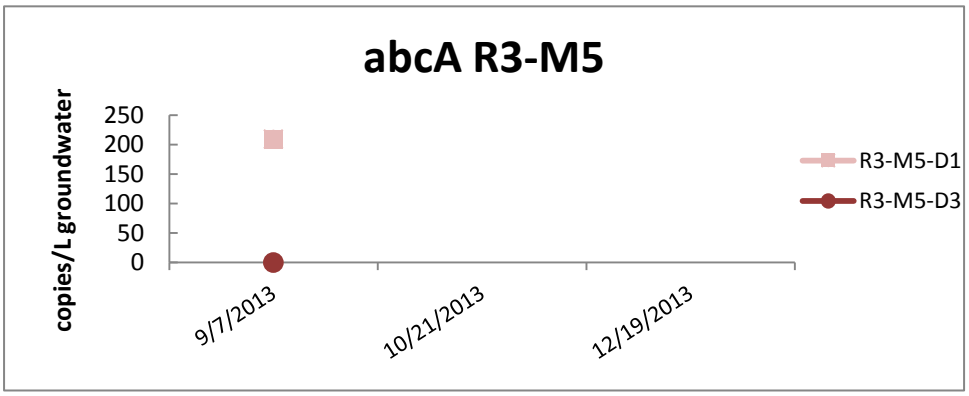
abcA R3-M5
copies/L groundwater
250
200
150
100
50
0
9/7/2013
10/21/2013
12/19/2013
R3-M5-D1
R3-M5-D3